THE MAGNETIC PROPERTIES OF A MODEL TWO-DIMENSIONAL DIPOLAR THIN FILM

CENTRE FOR NEWFOUNDLAND STUDIES

TOTAL OF 10 PAGES ONLY
MAY BE XEROXED

(Without Author's Permission)

ALLAN B. MacISAAC

001311

CENTRE FOR NFLD. STUDIES
MEMORIAL UNIVERSITY
OF NEWFOUNDLAND

INFORMATION TO USERS

This manuscript has been reproduced from the microfilm master. UMI films the text directly from the original or copy submitted. Thus, some thesis and dissertation copies are in typewriter face, while others may be from any type of computer printer.

The quality of this reproduction is dependent upon the quality of the copy submitted. Broken or indistinct print, colored or poor quality illustrations and photographs, print bleedthrough, substandard margins, and improper alignment can adversely affect reproduction.

In the unlikely event that the author did not send UMI a complete manuscript and there are missing pages, these will be noted. Also, if unauthorized copyright material had to be removed, a note will indicate the deletion.

Oversize materials (e.g., maps, drawings, charts) are reproduced by sectioning the original, beginning at the upper left-hand corner and continuing from left to right in equal sections with small overlaps. Each original is also photographed in one exposure and is included in reduced form at the back of the book.

Photographs included in the original manuscript have been reproduced xerographically in this copy. Higher quality 6" x 9" black and white photographic prints are available for any photographs or illustrations appearing in this copy for an additional charge. Contact UMI directly to order.

UMI

A Bell & Howell Information Company
300 North Zeeb Road, Ann Arbor MI 48106-1346 USA
313/761-4700 800/521-0600

The magnetic properties of a model two-dimensional dipolar thin film

by

Allan B. MacIsaac

B.Sc. First Class Honours (St. Francis Xavier University) 1990
M.Sc. (Memorial University of Newfoundland) 1993

A thesis submitted to the
School of Graduate Studies
in partial fulfilment of the
requirements for the degree of
Doctor of Philosophy

Department of Physics and Physical Oceanography
Memorial University of Newfoundland

(March, 1997)

St. John's Newfoundland

National Library of Canada
Acquisitions and Bibliographic Services
395 Wellington Street
Ottawa ON K1A 0N4
Canada

Bibliothèque nationale du Canada
Acquisitions et services bibliographiques
395, rue Wellington
Ottawa ON K1A 0N4
Canada

Your file Votre référence

Our file Notre référence

The author has granted a non-exclusive licence allowing the National Library of Canada to reproduce, loan, distribute or sell copies of this thesis in microform, paper or electronic formats.

L'auteur a accordé une licence non exclusive permettant à la Bibliothèque nationale du Canada de reproduire, prêter, distribuer ou vendre des copies de cette thèse sous la forme de microfiche/film, de reproduction sur papier ou sur format électronique.

The author retains ownership of the copyright in this thesis. Neither the thesis nor substantial extracts from it may be printed or otherwise reproduced without the author's permission.

L'auteur conserve la propriété du droit d'auteur qui protège cette thèse. Ni la thèse ni des extraits substantiels de celle-ci ne doivent être imprimés ou autrement reproduits sans son autorisation.

0-612-23153-4

Canada

The magnetic properties of a model two-dimensional dipolar thin film

Copyright 1996

by

Allan B. MacIsaac

Abstract

In this thesis the magnetic properties of a model for a two-dimensional, dipolar thin film are determined using Monte Carlo simulations. Three different versions of the model have been considered and the results have been compared to previous theoretical results as well as to recent experiments on ultra-thin magnetic films.

The first version of the model is a uniaxial model, with dipolar and exchange interactions. The ground states for this model are shown to be stripe phases for all $J/g > 0.85$, where J is the strength of the exchange interaction and g is the strength of the dipolar interaction. At finite temperature there is a phase transition from these stripe phases at low temperature to an orientationally disordered phase at higher temperatures. This orientational disordered phase appears to map continuously to the paramagnetic phase. The effect of an applied field on the stripe phases is also considered.

The second version of the model is a planar model. In this model the magnetic moments interact only via the dipole-dipole interaction. The results of Monte Carlo simulations are interpreted within the context of a linearised spin wave calculation. The comparison indicates that the model system orders at a finite temperature in the thermodynamic limit. The nature of the transition from the paramagnetic state to the low temperature ordered state is studied by considering the decay of the two-point correlation function, both above and below the critical temperature.

The third version of the model is a dipolar Heisenberg model, in which the mag-

netic moments interact via the dipole-dipole interaction. The moments are also subject to a magnetic surface anisotropy. This model is shown to exhibit a novel reorientation transition. The phase diagram for this model is developed and compared to that obtained for a similar system with a dominant ferromagnetic exchange interaction.

To my wife and to my parents.

Contents

List of Figures

List of Tables

Acknowledgements

I would like to take this opportunity to thank the many people who have made contributions to the work presented in this thesis.

Foremost I would like to thank Dr. John Whitehead, my supervisor, who's influence has made me a better researcher and may, in time, make me an acceptable writer. I have learned a considerable amount from John about both the methods of physics and also how one should properly conduct research. His tolerance of my wanderings, both physical and mental, has been greatly appreciated.

I have also been fortunate enough to have a very capable "substitute" supervisor in Dr. Keith De'Bell, to whom I owe a great deal. My collaborations with Keith have been very productive and informative, and I am looking forward to our working more closely.

I would also like to thank Dr. Mark Whitmore and Dr. John DeBruyn for acting as members of my supervisory committee. I must also thank both of them for their assistance in their administrative roles, as acting Head of the Department and as Deputy Head (Graduate Studies).

I have been lucky enough to have met and worked with three very fine students, during their years as undergraduates. I would like to thank Ivan N. Booth, Michael Robinson, and Jessica Arlett for their enthusiasm and hard work. I am certain they will all go far in life, and I hope they recall our interactions favourably.

I would like to acknowledge the Natural Science and Engineering Research Council

of Canada, and Memorial University of Newfoundland for financial assistance. I also wish to acknowledge research assistance from The High Performance Computer Centre in Calgary, The Pittsburgh Supercomputing Center in Pittsburgh and Digital Equipment Corporation.

I would like to thank my fellow students, Roman Baranoski, Raja Amruthavalli, Marc Pepin, Todd Andrews, Maria Kilfoil, Bojiong Yuan, and Todd Farrell for keeping life tolerable.

Finally a very heart felt thank you is extended to my wife, Sandra, who's patience I have severely tested over the last few years. You have stood by me through it all, and I assure you, Sandra, "I'm almost finished."

Chapter 1

Introduction

In this thesis the properties of a lattice-based model for two-dimensional magnetic thin films are investigated. The magnetic moments in the model interact via a dipole-dipole interaction as well as other possible interactions, but it is the effects of the dipolar interaction which are considered in depth. These effects on the magnetic properties of materials can be very dramatic and yet still quite subtle, and there has been keen interest in magnetic thin films over the past 20 years [1, 2, 3]. In recent years magnetic thin films have again become a "hot" topic for research due to enhancements in molecular beam epitaxy, and the ability of researchers to construct high quality thin films for study [4, 5].

In this thesis, the phase behaviour is established for a classical model of a thin magnetic film both at $T = 0K$ and at finite temperature. The results of analytical calculations for the energy of various phases are presented and used to predict the

ground states for the model. Monte Carlo simulations are used extensively to determine both the low temperature properties and the nature of the phase transitions present in the various versions of the model. Three different variants of the basic model are considered. The first is a system with uniaxial or one component magnetic moments. The magnetic moments are constrained to orient perpendicular to the film and interact via a dipole-dipole interaction and an exchange interaction. The influence of an applied field is also considered. The second is a system with planar or two component magnetic moments. The magnetic moments are confined to the plane of the film and interact via the dipole-dipole interaction only. For this variant of the model, the low temperature properties are examined with reference to a classical, linearised spin wave calculation. The third version of the model is a Heisenberg model in which the moments are fully three-dimensional vectors which interact via the dipole-dipole interaction and are subject to a perpendicular anisotropy.

Much of the work presented in this thesis has been published[6, 7, 8, 9, 10, 11, 12]. The outline of the thesis is given below.

1.1 Outline

This thesis is organised as follows: Chapter 1 will introduce the model being studied in general terms, and discuss the motivation for the study. It will also provide an introduction to previous experimental and theoretical work related to the work presented in this thesis.

Chapter 2 will give a brief introduction to Monte Carlo simulations. The difficulties associated with including a dipolar interaction within a Monte Carlo simulation will be discussed. The dipolar interaction is a long-range, anisotropic interaction and both of these properties make it a challenge to incorporate efficiently into a Monte Carlo simulation. The simulations carried out as part of this study are among the most comprehensive and involve the largest systems of any published studies.

Chapters 3 and 4 treat the case of a uniaxial dipolar system. In other words, these chapters deal with a system where the magnetic moments are constrained to point perpendicular to the film. Assuming that the direction perpendicular to the film is the $\hat{z}$ direction, the magnetic moment can assume only two states; either $\vec{\mu} = +\mu\hat{z}$ or $\vec{\mu} = -\mu\hat{z}$. The moments lie on a square lattice and interact via the dipolar interaction, and an exchange interaction and with an applied field. Chapter 3 deals exclusively with the problem of establishing the ground state as a function of the ratio between the exchange interaction and the dipolar interaction, in the absence of an applied field. Chapter 4 considers the finite temperature behaviour of this system, as well as the effects of an applied field.

In Chapter 5, a dipolar planar model is considered. In this model the magnetic moments or spins are assumed to lie within the plane of the thin film and to have full rotational freedom in that plane. Again assuming that the direction perpendicular to the film is the $\hat{z}$ direction, this means that, in the planar model, the magnetic moment may be specified by $\vec{\mu} = \mu^x\hat{x} + \mu^y\hat{y}$ with $|\vec{\mu}| = \mu$. The $\hat{x}$ and $\hat{y}$ directions

are chosen so they lie along the axes of the square lattice of the system. The nature of the ordering which takes place in this model is analysed while considering the results of a linearised, spin wave calculation. The spin wave calculation has been performed for both the full long-range dipolar interaction as well as for a short-range approximation. This model is also interesting because of the well known properties of the classical planar model, which is an isotropic short-range exchange model. In the classical planar model there is no order-disorder transition, but instead there is a Kosterlitz-Thouless transition [13].

In Chapter 6, a system with a dipolar interaction along with a magnetic surface anisotropy is considered. The magnetic moments are considered to be fully three-dimensional vectors, $\vec{\mu} = \mu^x\hat{x} + \mu^y\hat{y} + \mu^z\hat{z}$, with an anisotropy chosen such that the $\hat{z}$ direction (perpendicular to the plane) represents the easy axis for the system. In this part of the study the properties of a reorientation transition in the absence of an exchange interaction are examined.

The final chapter, Chapter 7, is the conclusion. In this chapter a brief summary is given of the major results presented in the thesis. As well it offers an overview of some of the remaining questions in this field.

1.2 Motivation and experimental results

1.2.1 Rare earth compounds

The original motivation for choosing to work with two-dimensional dipolar systems was to explain the ordering observed in the rare earth subsystem of (RE)$Ba_2Cu_3O_7$, which is a class of magnetic superconductors. High-temperature superconductors have vast technological potential, therefore understanding the properties of these systems is very important. In these compounds, the rare earth ions order at temperatures of the order of a few Kelvin, where the dipole-dipole interaction is significant. The ordered states observed in these compounds are also consistent with a significant dipole-dipole interaction [14, 15, 16, 17]. There are a large number of experiments on the low temperature properties of these compounds which have established that, for some rare earths, the ordering has characteristics which are distinctly two-dimensional. For example, Lynn *et al.* [18] showed that in $ErBa_2Cu_3O_7$, the rare earth sublattice orders at 618 mK, and they also showed that the neutron scattering by this material is characteristic of two-dimensional ordering within planes in the crystal. The neutron scattering indicates that three-dimensional ordering occurs only at lower temperatures [18]. Similar results have been found for $DyBa_2Cu_3O_7$ by Fischer *et al.* [19] and by Goldman *et al.* [15]. These experimental results have been compared with simulations in previous publications [20, 21, 22], and are not discussed explicitly in this thesis, however understanding the (RE)$Ba_2Cu_3O_7$ compounds represents an im-

portant potential application of the present work.

1.2.2 Magnetic thin films

In addition to (RE)$Ba_2Cu_3O_7$, the model studied can also be applied to magnetic thin films. This is a topic of considerable interest both from an experimental and a theoretical perspective. Recent progress in molecular beam epitaxy in ultra-high vacuum has allowed experimentalists to make great strides in the fabrication and analysis of ultra-thin (several mono-layers) magnetic films [4, 5, 23, 24, 25, 26, 27, 28, 29, 30, 31, 32]. It is apparent from these studies, and the related theoretical work, that the dipolar interaction plays an important role in determining the magnetic properties of these systems.

Thin epitaxial films of Fe on the Co(100) surface were studied by Pappas *et al.* [5] using spin-polarised secondary-electron spectroscopy. The films in this study were approximately 2.5–3.5 atomic layers thick. There are two results of this work which are of particular relevance to this thesis. The first is that, at low temperature, the system orders with the magnetic moments perpendicular to the film. This implies the existence of an anisotropy or interaction besides the typical short range exchange interaction, since an isotropic system with only short-range exchange interactions would not exhibit long-range order[33]. The dipolar interaction is the obvious additional interaction, but it favours in-plane ordering. This suggests that a magnetic surface anisotropy also exists. Pappas *et al.* also showed that at higher temperatures

there is a reorientation transition at which the direction of the net magnetisation switches from perpendicular to the film to parallel to the film.

Allenspach *et al.* [4] have studied thin epitaxial films of Co on the Au(111) surface using spin scanning electron microscopy (SEM). They found the intriguing result in a three mono-layer film that at temperatures of approximately 300 K the magnetic moments form domains of micron size with the magnetic moments oriented perpendicular to the plane of the film. This was the first time that an experiment had supported the theoretical predictions that domains would form in thin films, when the films had perpendicular anisotropies due to dipole-dipole interactions[8, 34]. Allenspach *et al.* also found the reorientation transition observed by Pappas *et al.* [5]. The reorientation transition occurs both as a function of temperature and as a function of the film thickness. For films with a thickness less than three mono-layers the magnetisation is perpendicular to the film, while films thicker than six mono-layers have a magnetisation which lies in the plane of the film. This reorientation is believed to be the result of a change in the effective strength of the magnetic surface anisotropy. In the thicker films the ratio of the number of moments at the surface to total number of moments is reduced, and hence the effect of the surface anisotropy is similarly reduced. With no surface anisotropy the lowest energy state is that with the moments in the plane of the film. This is due to the dipolar interaction, which favours the in-plane state. Allenspach and Bischof [23] have observed a reorientation transition both as a function of temperature and as a function of film thickness in thin films of

Fe on the Cu(100) surface as well. Using SEM they have shown that stripe domains form when the magnetisation is perpendicular to the film at low temperature.

Kerkmann *et al.* [24] studied Co films on the Cu(100) surface in an applied magnetic field. They made use of both the magneto-optic Kerr effect as well as spin-polarised SEM. They were able to observe an ordered phase at low temperature with definite domain formation, as well as the transition to a disordered phase at higher temperatures. They also studied the hysteresis curves due to the application of an applied field both above and below the transition temperature and showed that the results were very similar to those predicted for the 2-D Heisenberg model above the transition temperature. Speckmann *et al.* [30] have also looked at Co films on the Au(111) surface using SEM. They showed that after annealing, the films display a definite domain structure with perpendicular magnetisation and a characteristic domain size dependent upon the film thickness. They were able to measure the dependence of the domain size on the film thickness for films as thin as two mono-layers and the results are well fit by the predictions of Kaplan and Gehring [35], whose work will be discussed below.

The properties of Fe on the Ag(100) surface have been studied by Qui *et al.* [25], who confirmed that for very thin films the preferred direction for the ordered magnetic moments at low temperature is perpendicular to the plane of the film. Qui *et al.* studied a wedge shaped film as they were interested in the variation of the magnetisation as a function of the film thickness. They found that in a 7 mono-layer

film there is a reorientation transition at approximately $T = 375K$.

These results are relevant to all sections of this thesis, but are of particular relevance to Chapters 3 and 6. In Chapter 3 it is concluded that the lowest energy state for films with perpendicular magnetisation is a stripe phase that is qualitatively similar to that observed by Allenspach *et al.* In Chapter 6 the reorientation transition, as a function temperature, is explored. In many of the experiments, it is a change in the thickness of the film which leads to the reorientation transition. The film thickness is an experimentally controllable parameter while the magnitude of the magnetic surface anisotropy (MSA) is not. In a Monte Carlo simulation the MSA is a controllable parameter, and it is less computationally demanding to simulate a mono-layer than to simulate a multi-layered film. Therefore, in this thesis, only the case of a thermally induced reorientation transition in a mono-layer is considered.

Technologically, materials such as Co/Au(111) films are interesting due to potential applications in magnetic storage devices [4]. There are also a number of systems which have similar properties to dipolar thin films, which makes the understanding of thin films interesting from a purely theoretical point of view. These systems include such diverse systems as liquid crystals, Langmuir mono-layers and others [36, 37, 38]. The rich variety of spatially modulated phases which can be found in dipolar thin films also makes them ideal systems for the study of pattern formation[39, 40, 41] and self-organised behaviour [42].

1.3 The model in general

In this section the general Hamiltonian that defines the model discussed in this thesis is introduced. This is done in order to make the discussion of the previous theoretical work on this subject more cohesive, as most of the terms used in the rest of the thesis will be defined in this section.

The model attempts to capture the salient features of a magnetic thin film. or of the rare earth sublattice in the (RE)$Ba_2Cu_3O_7$ compounds. Hence the model treats a two-dimensional system on a square lattice, where the two in-plane directions are the $\hat{x}$ and $\hat{y}$ directions and the direction perpendicular to the plane is taken as the $\hat{z}$ direction. At each lattice point there is a magnetic dipole $\vec{\mu}$ and a net spin $\vec{S}$. The Hamiltonian for the model is, in general, given by

$$\begin{aligned}\mathcal{H} &= \frac{1}{2}{\sum_{\vec{R}_i,\vec{R}_j}}' \left[\frac{\vec{\mu}(\vec{R}_i)\cdot\vec{\mu}(\vec{R}_j)}{|\vec{R}_{ij}|^3} - 3\frac{(\vec{\mu}(\vec{R}_i)\cdot\vec{R}_{ij})(\vec{\mu}(\vec{R}_j)\cdot\vec{R}_{ij})}{|\vec{R}_{ij}|^5}\right] \\ &\quad -\frac{\mathcal{J}}{2}\sum_{(\vec{R}_i,\vec{R}_j)}\vec{S}(\vec{R}_i)\cdot\vec{S}(\vec{R}_j) \\ &\quad -\sum_{\vec{R}_i}\vec{H}\cdot\vec{\mu}(\vec{R}_i) - \sum_{\vec{R}_i}\lambda(\mu(\vec{R}_i)^z)^2, \end{aligned} \tag{1.1}$$

where the displacement is defined as $\vec{R}_{ij} = \vec{R}_i - \vec{R}_j$ and a primed sum means that the term with $\vec{R}_i = \vec{R}_j$ is excluded.

The first term in equation 1.1 is the dipolar interaction and the sum is over all pairs of spins $\vec{R}_i$, $\vec{R}_j$. The typical way of writing the interaction energy between two dipoles is

$$E(\vec{R}_i - \vec{R}_j) = \frac{\vec{\mu}_i\cdot\vec{\mu}_j}{|\vec{R}_{ij}|^3} - 3\frac{(\vec{\mu}_i\cdot\vec{R}_{ij})(\vec{\mu}_j\cdot\vec{R}_{ij})}{|\vec{R}_{ij}|^5}. \tag{1.2}$$

For mathematical reasons it is sometimes preferable to start from a different form of the interaction, which looks very much like the Coulomb interaction. In the form used in most of the calculations shown in this thesis, the interaction energy between two dipoles is written as

$$E(\vec{R}_i - \vec{R}_j) = \sum_{\alpha\beta} \mu^\alpha(\vec{R}_i)\mu^\beta(\vec{R}_j) \lim_{\vec{r}\to 0} \frac{\partial}{\partial r^\alpha} \frac{\partial}{\partial r^\beta} \frac{1}{\left|\vec{R}_{ij} + \vec{r}\right|}. \tag{1.3}$$

With a little work one can show that the two forms are equivalent. The dipolar interaction is a long-range interaction, which means that each spin in the system interacts with all the other spins in the system. It also means that, unlike an exchange interaction which typically decays exponentially with distance, the dipolar interaction decays with a power law dependence on distance. This can lead to convergence problems when treating systems in the thermodynamic limit.

The dipolar interaction is also an anisotropic interaction; in figure 1.1 the field produced by an isolated dipole is shown schematically. It can be seen that the dipole-dipole interaction can either be ferromagnetic or antiferromagnetic, depending on the relative displacement of two dipoles. This will be important, as will be seen later in this thesis, in determining the ground state spin configuration as a function of the various parameters in the Hamiltonian.

The second term in equation 1.1 is an exchange interaction. This sum is over all nearest neighbour pairs (the notation $\langle \vec{R}_i, \vec{R}_j \rangle$ is standard), as the exchange interaction is a short range interaction. A positive J denotes a ferromagnetic exchange interaction, while a negative J denotes an antiferromagnetic interaction. Exchange inter-

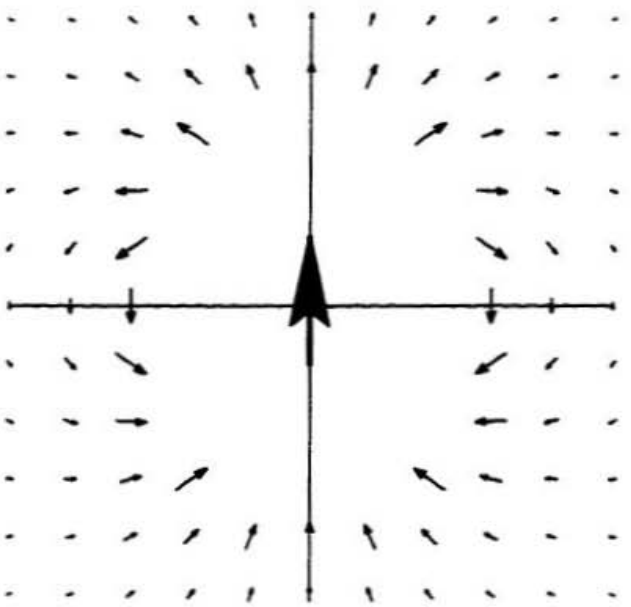

Figure 1.1: The field for an isolated magnetic dipole. The vectors show the magnetic field at various points about a magnetic dipole located at the origin.

actions arise as a consequence of charge overlap between ions. Figure 1.2 schematically illustrates three types of exchange interaction: direct, indirect and super-exchange. In a direct exchange the charge clouds of adjacent ions overlap and the electrons from one ion are able to directly interact with those of the second ion. The second type of exchange is known as an indirect exchange interaction. In this case the electrons of a magnetic ion interact with conduction electrons, which can then interact with a second magnetic ion, giving an effective coupling between the two magnetic ions. The third type of exchange is a super-exchange. In this type of exchange there is an intermediate non-magnetic ion which has a charge overlap with the two magnetic ions. The non-magnetic ion mediates the exchange interaction as its electrons interact

with the electrons of the first ion, and they then interact with the second magnetic ion. In all of these cases the interaction may be approximated by the form given by the second term in equation 1.1.

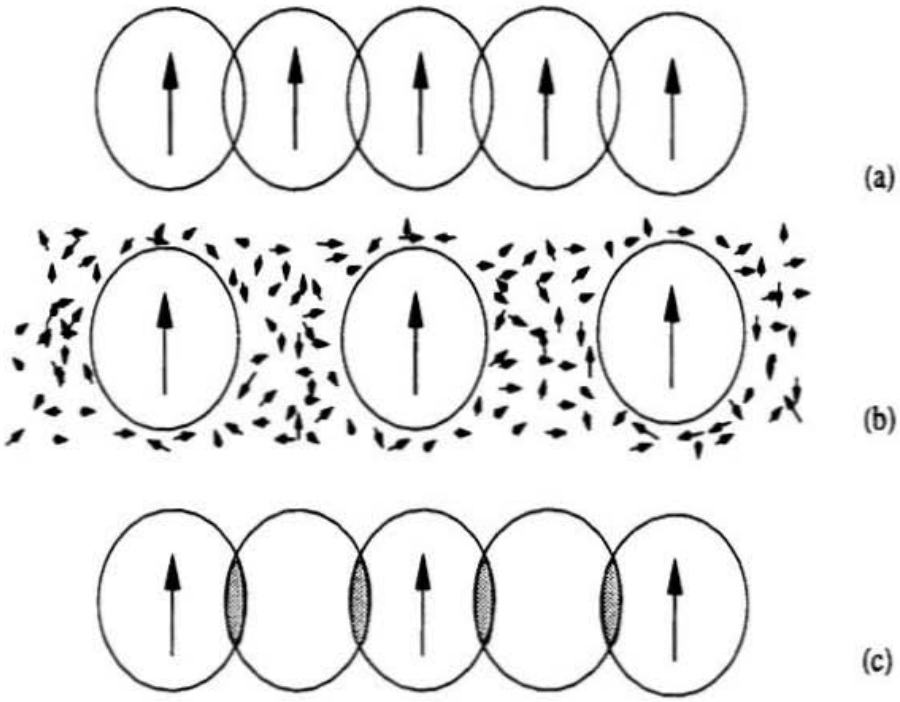

Figure 1.2: Schematic diagram of a direct exchange (a), an indirect exchange (b) and a super-exchange interaction (c).

The third term in equation 1.1 allows for the application of an applied external field which can have components in any of the three spatial directions. The effect of an applied field is studied only in the case of uniaxial moments, in Chapter 4.

The fourth term in equation 1.1 is the magnetic surface anisotropy. In a material it is possible for a preferred axis or axes to exist, about which it is energetically favourable for the system to order. This can be the result of a number of things.

For example, the lack of spherical symmetry in the charge overlap between ions, due to spin-orbit coupling, can lead to a preferred orientation for the ions. The isotropic exchange interaction does not account for this. This is the case for cobalt crystals [43]. Another possible cause is crystalline electric fields, which are the result of the inhomogeneous fields of the neighbouring ions. Crystalline electric field effects will be much stronger in magnetic thin films composed of transition metals than in rare earth superconductors, since in the magnetic thin films it is the outer shell, the 3d shell, which is responsible for the magnetic moment, while in the rare earth ions it is the inner 4f shell.

In the model magnetic film considered in this thesis it is sufficient that the anisotropy couple only to the $\hat{z}$ component of the magnetic moment, due to the symmetry between the two in-plane directions. A positive anisotropy, $K > 0$ gives an easy axis along $\hat{z}$, while a negative value makes $\hat{z}$ a hard axis and gives an easy plane within the film. The case of $K < 0$ is treated in Chapter 6, where the system is studied as a function of K.

Before proceeding it is useful to rewrite equation 1.1 in terms of the dimensionless quantities which are used in the Monte Carlo simulations. The magnetic moments are rewritten as $\vec{\mu} = \mu_{eff}\vec{\sigma}$, where $|\vec{\sigma}| = 1$. Similarly the spin is rewritten as $\vec{S} = S_{eff}\vec{\sigma}$. Also all displacements are scaled by the lattice constant, a, so that $\vec{R} \rightarrow \vec{R}/a$.

Substituting these definitions in to equation 1.1 yields

$$\begin{aligned}\mathcal{H} &= \frac{\mu_{eff}^2}{a^3}\frac{1}{2}{\sum_{\vec{R}_i,\vec{R}_j}}' \left[\frac{\vec{\sigma}(\vec{R}_i)\cdot\vec{\sigma}(\vec{R}_i)}{|\vec{R}_{ij}|^3} - 3\frac{(\vec{\sigma}(\vec{R}_i)\cdot(\vec{R}_{ij}))(\vec{\sigma}(\vec{R}_i)\cdot(\vec{R}_{ij}))}{|\vec{R}_{ij}|^5}\right] \\ &\quad -\frac{\mathcal{J}S_{eff}^2}{2}\sum_{\langle\vec{R}_i,\vec{R}_j\rangle}\vec{\sigma}(\vec{R}_i)\cdot\vec{\sigma}(\vec{R}_j) \\ &\quad -\mu_{eff}\sum_{\vec{R}_i}\vec{H}\cdot\vec{\sigma}(\vec{R}_i) - \mu_{eff}^2\sum_{\vec{R}_i}\lambda(\sigma^z(\vec{R}_i))^2. \end{aligned} \tag{1.4}$$

Finally new coupling constants are defined such that the Hamiltonian can be written as

$$\begin{aligned}\mathcal{H} &= g\left\{{\sum_{\vec{R}_i,\vec{R}_j}}'\sigma^\alpha(\vec{R}_i)\Gamma^{\alpha\beta}(\vec{R}_{ij})\sigma^\beta(\vec{R}_j) - \frac{J}{2}\sum_{\langle\vec{R}_i,\vec{R}_j\rangle}\vec{\sigma}(\vec{R}_i)\cdot\vec{\sigma}(\vec{R}_j) - \sum_{\vec{R}_i}\vec{h}\cdot\vec{\sigma}(\vec{R}_i)\right. \\ &\quad \left. -K\sum_{\vec{R}_i}(\sigma^z(\vec{R}_i))^2\right\}, \end{aligned} \tag{1.5}$$

with

$$\Gamma^{\alpha\beta}(\vec{R}_{ij}) = \frac{\delta_{\alpha\beta}}{|\vec{R}_{ij}|^3} - 3\frac{R_{ij}^\alpha R_{ij}^\beta}{|\vec{R}_{ij}|^5}. \tag{1.6}$$

The new coupling constants are defined to be

$$g \equiv \frac{\mu_{eff}^2}{2a^3} \tag{1.7}$$

$$\begin{aligned} J &\equiv \frac{S_{eff}^2\mathcal{J}}{g} \\ &= 2a^3\mathcal{J}\left(\frac{S_{eff}^2}{\mu_{eff}^2}\right) \\ &\approx 2a^3\mathcal{J}\left(\frac{g_J-1}{g_J}\right)^2 \end{aligned} \tag{1.8}$$

$$\begin{aligned} \vec{h} &\equiv \frac{\mu_{eff}\vec{H}}{g} \\ &= \frac{2a^3\vec{H}}{\mu_{eff}} \end{aligned} \tag{1.9}$$

$$K \equiv \frac{\mu_{eff}^2 \lambda}{g}$$
$$= 2a^3\lambda, \tag{1.10}$$

where g_J is the Landé g factor [44]. In the remainder of the thesis, unless otherwise stated, all energies, J, h,and K will be measured in units such that $g \equiv \mu_{eff}^2/2a^3 \equiv 1$.

In this thesis the magnetic moments are treated classically. It is important to establish when this simplification is reasonable, since magnetism is an intrinsically quantum mechanical phenomenon. Unfortunately this is not always a trivial task[45]. Certainly the assumption is valid near a second order phase transition. The relevant length scale near such a transition is the correlation length, which diverges at the transition. No such divergence occurs near a first order transition, and hence all predictions made concerning such transitions must be made with the caveat that quantum effects have been ignored. This may be reasonable when comparing results to experiments on magnetic thin films in which the transitions take place near room temperature. It may not be reasonable in the rare earth superconductors in which the transitions occur near 1 K. The predictions for the ground states, which are based on classical calculations, must be considered to be, at best, a first approximation valid in some low temperature region. A complete calculation of the $T = 0K$ state of an experimental magnetic system must include a consideration of quantum effects.

1.4 Relevant theory

The experimental work discussed above is relevant to the results presented in all of the upcoming chapters, However the theoretical studies are best divided based on the spin dimensionality. This division is employed because the spin dimensionality is an important parameter in determining the critical behaviour and phase behaviour of a system. This does not imply that the results of one section will not be relevant to other sections. In fact the chapter concerned with the Heisenberg model is very much dependent on the results found for both the uniaxial and planar systems. Since in each chapter the important literature for that section is reviewed, the survey here will be in the form of a brief overview of what has been published and the methods employed, rather than a detailed analysis of the final results of these studies.

1.4.1 Uniaxial system

For uniaxial systems, where the magnetic moments are oriented perpendicular to the plane of the film, one of the fundamental questions is to establish the ground state when one has both a nearest neighbour exchange interaction and a long-range dipolar interaction. The dipolar interaction makes this a subtle calculation and there has been some contradiction between published results. The contradiction arises because ground state energies calculated within a continuum approximation by Garel and Doniach[46], Yafet and Gyorgy[34], and Kaplan and Gehring [35] disagree with those of Czech and Villain [47] who did not make use of a continuum limit but retain

the discrete nature of the underlying lattice. The continuum calculations by Garel and Doniach and the other groups all predicted a ground state consisting of striped domains. while the calculations of Czech and Villain predicted a ground state of square domains. As well, Taylor and Gyorffy [48], using a discrete approach, agreed with the results of the continuum calculations, and hence disagreed with Czech and Villain, although their calculation was valid in a different regime. This problem is discussed in some detail in Chapter 3.

At finite temperature an important question concerns the nature of the transition from a low temperature ordered phase to the high temperature, paramagnetic phase, both in zero applied field and non-zero applied field. The behaviour of the system in an applied field is important because of the technological implications for materials used for magnetic storage. The relevant theory in zero field has been developed by many of the same authors listed in the previous paragraph, using a number of different methods. Garel and Doniach [46] used a Ginzburg-Landau approach to study a film with a finite thickness at finite temperature including the possibility of an applied field. Gehring and Keskin [49] considered a model film using a mean field approach and looked at the temperature dependence of the domain size. Mean field approximations have been used in the limit of a discrete system by Czech and Villain [47] and by Taylor and Gyorffy[48] and in the continuum limit by Abanov *et al.* [50]. Lattice gas simulations have been used by Hurley and Singer[42, 51, 52]. A discussion of the finite temperature phase behaviour is presented in Chapter 4.

1.4.2 Planar system

The dipolar 2-D planar model is interesting, particularly in light of what is known about the classical 2-D planar model. In the classical 2-D planar model the magnetic moments interact via an isotropic, short-range exchange interaction. The classical 2-D planar model contains a zero energy spin wave mode (a gapless mode) which prevents long-range order at any finite temperature. However, the model does undergo a phase transition. At low temperature it is possible for bound pairs of vortices to exist and the two-point correlation function exhibits a power law decay. When the temperature reaches a critical point the vortex pairs unbind and the two-point correlation function decays exponentially. This type of phase transition is known as a Kosterlitz-Thouless transition [13, 53, 54].

The effect of the dipolar interaction on a system with a dominant, ferromagnetic exchange interaction was considered by Maleev [3]. Maleev showed that it was possible for the dipolar interaction to stabilise long-range order in a planar model as a direct result of the long-range nature of the dipolar interaction. Zimmerman *et al.* [55] considered a system of dipoles on the honeycomb lattice, using a mean field approach as well as Monte Carlo simulation, and developed a phase diagram for that model. They also noted the subtle nature of the spin wave spectrum due to an anisotropic interaction, such as the dipole-dipole interaction. This was expanded upon by Henley[56] who introduced the concept of thermally induced ordering, and Prakash and Henley, [57] who applied this concept to the low temperature behaviour

of an anisotropic model with a short-range interaction which was chosen to mimic the nearest neighbour part of the dipole-dipole interaction. Prakash and Henley were able to derive expressions for the free energy and magnetisation of their model within the context of a spin wave approximation.

Using a spin wave calculation as well as Monte Carlo simulation, and working on the triangular lattice, Bedanov [58] concluded that this model orders at low temperature. The results of his spin wave calculation agreed with his Monte Carlo results. The Monte Carlo results, however, were for very small systems. Numerical studies for larger square lattices have been done by Bajaj *et al.* [59]. In these studies, using spin dynamic stimulations, the spin wave spectra have been calculated for a dipolar model using the same nearest neighbour approximation as used by Prakash and Henley. The results of the present work concerning the planar dipolar model are presented in Chapter 5.

1.4.3 Heisenberg system

In the experiments discussed above, the systems studied are generally believed to have a dominant ferromagnetic exchange interaction, potentially a strong magnetic surface anisotropy, and a much weaker dipolar interaction. Almost all of the previous theoretical work on dipolar Heisenberg models has been on models in which the relative strengths of the interactions were chosen to be similar to those in experiments. Early work includes a spin wave calculation by Yafet, Kwo and Gyorgy[60] for a system

which orders with a magnetisation perpendicular to the plane of the film. Pescia and Pokrovsky[61] treated the same problem within the context of the Renormalisation Group and concluded that this system should have a reorientation transition for a range of ratios between the strength of the dipolar interaction and the strength of the magnetic surface anisotropy. Politi *et al.* [62] also studied the reorientation transition in a thin film. They used a Renormalisation Group proposed by Polyakov [63], which they generalised to study the reorientation transition in terms of both film thickness and temperature.

Spin wave results have also been published by a number of groups. Pich and Schwabl[64] considered the dipolar antiferromagnet with a dominant antiferromagnetic exchange, predicting that the dipolar interaction leads to a gap in the spin wave spectrum and hence the existence of an ordered ground state, with the assumption that the ground state is perpendicular to the plane of the film. Corruccini and White [65] considered a model with only the dipole-dipole interaction and, based on their linearised spin wave calculation, concluded that the model will not exhibit long-range order on the square lattice. Stamps and Hillebrands[66] and Bruno[67] have considered two-dimensional ferromagnetic systems with dipolar interactions within the spin wave approximation.

The problem of a ferromagnetic system with a small dipolar interaction has also been approached using mean field techniques by both Moschel and Usadel[68, 69, 70] and Hu and Kawazoe[71]. As well, Monte Carlo simulations have been done by

Chui[72] and Hucht *et al.* [73, 74]. Both the mean field studies and the Monte Carlo studies considered both the effect of temperature and film thickness as they related to the reorientation transition. Abanov *et al.*[50], in a detailed study of a model thin film, have made a number of predictions concerning the phase behaviour, both in zero and non-zero applied field, which are relevant for all chapters in this thesis. They have also made a number of predictions concerning the phase diagram for their model using a mean field approach.

These studies all provide information concerning the phase behaviour of the model system in a small region of phase space where the ferromagnetic exchange interaction and a magnetic surface anisotropy dominate over a much smaller dipole-dipole interaction. In Chapter 6 an alternative region of phase space is probed. This region is characterised by the absence of an exchange interaction ($J = 0$). The phase behaviour is explored as a function of the strength of the magnetic surface anisotropy relative to the strength of the dipolar interaction.

Chapter 2

Methods

While there is a substantial body of literature concerned with the computational aspects of magnetic systems with short range interactions, [75, 76] it is only recently that much attention has been given to the effects of long-range interactions and how to effectively treat these interactions within a Monte Carlo simulation [58, 72, 73]. This chapter is intended as a review of the basics of Monte Carlo simulation methods and some of the theory behind the technique. The chapter also contains a discussion of how the long-range nature of the dipolar interaction makes the simulations much more difficult than when only local interactions are included. The final section is a discussion of the techniques used on the various computer architectures to minimise the problems associated with the long-range interaction

2.1 Monte Carlo simulation

Evaluation of the thermodynamic properties of a magnetic system involves the calculation of the expectation values of various local operators with respect to the Boltzmann probability distribution. Specifically, it involves calculating integrals of the form

$$\langle A \rangle = \frac{\int d\{x\} A(\{x\}) \exp(-\beta E(\{x\}))}{\int d\{x\} \exp(-\beta E(\{x\}))}, \tag{2.1}$$

where $\{x\}$ denotes a set of variables that serve to uniquely specify the configuration of the system of interest. $A(\{x\})$ and $E(\{x\})$ denote the value of a local operator and the energy of the system in configuration $\{x\}$, respectively, and β denotes the inverse temperature ($\beta = 1/k_B T$). Note that if one or many of the x's in $\{x\}$ is discrete, then the integrals associated with those variables become the appropriate summations. While it is not always possible to analytically evaluate averages such as those expressed by equation 2.1, for many systems of interest it is often possible to evaluate them numerically for finite systems by means of Monte Carlo simulation. It is then possible to extrapolate the results for these finite systems to systems of infinite size, by means of finite size scaling techniques [77, 78]. The reliability of the procedure is, however, critically dependent on the size of the systems which can be usefully studied and the precision of the results obtained. These factors are determined by the complexity of the model under investigation, the efficiency of the algorithm used and the speed and capacity of the computer on which the simulation is being performed. Hence computational considerations are crucial to the successful

application of Monte Carlo simulation to problems of physical interest.

The Monte Carlo simulation is, in simplest terms, a method of integration. In the Monte Carlo method, a subset of all possible states of a system are used to approximate the entire set. One way of choosing the states to include in the evaluation of the integral is to pick the states randomly, that is with probability $P(\{x\}) = 1/N$, where N is the total number of possible configurations. This method of Monte Carlo simulation is very inefficient at evaluating quantities such as $\langle A \rangle$ in equation 2.1. This is because the exponentials in the integrand of equation 2.1 can vary over several orders of magnitude, and hence there are large regions of phase space which do not contribute significantly to the integration. To improve the efficiency of the Monte Carlo simulation the concept of "importance sampling" is employed. Importance sampling means that from the total phase space of the system, only those regions which will contribute significantly to the integrations are sampled.

In this work, points are selected according to the probability $P_{\text{eq}}(\{x\})$, where

$$P_{\text{eq}}(\{x\}) \propto \exp(-\beta E(\{x\})) \,. \tag{2.2}$$

Selecting points according to this probability allows one to estimate the value of the expectation value $\langle A \rangle$ from M points quite simply as

$$\langle A \rangle \approx \frac{1}{M} \sum_{\nu=1}^{M} A(\{x\}_\nu) \,. \tag{2.3}$$

Obviously the more points used in the evaluation of $\langle A \rangle$ the more accurate the value obtained[79].

It has been shown that one may generate a set of states $\{x\}_\nu$ according to the probability $P_{\rm eq}(\{x\})$ by means of a trajectory $\{y\}_\tau$ through phase space [79]. This trajectory is generated by means of a Markov process defined in terms of a transition probability, which is denoted by $W(\{y\}_\tau \rightarrow \{y\}_{\tau+1})$, and is required to satisfy the condition of detailed balance, specifically

$$P_{\rm eq}(\{y\}_\tau)W(\{y\}_\tau \rightarrow \{y\}_{\tau+1}) = P_{\rm eq}(\{y\}_{\tau+1})W(\{y\}_{\tau+1} \rightarrow \{y\}_\tau)\ . \qquad (2.4)$$

The states $\{x\}_\nu$ used in the evaluation of the expectation value given by equation 2.3 are typically determined from the trajectory $\{y\}_\tau$ as

$$\{x\}_\nu = \{y\}_{\tau_0+n\nu}\ , \qquad (2.5)$$

where τ_0 denotes the number of Monte Carlo steps (MCs) required for the system to reach equilibrium and n is determined by the number of MCs it takes for correlations within a system (in equilibrium) to effectively decay to zero. In this way the evaluation of the weighted average over phase space, expressed by equation 2.1, is replaced by an average over a trajectory in phase space generated by the transition probability $W(\{y\}_\tau \rightarrow \{y\}_{\tau+1})$. The specific form of the transition probability $W(\{y\}_\tau \rightarrow \{y\}_{\tau+1})$ may be chosen in a variety of ways to satisfy equation 2.4 and many different choices have been studied. It should be noted however that the particular choice of $W(\{y\}_\tau \rightarrow \{y\}_{\tau+1})$ can have a dramatic effect on the values of τ_0 and n required to obtain good statistics and hence will have a crucial effect on the efficiency of the simulation and the accuracy of the results[75, 76, 79].

It is important to make one point concerning the definition of n in equation 2.5. n is the number of steps along a trajectory, in phase space, required to allow correlations to effectively decay to zero, and hence it is also the number of Monte Carlo steps between taking samples of the system when calculating thermodynamic averages. The best choice for n depends upon the correlations which are present in the system, since an uncorrelated set of configurations is required. It is difficult to make estimates of n *a priori*, since this requires knowledge of equilibrium relaxation times. It is possible to determine if an appropriate value has been chosen *a posteri*, by choosing a larger value of n and confirming that the thermodynamic averages are unaffected by the increase. This is part of the "art" of doing simulation physics.

The reason for expanding upon the definition of n is that it is very important when studying critical phenomenon. Close to a phase transition the correlation times increase dramatically, becoming divergent in an infinite system, an effect known as "critical slowing down". This presents particular problems for simulations on large systems close to criticality, as the value of n required to obtain reliable results will increase as a consequence of the increased correlation times. The value of n needed is also dependent greatly on the dynamics that is used in the Monte Carlo simulation. There have been a number of algorithms developed to minimise these problems in systems with short-range interactions [80]. This is in fact still a very active research area. Unfortunately it is not clear if these acceleration algorithms are applicable to systems with long-range interactions. As a consequence, near a phase transition one

is forced to use a large value of n, greatly increasing the time required for a simulation of a system with long-range interactions.

A detailed discussion of Monte Carlo simulation methods can be found in many books. In particular the two volumes edited by K. Binder in the Topics in Current Physics series[79, 81] are very useful.

2.1.1 General Algorithm

For magnetic systems the degrees of freedom are those associated with the orientation of magnetic dipoles in a lattice. The quantities to be calculated include the average internal energy, the specific heat, appropriate order parameters and their associated magnetic susceptibility. Either the Metropolis algorithm[82] or the heat bath algorithm[76] is used in all of the simulations presented in this thesis. In the Metropolis algorithm the transition probability is given by

$$W(\{x\}_\tau \rightarrow \{x\}_{\tau+1}) = \begin{cases} 1 & \text{if } \Delta E < 0 \\ \exp(-\beta \Delta E) & \text{if } \Delta E > 0 \end{cases}, \tag{2.6}$$

where ΔE is the difference in energy between the state $\{x\}_\tau$ and the state $\{x\}_{\tau+1}$. In the heat bath algorithm the transition probability is given by

$$W(\{x\}_\tau \rightarrow \{x\}_{\tau+1}) = \frac{1}{(1 + \exp(\Delta E / k_B T))}. \tag{2.7}$$

A simulation then consists of generating a trajectory in phase space starting with some initial spin configuration by means of the following steps:

1. Generate a new configuration by randomly choosing a spin to update and rotating the spin to some new direction ($\vec{S}_i \rightarrow \vec{S}_i' = \vec{S}_i + \Delta\vec{S}_i$).

2. Calculate the difference in energy, ΔE, between the original configuration and the new one.

3. Generate a random number R between 0 and 1.

4. If $R < W(\vec{S}_i \rightarrow \vec{S}_i')$ then accept the new spin configuration.

5. If $R > W(\vec{S}_i \rightarrow \vec{S}_i')$ then retain the old spin configuration.

6. Return to step 1.

This procedure is repeated over and over again, with data taken every n steps.

2.2 Monte Carlo simulations with dipolar interactions

Much of the current interest in these models stems from the effects of the long-range character of the dipolar interaction. In earlier studies on three-dimensional dipolar systems [1] it was found that finite size effects can be best treated by assuming that the spin system is periodic. In the following arguments the system is assumed to be a square lattice with lattice constant a, and L^2 magnetic ions. The square lattice is used since the experimental systems being considered have this symmetry. However

the methods can be generalised to other lattices. By imposing this periodicity, the configuration of the system can be specified in terms of the L^2 spin variables contained within a single cell. The energy of a particular configuration can then be written in terms of this finite cell by "folding in" the interactions between the spins inside the cell and those outside, to leave an effective interaction between two spins within the basic unit cell. Figure 2.1 illustrates what is meant by "folding in". The part of the system inside the dark lines is the finite system, and the infinite system is comprised of infinitely many copies of this finite system. Thus knowing the state of each spin in

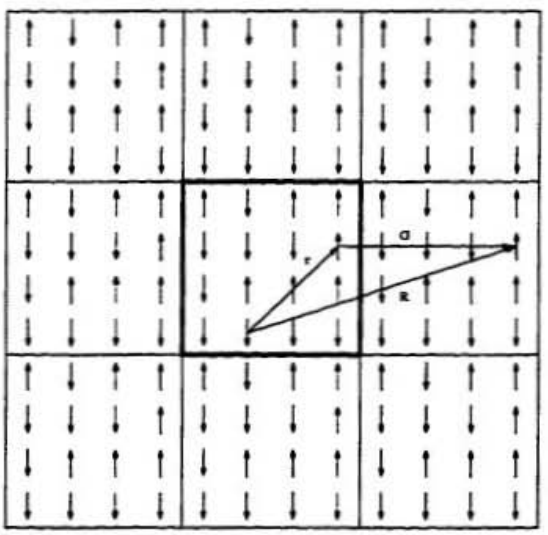

Figure 2.1: The infinite system is comprised of replicas of the finite cell. All interactions between spins outside the finite cell are included in an effective interaction between spins within the unit cell.

the finite system means that one knows the state of every spin in the infinite system. The Hamiltonian can then be rewritten such that the spins outside of the finite system can be replaced with the equivalent spins from inside the finite system. The cost of

this technique is a greatly increased complexity in the form of the interaction.

Mathematically, this means that the allowed spin configurations satisfy the requirement that

$$\vec{\sigma}(\vec{R}) = \vec{\sigma}(\vec{R} + \vec{G}), \tag{2.8}$$

where $\vec{G}$ is a lattice vector given by

$$\vec{G} = L(g_1\hat{x} + g_2\hat{y}), \tag{2.9}$$

with g_1 and $g_2 = 0, \pm 1, \pm 2 \ldots$. Note that distances have been scaled by the lattice spacing a. The square lattice is defined in terms of the unit vectors $\hat{x}$ and $\hat{y}$. This assumed periodicity presents no problems for treating the MSA or the applied field in a simulation. For the exchange interaction it is equivalent to the application of periodic boundary conditions. Because the dipolar interaction is a long-range interaction and the simulation uses a finite size system, incorporating the dipolar interaction into a simulation is more complicated than incorporating the exchange interaction. The dipolar part of the Hamiltonian, given in equation 1.5,

$$\mathcal{H}_{dd} = g \sum_{\vec{R}_n, \vec{R}_m}{}' \sigma^{\alpha}(\vec{R}_n)\Gamma^{\alpha\beta}(\vec{R}_{nm})\sigma^{\beta}(\vec{R}_m), \tag{2.10}$$

can be rewritten such that it only depends on the moments and lattice vectors in the finite system. This can be done by writing the vector $\vec{R}_{nm}$ in terms of a reduced vector $\vec{r}_{nm}$ where

$$\vec{R}_{nm} = \vec{r}_{nm} + \vec{G}, \tag{2.11}$$

and $\vec{G}$ is chosen such that $\vec{r}_{nm}$ lies within the finite system. Using the fact that the allowed spin configurations satisfy equation 2.8, the Hamiltonian then becomes

$$\mathcal{H}_{dd} = g\frac{N}{L^2}\sum_{\vec{r}_n,\vec{r}_m}^{L^2}{}'\sigma^\alpha(\vec{r}_n)\sum_{\vec{G}}\Gamma^{\alpha\beta}(\vec{r}_{nm}-\vec{G})\sigma^\beta(\vec{r}_m). \tag{2.12}$$

To remind the reader, N is the number of magnetic moments in the system ($N \to \infty$ in the thermodynamic limit), and L^2 is the number of moments in the finite cell. The notation used for the sums over $\vec{r}_n$ and $\vec{r}_m$ is intended to signify that these sums are over the lattice sites in the finite L^2 system. Substituting the expanded form for $\Gamma^{\alpha\beta}$ gives

$$\mathcal{H}_{dd} = \frac{Ng}{L^2}\left[C + \sum_{\vec{G}}\sum_{\vec{r}_n,\vec{r}_m}^{L^2}{}'\sigma^\alpha(\vec{r}_n)\sigma^\beta(\vec{r}_m)\lim_{\vec{r}\to 0}\frac{\partial}{\partial r_\alpha}\frac{\partial}{\partial r_\alpha}\frac{1}{|\vec{r}_{nm}+\vec{G}-\vec{r}|}\right], \tag{2.13}$$

where C denotes the interaction between spins at equivalent lattice sites and is therefore independent of the configuration of the system by virtue of the assumed periodicity. The prime on the sum indicates that the all terms with $\vec{r}_n = \vec{r}_m$ are excluded from the sum. The Hamiltonian can then be rewritten in terms of an effective interaction

$$\mathcal{H}_{dd} = \frac{gN}{L^2}\left[C + \frac{1}{2}\sum_{\vec{r}_n,\vec{r}_m}^{L^2}{}'\sigma^\alpha(\vec{r}_n)W^{\alpha\beta}(\vec{r}_{nm})\sigma^\beta(\vec{r}_m)\right], \tag{2.14}$$

with

$$W^{\alpha\beta}(\vec{r}_{nm}) \equiv \sum_{\vec{G}}\lim_{\vec{r}\to 0}\frac{\partial}{\partial r_\alpha}\frac{\partial}{\partial r_\alpha}\frac{1}{|\vec{r}_{nm}+\vec{G}-\vec{r}|}. \tag{2.15}$$

The numerical evaluation of the effective interaction is best accomplished by means of a generalisation of the Ewald summation technique. The details of this calculation have been published previously [2, 20].

With the Hamiltonian of the system given by equation 2.14, the change in energy due to the rotation of a magnetic moment can be calculated at an arbitrary site n. If the magnetic moment changes according to

$$\vec{\sigma}_n \rightarrow \vec{\sigma}_n + \Delta\vec{\sigma}, \tag{2.16}$$

then the change in energy can be expressed in terms of an effective field $\vec{H}_n$ defined at each lattice point as

$$\Delta E = \sum_{\alpha} \Delta\sigma_n^{\alpha} H_n^{\alpha}, \tag{2.17}$$

where the effective field is given by

$$H_n^{\alpha} = \sum_{m \neq n} \mathcal{W}^{\alpha\beta}(\vec{r}_{nm})\sigma_m^{\beta}. \tag{2.18}$$

2.3 Computational aspects

With the Hamiltonian of the system given by equation 2.14, the Monte Carlo algorithm described in the previous section proceeds as follows. From the initial spin configuration the effective field $\vec{H}_n$, defined by equation 2.18, can be calculated at each site on the lattice. The change in energy, given by equation 2.17, is then calculated for the rotation of a randomly chosen spin. If the new spin configuration is accepted then the effective field at each site is updated:

$$H_n^{\alpha} \rightarrow H_n^{\alpha} + \sum_{\beta,m} \mathcal{W}^{\alpha\beta}(\vec{r}_{nm})\Delta\sigma_m^{\beta}\ . \tag{2.19}$$

This operation is much more time consuming for a long-range interaction than for a similar simulation with a short range interaction. This is because rotating a spin at one site induces a change in the effective field at all other sites on the lattice. Thus each spin change requires the updating of the L^2 effective field matrix, and since one must update each spin in the system, which means L^2 spins, the time for one MCs/site scales like L^4 in two-dimensions and L^6 in 3-dimensions. The amount of computation required is also strongly correlated to the acceptance rate, since the decision to flip or not requires very little computation time relative to the updating of the effective fields. At low temperature very few spin changes are accepted, but near a second order phase transition the acceptance rate increases considerably. Combined with the phenomenon of critical slowing down, mentioned earlier, this means that in the vicinity of the critical point, one requires much longer simulations, in terms of MCs/site, in order to obtain good statistics[81, 79].

A further concern is that the effective interaction $W^{\alpha\beta}(\vec{r}_{nm})$, defined by equation 2.15, is not a simple function. It must be pre-computed and stored as an array. It is not generally feasible to store the full L^4 array (one L^2 array for each pair of α and β) of floating point numbers, since the goal is to have L as large as possible. (This restriction is starting to be removed as computers with 64 bit address mapping are now becoming available and the amount of memory which can be addressed has increased significantly.) Fortunately there is a large amount of symmetry in the system and it is only necessary to store a single L^2 array. The cost of using this symmetry is

that now a mapping from the L^4 array to the L^2 array must be used. Doing this mapping efficiently is currently the limiting factor on the efficiency of the code, and considerable time and effort have been spent in trying to make this section of code as efficient as possible. To accomplish this a $(2 \times L) \times (2 \times L)$ array is used, where $\mathcal{W}^{\alpha\beta}(\vec{r}_0 - \vec{r}_m)$ is repeated in each of the 4 $L \times L$ sections of the large array. Because of the periodicity assumed in equation 2.8, finding the correct interaction between the spin that has rotated and all other spins can be accomplished by assuming the rotated spin is at the origin of the system. By storing the larger array, stepping through memory is now done partially in unit strides and partially in strides of $2L$, which is a more efficient method of accessing memory then accessing array elements in a random order.

The code used to perform the update of the effective field is given below. The variables Wxx, Wyy, Wxy, and Wzz are the interaction matrices for $(\alpha\beta)$ equal to xx, yy, xy (and yx) and zz, respectively. Wxz and Wyz are zero in a two-dimensional system, and Wxy = Wyx. Hx, Hy, and Hz are arrays which store the effective field in the x, y, and z directions. Note that the two-dimensional arrays have been stored as one-dimensional arrays, because this allows a more efficient access to the arrays. The variables rowspin and colspin refer to the row and column of the spin which has rotated and deltax, deltay and deltaz are the changes in the x, y and z components of the rotated spin. This update loop is one of the benchmarks used in evaluating the efficiency of the code on the different machines used to do the simulations.

```
c---- UpdateFields spin at ( rowspin, colspin) has changed------
           DO 92 j = 0, L-1
              Fn = 2*L*(L+j-rowspin)-colspin+1+L
              jl = L*j + 1
              DO 93 k = 0, L-1
                 Hx(k+jl)=Hx(k+jl)+deltax*Wxx(Fn+k)+deltay*Wxy(Fn+k)
                 Hy(k+jl)=Hy(k+jl)+deltay*Wyy(Fn+k)+deltax*Wxy(Fn+k)
                 Hz(k+jl)=Hz(k+jl)+deltaz*Wzz(Fn+k)
93            CONTINUE
92         CONTINUE
```

2.4 Benchmarks

Benchmarking the Monte Carlo code is important for a number of reasons. The most obvious is that it gives an indication of how efficiently one is making use of the available computational resources. It also allows one to gauge if changes to a code have improved the performance and how significant that improvement is (or perhaps even how much a change in the code has degraded the performance). Monte Carlo simulations with long-range interactions require very high-performance computational resources, which are expensive, and should not be wasted or used inefficiently. The simulations which constitute a large portion of the new results in this thesis would not have been feasible using the computational resources available only five years ago.

The simulations presented in this thesis were run on a number of different computers, using resources provided by many sources. At Memorial University of Newfoundland the code was run on a Silicon Graphics R4000 Crimson, a DEC 2100/A500MP, a DEC 300/M600, and a DEC AXP 3400. Through a scholarship provided by The

High Performance Computing Centre in Calgary, Alberta, access was granted to their Fujitsu VPX240, which is a vector supercomputer with a peak rate of 2.5 gigaflops. (2.5×10^9 floating point operations per second). Access to a 64 node Connection Machine 5 (CM5), was obtained from the HLRZ Research Centre in Julich, Germany. The CM5 is a massively parallel machine. The Pittsburgh Supercomputing Center and Digital Equipment Corporation graciously provided time on an 4 processor DEC 8400/300.

In benchmarking the performance of the code used for the simulations, two important measures were used. The first is a floating point operations per second (flop/s) rating for the basic kernel which updates the effective field matrix and is shown above. The second is a measure of the time per Monte Carlo step per site. This second benchmark is the CPU time required to pick a new state, decide whether to accept the new state, and to update the system assuming the change was accepted. The time/MCs/site is calculated using a 40×40 system. For the two supercomputers used in this work, particularly the Connection Machine 5 (CM5), their performance relative to the workstations would be better if larger systems were used, although the amount of memory then becomes a concern. On the DEC Alpha 8400 5/300, benchmarks were gathered for a Fortran77 and a Fortran90 code. The DEC Alpha 8400 5/300 is a shared memory multiprocessor, and the Fortran90 code was developed to take advantage of the parallel nature of the machine. Therefore benchmarks are given for the Fortran90 code using both 1 processor and using 4 processors. The Mflop/s

rating allows the comparison of the efficiency of the code to that of other programs on the various machines and to the peak efficiency of the machine. The time per Monte Carlo step per spin is a less general benchmark since it is a comparison of the speed of the machines for this one problem, but it is the more informative to the physicist, since it is more closely related to the real time to complete a simulation.

In Table 1 both sets of benchmarks are shown for some of the machines which have been used to test the code. It should be noted that the programming experience of the author in a high-performance environment is somewhat limited and some of the benchmark numbers reflect this fact. In particular the numbers for the CM5 are very much influenced by the limited opportunity to interact with people with experience in this environment. Comparison of the Mflop/s ratings on the various machines to their peak Mflop/s ratings, shows that the code is using the hardware very efficiently. The numbers showing the time/MCs/site also reflect the type of problem treated. The main CPU intensive loop in the program is perfectly vectorisable and parallelisable, but the mapping from the L^4 array to the L^2 array makes the algorithm less than ideal for the distributed memory of the CM5. On the CM5 it is more efficient to store the entire L^4 interaction matrix. Thus the Mflop/s rating for the CM5 is very impressive, while the time per MCs/site is less so. This is because parts of the code must be done serially and the massively parallel nature of the CM5 is wasted, and because communication between the nodes is necessary with each spin rotation. The DEC 8400/300 is a very new machine which features 64 bit memory addressing and

shared memory with 4 processors (on the machine which was used for this study). The ability to address large amounts of memory allowed the use of the full L^4 arrays, and the shared memory architecture also reduced the time per step required for communication.

Machine	Benchmark #1 in Mflop/s	time/MCs/site in seconds	Peak rate in Mflop/s
SGI Crimson R4000	11.1	5.53×10^{-4}	50
IBM 320H	16.7	4.87×10^{-4}	50
DEC 3400/300 AXP	32.2	2.64×10^{-4}	133
DEC 2100 A500MP	55.0	2.24×10^{-4}	190
DEC 8400/300 (1 CPU,f90)	71.2	1.63×10^{-4}	600
DEC 8400/300 (1 CPU,f77)	129.3	5.87×10^{-5}	600
IBM 590 R6000	151.2	5.68×10^{-5}	256
DEC 8400/300 (4 CPU,f90)	250.8	3.06×10^{-5}	2400
Fujitsu VPX240/10	398.4	1.82×10^{-5}	2400
CM5 (64 proc)	510.0	1.11×10^{-4}	2560

Table 2.1: Benchmarks of the code using a 40×40 lattice. These benchmarks are provided only for interest. The timings were not all done under equivalent load conditions or in accordance with generally accepted procedures. The peak Mflop/s rate was obtained from various sources and should be viewed as an estimate. (The third column for the CM5 is not a misprint)

2.5 A typical simulation

In a simulation the choice of various parameters necessary for the simulation depend upon a number of factors. For example the choice of n, depends very much on how close the temperature of the simulation is to any phase transitions. Near the transition temperature, where one requires a larger number of initialisation steps,

$n = 20$ MCs/site is normally used, while in a simulation away from the critical region n is typically 10 MCs/site. As a reminder, n is the number of steps along a trajectory required to allow correlations to effectively decay to zero, and hence it is also the number of Monte Carlo steps between taking samples of the system when calculating thermodynamic averages. A typical simulation consists of 10000 to 100000 initialisation steps per spin followed by from 10^6 to 10^8 more MCs/site for collecting data.

As was stated earlier there is an art to simulations much as there is an art to doing experiments and, as in experiments, reproducibility of results is one of the best tests. The code used for the simulations has been modified many times during the period of this study. These modifications have always been coupled with attempts to improve the efficiency of the code and to better take advantage of the available hardware. In these efforts the code was rewritten no less than four times, and each time the results were compared with our previous results and those published by others to confirm that the program was functioning properly. The effort allocated to redoing simulations and confirming old results has led to a set of code in which the author has a great deal of confidence.

Chapter 3

The uniaxial dipolar model: Ground states

3.1 Introduction

In this chapter the ground state properties for a two-dimensional spin system on a square lattice are examined. It is assumed that the crystalline electric fields are sufficiently large that the orientation of the magnet dipoles is constrained to lie perpendicular to the plane of the magnetic film. This corresponds to the case of $K \to \infty$ in the Hamiltonian of equation 1.5. In this case the components of the magnetic dipoles within the plane of the film will be zero. Thus $\sigma_x = \sigma_y = 0$ and the Hamiltonian reduces to

$$\mathcal{H} = \sum_{\vec{r}_n, \vec{r}_m}{}' \sigma^z(\vec{r}_n)\Gamma^{zz}(\vec{r}_n - \vec{r}_m)\sigma^z(\vec{r}_m) - \frac{J}{2} \sum_{<\vec{r}_n, \vec{r}_m>} \sigma^z(\vec{r}_n)\sigma^z(\vec{r}_n), \qquad (3.1)$$

where $\sigma_z = \pm 1$. In the absence of the dipolar interaction, the above Hamiltonian reduces to the well known Ising model [83], which can be solved exactly in two-dimensions [84] and which has been the subject of considerable theoretical study. For $J > 0$ and in the absence of the dipolar interaction, the ground state is the ferromagnetic state, while for $J < 0$ the ground state is the pure antiferromagnetic state, where each spin is anti-aligned with its four nearest neighbours. For the pure dipolar system ($J = 0$) the ground state is an antiferromagnetic state where the spins form ferromagnetic rows along one axis which are ordered antiferromagnetically along the second axis. The ground state for the uniaxial model, that includes both the exchange and the dipolar interactions, is somewhat more complex. Our preliminary Monte Carlo studies revealed that gradually increasing J from zero did not induce a transition from the antiferromagnetic ground state of the pure dipolar system to the ferromagnetic ground state of the ferromagnetic Ising system as one might expect [6]. Instead the Monte Carlo studies revealed a sequence of transitions with increasing J between states in which the magnetic dipoles formed stripes along one of the principal axes of the square lattice. A typical stripe configuration is shown in figure 3.1.

A review of the published literature at that time revealed that no one had reported seeing these phases in a Monte Carlo simulation, and considerable effort was expended in rigorously checking the code and in obtaining analytical and numerical results for the energy of various ground state configurations. While no Monte Carlo results were available, there were, however, some theoretical results which indicated that the

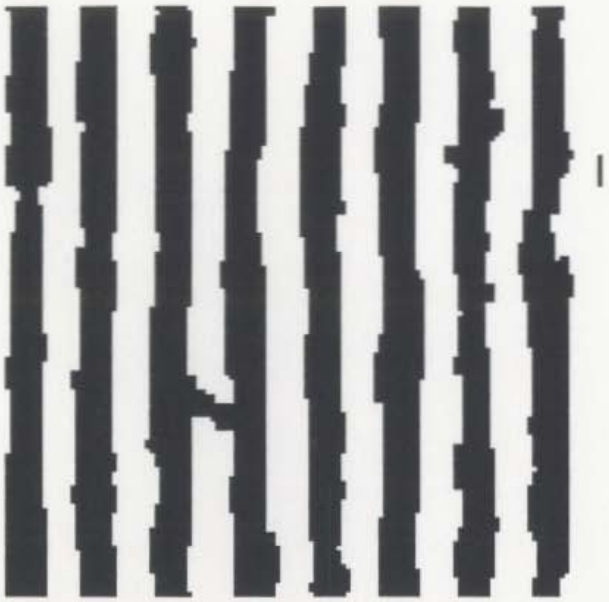

Figure 3.1: An example configuration showing the low temperature ordering in a stripe phase. ($L^2 = 128 \times 128$) and $J = 8.9$. Black indicates regions where the magnetic moment points in the $+\hat{z}$ direction and white shows magnetic moments in the $-\hat{z}$ direction.

ground states in this region should be the stripe phases. The earliest of these works was by Garel and Doniach [46]. Garel and Doniach showed, using a Ginzburg-Landau approach, that the stripe phases were stable with respect to the ferromagnetic phase. Their calculation treated the case of a slab of finite thickness at low temperatures in an applied field. They developed a mean field phase diagram for the system. Published later, the work of Yafet and Gyorgy[34] used a mean field approach to study domain formation in mono-layers and their results agreed qualitatively with the results of Garel and Doniach. Yafet and Gyorgy explicitly treated the case of a mono-layer, while Garel and Doniach had considered a film of small, but finite thickness. Yafet and Gyorgy assumed a finite anisotropy and worked within a continuum approximation, as

had Garel and Doniach. The Monte Carlo results of the present study were done using a discrete system and assumed an infinite anisotropy. As cited by Yafet and Gyorgy as a private communication and later published, Czech and Villain [47] reported that when the discrete nature of the lattice was retained, the stripe phases were no longer the ground state. Instead Czech and Villain predicted that the ground states would be a sequence of checkerboard phases, where blocks of ferromagnetically ordered moments would be arranged antiferromagnetically, much like the arrangement of black and red squares on a checkerboard. The difference in the two results was not surprising considering the subtle nature of the dipolar interaction.

The Monte Carlo results of the present study were therefore somewhat unsettling since they agreed with the theoretical predictions based on continuum models, but disagreed with the results which claimed to retain the discrete nature of the lattice. Obviously the resolution of the apparent discrepancy was very important in order to properly understand the results obtained. It was, therefore, necessary to explore more closely the ground state energies for the dipolar systems in the limits which are appropriate for the Monte Carlo simulations.

3.2 Ground state energies

Figure 3.2 summarises the low temperature results obtained from our early Monte Carlo simulations [20]. The phases shown in the figure are named using 2 letters and an optional number. The first letter refers to the ordering along the $\hat{x}$ direction and

the second letter to the ordering along the $\hat{y}$ direction. An F indicates ferromagnetic ordering and an A indicates antiferromagnetic ordering. The optional number gives the width of the ferromagnetically ordered stripe in the case where there is a stripe phase. For example, AF8 refers to a stripe phase in which there are ferromagnetic stripes of width 8 magnetic moments along the $\hat{y}$ direction, which are ordered antiferromagnetically along the $\hat{x}$ direction. The results shown in Figure 3.2 indicate that as J increases, so does the width of the stripes in the ground state. The system size used to determine the phase diagram shown in figure 3.2 was only 16×16. Only a few different stripe phases are indicated, as the periodicity of the stripes must be commensurate with the system size and obviously if the stripe width is greater than or equal to 16 then the system would look ferromagnetic. This is always a concern in Monte Carlo simulations with spatially modulated phases, where the boundary conditions impose a periodicity on the system. If this imposed periodicity is not commensurate with the natural period of the system, then one is not seeing the true behaviour of the infinite system. These studies on small systems suggested not only the need for simulations on larger systems, but also the need to be able to determine the proper ground state for a given value of J.

In order to predict the correct ground state, an expression for the energy of both stripe phases and checkerboard must be derived. For a stripe phase of width h, the exchange interaction contribution to the energy is given by

$$E_{ex} = -2J\left(1 - \frac{1}{h}\right), \tag{3.2}$$

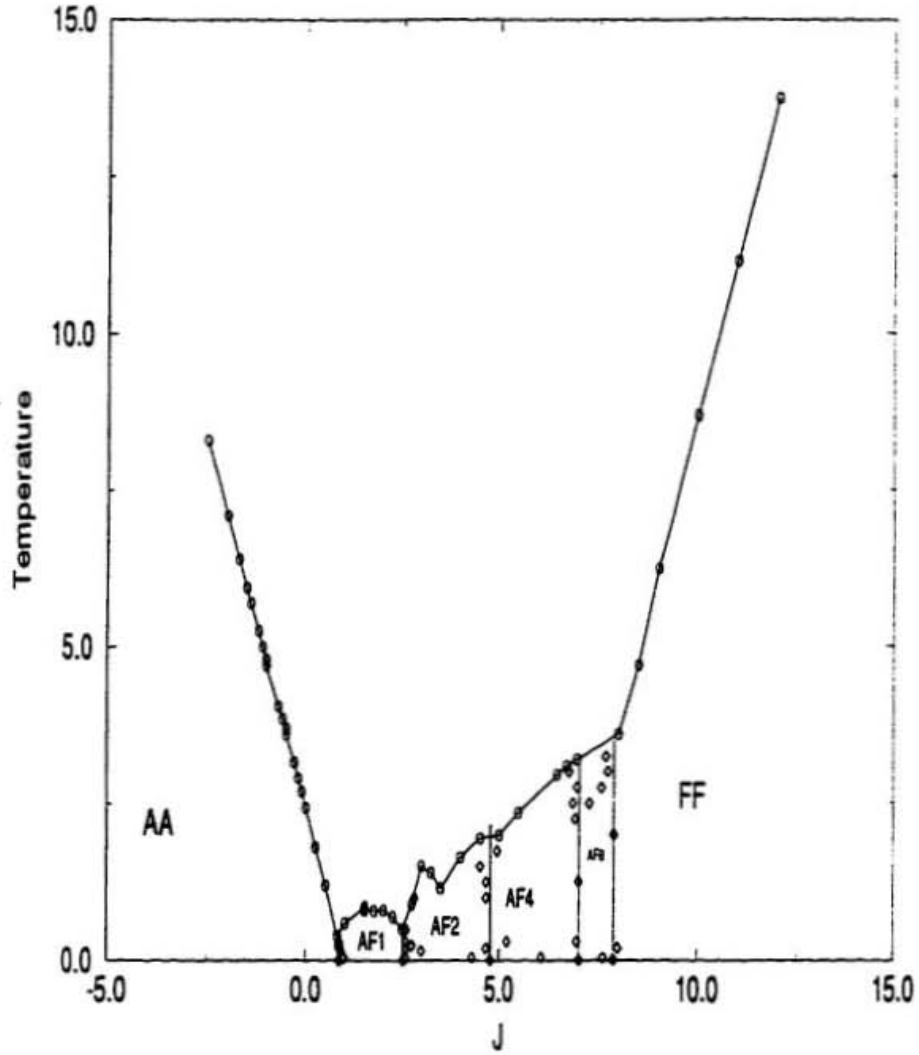

Figure 3.2: The phase diagram found using Monte Carlo simulations with a $L^2 = 16 \times 16$ system. Of interest in this figure is the low temperature region, which shows that the ground state for some values of J are stripe phases. These phases are the AF1, AF2, AF4, and AF8 phases, where the number refers to the width of the stripes. The vertical lines are estimates of the phase boundaries between the stripe phases based on energy calculations, as discussed in the text. Temperature is in units of g/k_B.

while for a checkerboard phase of size h by h the exchange contribution is

$$E_{ex} = -2J\left(1 - \frac{2}{h}\right). \tag{3.3}$$

The use of h to describe the characteristic domain size in the stripe and checkerboard phases should not be confused with the applied field h, the context in which h is used should lead to no confusion. The expressions for the dipolar contribution to the energy are not quite as compact. For a stripe phase

$$\begin{aligned} E_{dd} &= \frac{4}{\sqrt{\pi}}\left(\sum_{\vec{G}\neq 0}(-1)^{g_1}\frac{F_1(\eta|\vec{G}|)}{|\vec{G}|^3} + \frac{1}{h}\sum_{\vec{G}}\sum_{m=1}^{h}{\sum_{n=1}^{h}}'(-1)^{g_1}\frac{F_1(\eta|\vec{r}_{mn}+\vec{G}|)}{|\vec{r}_{mn}+\vec{G}|^3}\right), \\ &+ \frac{4\sqrt{\pi}}{h}\sum_{\vec{Q}}\frac{|\vec{Q}|}{2}F_2(\frac{|\vec{Q}|}{2\eta})\left(1+\frac{1}{h}\sum_{m=1}^{h}{\sum_{n=1}^{h}}'e^{i\vec{Q}\cdot\vec{r}_{mn}}\right) - \frac{4\eta^3}{3\sqrt{\pi}}, \end{aligned} \tag{3.4}$$

and for a checkerboard phase,

$$\begin{aligned} E_{dd} &= \frac{4}{\sqrt{\pi}}\left(\sum_{\vec{G}\neq 0}(-1)^{g_1+g_2}\frac{F_1(\eta|\vec{G}|)}{|\vec{G}|^3} + \frac{1}{h^2}\sum_{\vec{G}}\sum_{m=1}^{h^2}{\sum_{n=1}^{h^2}}'(-1)^{g_1+g_2}\frac{F_1(\eta|\vec{r}_{mn}+\vec{G}|)}{|\vec{r}_{mn}+\vec{G}|^3}\right) \\ &+ \frac{4\sqrt{\pi}}{h^2}\sum_{\vec{Q}}\frac{|\vec{Q}|}{2}F_2(\frac{|\vec{Q}|}{2\eta})\left(1+\frac{1}{h^2}\sum_{m=1}^{h^2}{\sum_{n=1}^{h^2}}'e^{i\vec{Q}\cdot\vec{r}_{mn}}\right) - \frac{4\eta^3}{3\sqrt{\pi}}. \end{aligned} \tag{3.5}$$

F_1 is defined as

$$F_1(x) = \frac{1}{2}xe^{-x^2} + \frac{\sqrt{\pi}}{4}\mathrm{erfc}(x), \tag{3.6}$$

and F_2 is defined as

$$F_2(x) = \frac{e^{-x^2}}{x} - \sqrt{\pi}\mathrm{erfc}(x). \tag{3.7}$$

The definitions of η, $\vec{G}$, and $\vec{Q}$ are all given in Appendix A, in which the exact details of the calculation are presented. Only the final results are presented here along with a discussion of the analysis. These expressions are exact, and can be evaluated

numerically for any value of h, although one is still limited by the computation time required when h is large. This is in contrast to the calculations of Czech and Villain, Garel and Doniach, and Yafet and Gyorgy, which are intended to be approximations valid in the limit of large h. The expressions for the energy of the stripe and checkerboard phases are quite complex. This is a direct result of the long-range nature of the dipole-dipole interaction and the slow convergence of the sums in equation 3.1. The sums in equation 3.4 and 3.5 converge quickly, with seven figure accuracy generally obtained by taking only terms with $|G| \leq 5$. The energies given by equations 3.4 and 3.5 for small values of h have been compared to those given by the Monte Carlo calculation as an extra check of the Monte Carlo program.

In figure 3.3 the energy of the stripe phases with $h = 1, 2, 3, 4,$ and 5 along with the energy of the ferromagnetic and antiferromagnetic phases are plotted as functions of J. For $J < 0.85$ the ground state is the pure antiferromagnetic state preferred by the dipolar interaction. At $J = 0.85$ the ground state changes to a stripe phase with $h = 1$. As J increases the ground state changes to stripe phases with larger and larger strip width. The checkerboard phases are never the lowest energy phase for the values of J shown, and therefore are not shown in figure 3.3. Although it is difficult to discern from figure 3.3, as J increases, the differences in energy between successive stripe phases get smaller at any given temperature. Also the region of stability for the lowest energy stripe phase gets narrower as the stripe width grows. It is evident in figure 3.3 that as h increases the energy of that stripe phase becomes closer to that

of the ferromagnetic phase. It is not clear if the stripe phases will continue to be of lower energy than the ferromagnetic phase or the checkerboard phases at larger values of J. However, the range of stripe widths shown in figure 3.3 is the relevant range for comparison to the Monte Carlo results. In figure 3.2 the $T = 0$ phase boundaries predicted by the above energy calculations are shown as solid vertical lines. They are in good agreement with the Monte Carlo results. While this partially validated the results of the Monte Carlo simulation, which indicated that the system orders in a stripe phase at low temperature rather than a checkerboard phase, it did not resolve the apparent discrepancy between the ground state predictions of continuum and discrete calculations.

3.2.1 In the limit of large stripe width

Figure 3.3 includes only phases up to $h = 5$, and while the results suggest the stripe phases will continue to be the lowest energy phase for larger values of J, the results are not conclusive. Thus an asymptotic form of the energy for the various phases as a function of J is required. This calculation has been done by Whitehead and De'Bell[85] and leads to a dipolar contribution to the energy for both the stripe phases and the checkerboard phases of

$$\lim_{h\to\infty} E_{dip}(h) = E^0_{dip} - \frac{1}{h}\left(A + B\ln(h)\right) + \mathcal{O}\left(\frac{1}{h^2}\right), \tag{3.8}$$

with E^0_{dip} equal to the dipolar contribution to the ferromagnetic state. A and B are positive constants, which differ for the stripe phases and for the checkerboard phases.

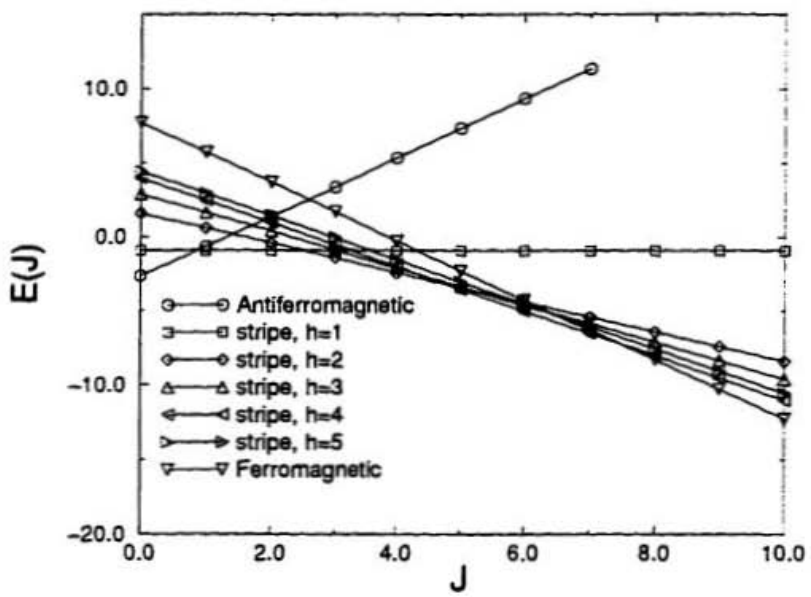

Figure 3.3: The energy of the stripe phases with $h = 1$, 2, 3, 4, and 5, as well as the ferromagnetic and antiferromagnetic phases as functions of J. Temperature is in units of g/k_B.

The calculations of A and B are quite difficult. The B's have been calculated exactly for both the checkerboard and stripe phases [35, 85]. For the stripe phases $B = 8$. while for the checkerboard phases $B = 16$. The difficulties associated with the long-range dipolar interaction manifest themselves in the calculation of the A's. To calculate the A's, the energies of the various phases were fit to the functional form given in equation 3.8 using the larger values of $h(h > 50)$. Fortunately the higher order terms in equation 3.8 are very small and the functional form holds even for stripes as small as $h = 10$, and for checkerboards as small as $h = 20$. To show how well this functional form holds the results are plotted in figure 3.4. The slope in each case yields an estimate of B and the y-intercept gives an estimate for A. The agreement between the numerical data and the asymptotic form is excellent. The estimates for A from this analysis are $A = 9.105 \pm 0.005$ for the stripe phases and $A = 2.819 \pm 0.005$ for the checkerboard phases.

After combining equations 3.2 and 3.3 with equation 3.8 the total energy of a stripe or checkerboard phase as a function of J and h can be written as

$$\lim_{h\to\infty} E(h) = E_{dip}(h) + E_{ex}(h, J). \tag{3.9}$$

For stripes one has

$$\lim_{h\to\infty} E(h) = E_F - \frac{1}{h}\left(A - 2J + B\ln(h)\right) + \mathcal{O}\left(\frac{1}{h^2}\right), \tag{3.10}$$

and for the checkerboard phases one has

$$\lim_{h\to\infty} E(h) = E_F - \frac{1}{h}\left(A - 4J + B\ln(h)\right) + \mathcal{O}\left(\frac{1}{h^2}\right). \tag{3.11}$$

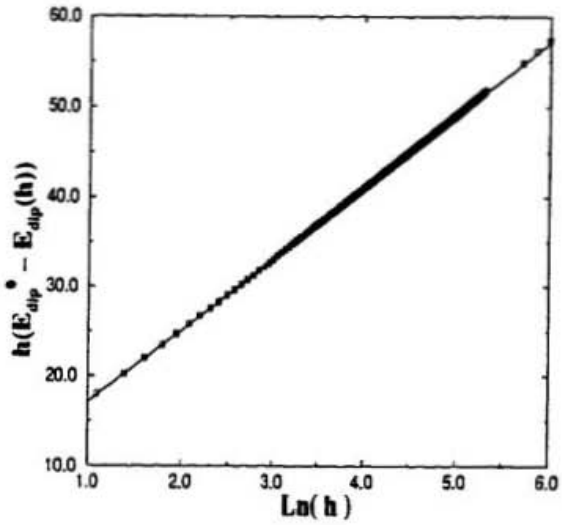

(a)

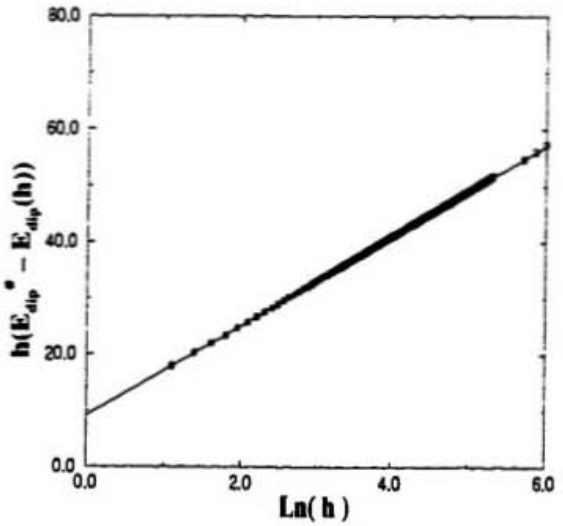

(b)

Figure 3.4: A plot of $\left\{h\left[E^0_{dip} - E_{dip}(h)\right]\right\}$ as a function of $\ln(h)$ for the stripe (a) and checkerboard phases (b) [6].

where $E_F = E^0_{dip} - 2J$ is the combined energy of the ferromagnetic phase. The minima of the energies in equations 3.10 and 3.11 define a lowest energy domain size for each class of phases, which is denoted by h^*. It is straightforward to derive that for both stripe and checkerboard phases

$$h^* = h_0 \exp\left(\frac{J}{4}\right), \tag{3.12}$$

with $h_0 \equiv \exp(1 - A/B)$ (the exact values of B have been substituted into the exponential to obtain the $J/4$ dependence). Substituting back into equations 3.10 and 3.11 leads to an expression for $E(h^*)$, which is the energy of the lowest energy state in each class. The resulting equation for both stripe and checkerboards is

$$\begin{aligned} E(h^*) &= E_F - \frac{B}{h^*} + \mathcal{O}\left(\frac{1}{h^{*2}}\right), & (3.13) \\ &= E_F - \frac{B}{h_0}\exp(-J/4) + \mathcal{O}\left(\frac{1}{h^{*2}}\right). & (3.14) \end{aligned}$$

Thus both the stripes and checkerboards would destabilise the ferromagnetic state, as B and h_0 are positive by definition. Which of the two phases is the ground state is determined by the value of B/h_0. For the stripes $B/h_0 \approx 9.2 \pm 0.05$ and for the checkerboard $B/h_0 \approx 7.0 \pm 0.05$. Thus the stripe phases constitute the ground state in a discrete system.

Kaplan and Gehring [35] arrived at a similar conclusion regarding the stability of the stripe phase over the checkerboard phase. They also correctly identified the approximation in the analysis of Czech and Villain[47] that leads to their conclusion regarding the stability of the checkerboard phase. However a detailed comparison of

the analysis of Kaplan and Gehring with the present results reveals that the continuum approximation leads to a slightly different value of the coefficient A (defined as $4\pi b$ and $4\pi b'$ for the stripe phase and the checkerboard phase respectively in [35]) for both the stripe and the checkerboard phases. This arises as a consequence of the fact that corrections to the $\ln(h)$ term in the asymptotic expansion of the dipolar energy are very sensitive to the nature of the approximations used in the analysis. While such corrections are relatively small, they are nevertheless significant in calculating the difference between the minimum energy of the stripe and checkerboard phase for a given value of J. This serves to emphasise the subtle nature of the dipolar interaction and the care that has to be taken in treating a long-range interaction. This point is also emphasised in the work of Hurley and Singer [51].

As stated above, the results of Czech and Villain highlight the subtle nature of calculations involving the dipolar interaction and it is worthwhile to look more closely at their analysis. In their analysis they make one improper assumption, which leads to their conclusion that the checkerboard phases are the ground state. They arrive at a result similar to equation 3.8 for the dipolar contributions to the energy (their equation (12)) for both the stripes and checks. In this result there is a term which varies as A/h where A is of order unity. In the expression for the contribution to the energy due to the exchange interaction, there is a term which varies as J/h. Their improper assumption was that for $J >> 1$, they assumed that they could ignore the term which varies as A/h, since it will be dominated by the term which varies as J/h

from the exchange contribution. This is equivalent to setting $A = 0$, and in fact for large values of J, the term they ignore does not contribute significantly to the energy of either the stripes or the checkerboard phases as both asymptotically approach the same value of the energy. The problem arises because this term does contribute significantly to the determination of h^*. By taking $A = 0$, Czech and Villain have let $h^* = \exp\left(1 + \frac{J}{4}\right)$ for both stripes and checks and the determination of the ground state is dependent only on the B's. One can see quite clearly how the conclusions drawn from any analysis will be strongly dependent on any approximations used to estimate A. Kaplan and Gehring[35] also pointed out the flaw in the argument of Czech and Villan.

In figure 3.5, the energies of the lowest energy stripe phase, the lowest energy checkerboard phase and the ferromagnetic phase are all plotted as functions of J. As well, the corresponding set of points found for small J, from the exact calculation of the energies for small stripes and checkerboards are plotted; each point indicates where the domain size of the lowest energy stripe or checkered state changes from h to $h+1$.

While the work discussed above was in still progress, two related papers were published[42, 48]. The first, by Taylor and Gyorffy [48], dealt with a mono-layer coupled via dipolar, exchange, and spin-orbit interactions. They calculated the ground state energies and predicted the existence of stripe phases in the limit of small J, while maintaining the discrete nature of the magnetic moments. They were, however,

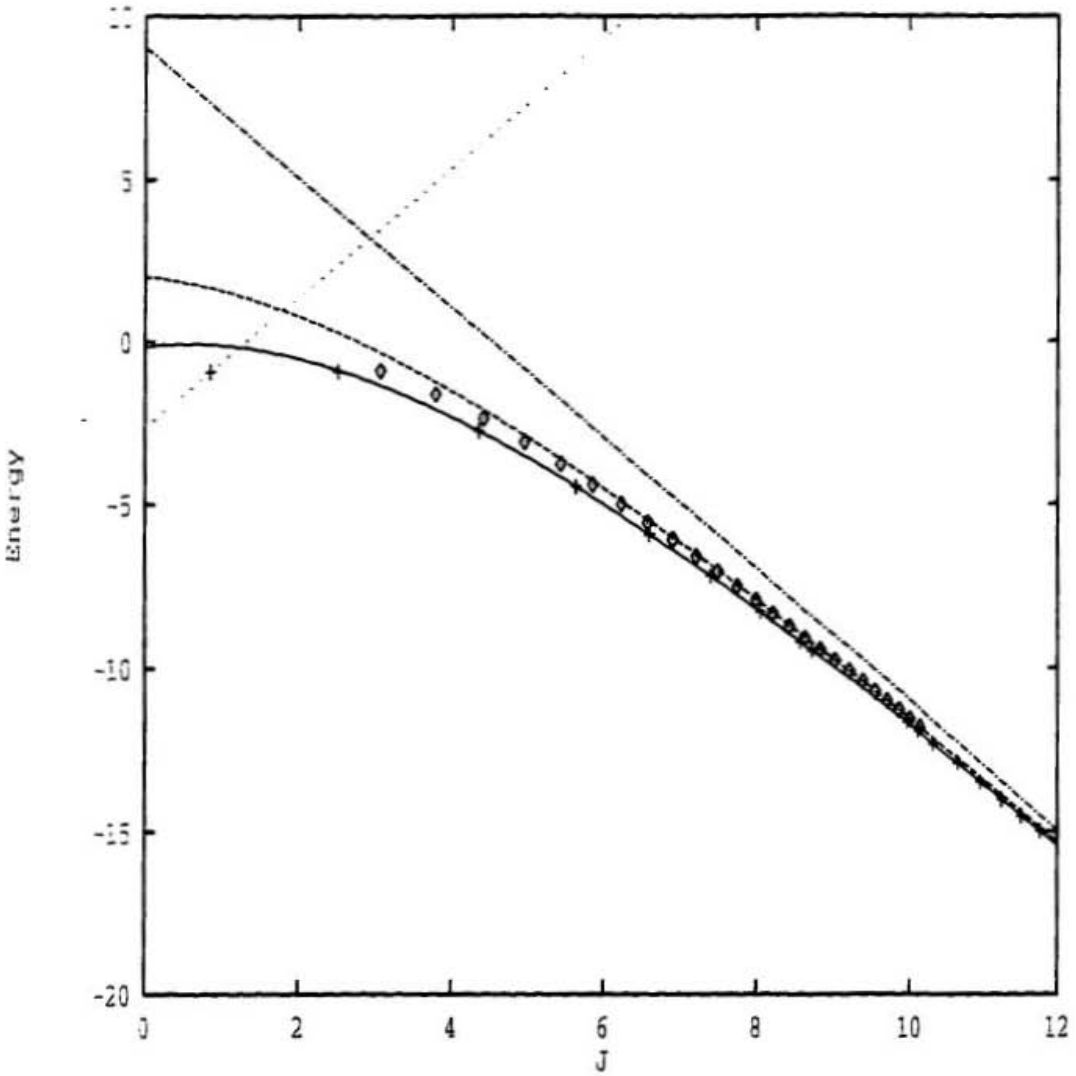

Figure 3.5: Comparison of the energies of the stripe and checkerboard phases. The solid line shows the energy calculated from the asymptotic expression for the stripe phase with the coefficients given in the text. The dashed line shows the corresponding energies for the checkerboard phase. Crosses represent the points at which the width of the stripes changes from h to h + 1. Diamonds are the corresponding points for the checkerboard phases. For reference, the dot-dashed line and the dotted line show the energies of the ferromagnetic and antiferromagnetic phases, respectively.

unable to determine the ground state in the limit of large J as done above, and left this as an open question. Also, they did not discuss the work of Czech and Villain concerning the checkerboard phases. Their predicted ground state energies matched the results found in the above analysis, within the precision quoted. Taylor and Gyorffy also noted that their initial attempts at Monte Carlo simulation had proved inconclusive, due to meta-stability effects. There was also a paper by Hurley and Singer [42] which predicted the existence of stripe phases and provided some Monte Carlo evidence of stripe phases. This work was done on a triangular lattice using a lattice gas model, hence it is not possible to make direct comparisons to their results. The work of Hurley and Singer is very similar to that of Yafet and Gyorgy.

3.3 Summary

The ground states for a uniaxial spin system on a square lattice were established as a function of the ratio of the short range exchange interaction and the long-range dipolar interaction. The ground states for $J > 0.85$ consist of a series of stripe phases, with the stripe width increasing with increasing J, rather than checkerboard phases as was predicted previously. Using the exact values for the energy of stripes with moderate widths as well as for checkerboard phases of moderate size, the energies of the two classes of phase were calculated analytically in the limit of large J. It was then established that the stripe phases are always the lower energy phase and will destabilise the ferromagnetic phase even in the limit of J going to infinity.

Chapter 4

The uniaxial dipolar model: Finite temperature

4.1 Introduction

In this chapter, the treatment of uniaxial systems is extended to finite temperature using Monte Carlo simulation. In the first half of the chapter, the moments are assumed to interact via the dipolar and exchange interactions as in the previous chapter. In the second half of the chapter the effect of an applied external field perpendicular to the film is examined.

The phase behaviour of a uniaxial dipolar model in zero field has been analysed by Czech and Villain [47], for a discrete lattice. Although, as was shown in the previous chapter, Czech and Villain assumed the wrong ground state, much of their argument

is still valid. Czech and Villain predict a depinning transition where the magnetic superlattice depins itself from the underlying square lattice. Thus the system forms a "floating solid" at all but the lowest temperatures. These predictions are based largely on a mean field analysis of the problem. Abanov *et al.* [50] have also treated the problem as part of a more general treatment of dipolar systems in the continuum limit. Abanov *et al.* use a phenomenological Hamiltonian. which they write in terms of a Fourier transform of the displacement of domain walls from an ordered configuration. The displacement of the nth domain wall is given by $u_n(\vec{r})$, and its Fourier transform is given by

$$u_n(\vec{p}) = \frac{1}{\Omega} \int d\vec{r} u_n(\vec{r}) \exp\left(-i\vec{p}\cdot\vec{r}\right). \tag{4.1}$$

When the Hamiltonian is expanded in terms of the wavenumber associated with the Fourier transform of the displacement of the domain walls, they obtain a term of the form $\kappa p_x^2 p_y^2$. The sign of κ determines the stability of the Ising nematic phase and hence also determines the predicted phase diagram. They find, to lowest order, $\kappa < 0$. but show that thermal fluctuations can lead to a positive κ by taking the one-loop correction to κ. Both predictions of Abanov *et al.* are shown in figure 4.1. The exact nature of the various phases will be discussed below, but it is important to note that Abanov *et al.* have not assumed a uniaxial system in their study.

The phase diagram of Abanov *et al.* shows the effects of temperature, an applied film perpendicular to the film (H_{perp}) and an applied field parallel to the film (H_{para}) on the phase behaviour of a dipolar system. In this thesis $H_{para} = 0$ as the effects

of a parallel applied field are not considered. Also Abanov *et al.* have considered a Heisenberg model, rather than a uniaxial model. Therefore their phase diagram includes a reorientation transition at T_R, which is not relevant to this chapter, but which will be considered in chapter 6. Abanov *et al.* have named the various phases based on an analogy to liquid crystal phases. This will be discussed later in the chapter, but the smectic phase in figure 4.1 refers to the stripe phases. The tetragonal phase is similar to the stripe phases, but lacks orientational order as will be discussed below. Abanov *et al.* also predict that an Ising-nematic phase may be stable. This phase will be defined below. The naming scheme used to identify the various phase transitions will be described below.

The addition of a field further complicates the problem. On the basis of a phenomenological Landau-Ginzburg model, Garel and Doniach[46] predict that for sufficiently large applied fields, the stripe phases will be unstable with respect to the formation of two-dimensional cylinders or bubbles and postulate the phase diagram shown in figure 4.2. This phase diagram shows the effects of temperature and an applied field directed perpendicular to the film. The bubble phase consists of compact domains of ferromagnetically ordered magnetic moments, which are ordered in a hexagonal pattern, with the surrounding moments aligned in the opposite direction. Abanov *et al.* predicted in their work that on the square lattice the four-fold anisotropy of the underlying lattice will stabilise the stripe phases at sufficiently low temperatures, as shown in figure 4.1. Monte Carlo simulations have been done on

the triangular lattice using a lattice gas model by Hurley and Singer [42], leading to the phase diagram shown in figure 4.3. In this figure, S refers to the stripe phase, H refers to the hexagonal or bubble phase and I refers to the isotropic phase. The phase diagram of Hurley and Singer is in the density-temperature plane, which makes it difficult to compare to the results of this thesis. It is possible, however, to map the lattice gas approach to our standard Monte Carlo simulations.

4.2 Zero field

The phase diagram shown in the previous chapter, figure 3.2, is for an $N = 16 \times 16$ system, and a system of this size is too small for extracting phase behaviour. Nevertheless the Monte Carlo simulation of this small system provided some of the first simulation evidence of some interesting finite temperature behaviour. The upper line in figure 3.2 is a phase boundary which was determined from the peaks in the specific heat. The low temperature phases are the ordered stripe phases, but the detailed nature of the higher temperature phase isn't clear in a system this small. To help in determining the nature of this phase, the structure factor was calculated. The structure factor is defined as

$$S\left(\vec{K}\right) = \left\langle \left| \sum_{\vec{r}} S\left(\vec{r}\right) e^{i\vec{K}\cdot\vec{r}} \right|^2 \right\rangle . \tag{4.2}$$

In figure 4.4 the structure factor is plotted at three temperatures for $J = 6.0$: at $T = 0.5$, a low temperature well below the transition line, at $T = 3.00$, which is

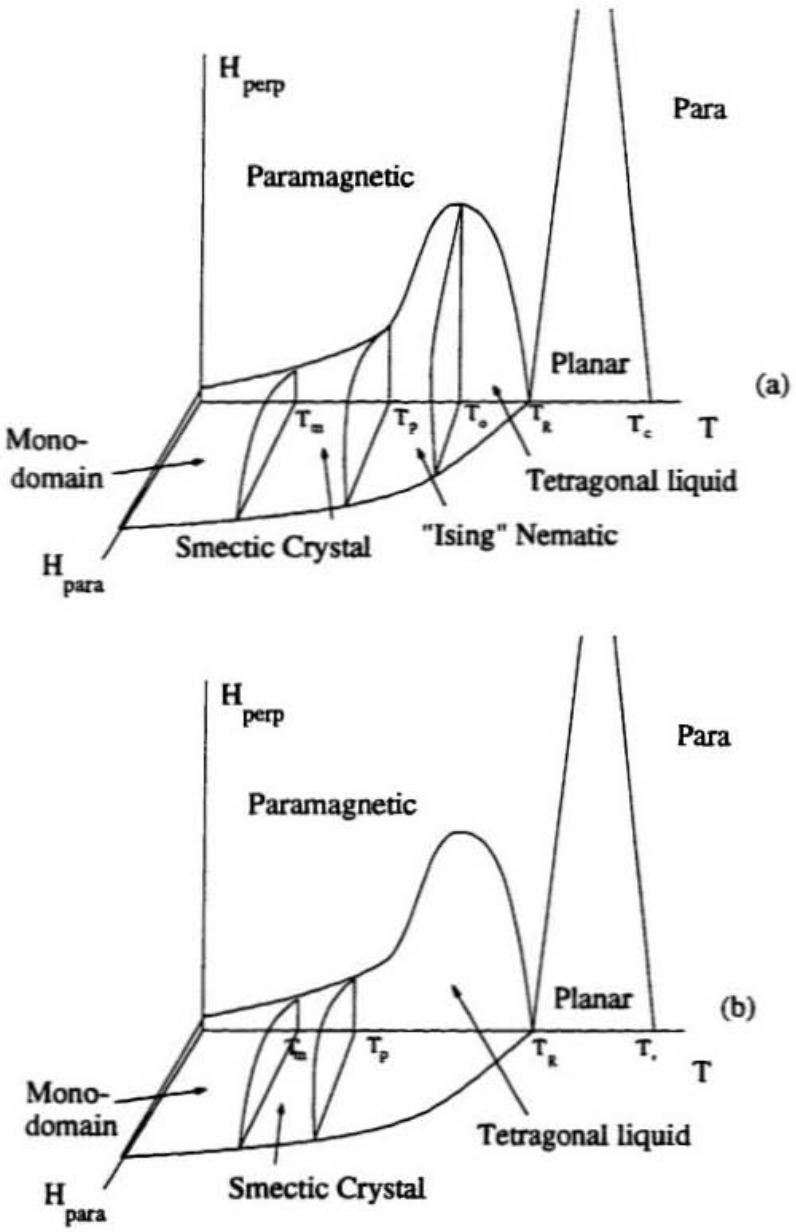

Figure 4.1: The phase diagram as predicted by Abanov *et al.* [50]. The figure (a) is a prediction for $\kappa > 0$ while figure (b) is for $\kappa < 0$. This phase diagram shows the stable phases as a function of temperature, an applied field perpendicular to the film and an applied field parallel to the film. The scheme used to name the transition temperatures by Abanov *et al.* is not used in this thesis.

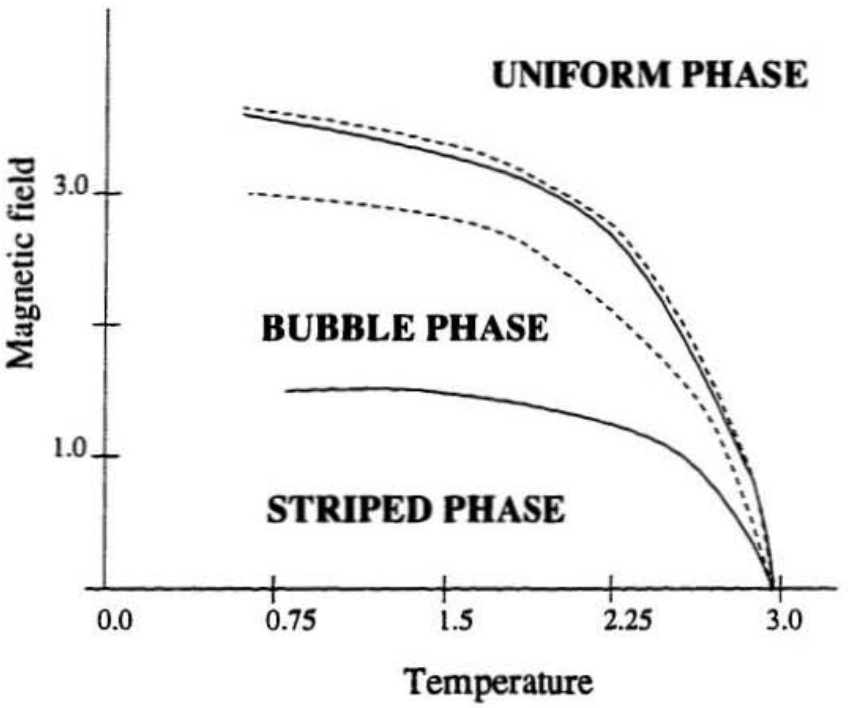

Figure 4.2: The phase diagram as predicted by Garel and Doniach [46]

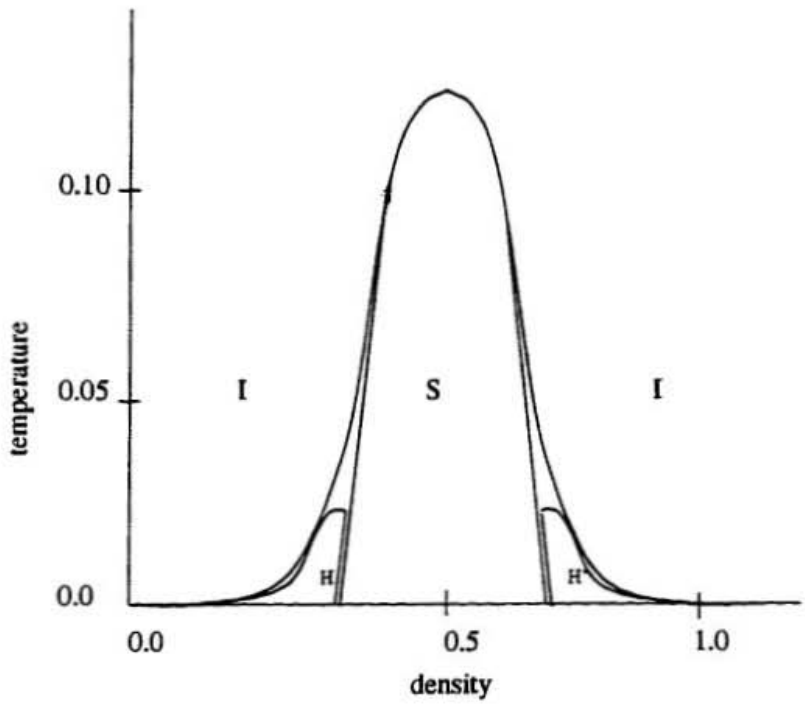

Figure 4.3: The phase diagram as predicted by Hurley and Singer [42]. The S refers to the stripe phase, the H to the hexagonal or bubble phase and the I to the isotropic phase.

near the transition, and at $T = 5.00$, which is well above the transition. At low temperature, the peaks in the structure factor are characteristic of the stripe phase with $h = 4$, in which the stripes are ferromagnetic along the $\hat{x}$ direction Just above the transition, the primary peaks associated with the FA4 and AF4 phases are present. At still higher temperature there is also structure with a characteristic $|\vec{K}|$ which is the same as that in the AF4 and FA4 phases. This indicates that the transition might not be a simple order-disorder transition as is typically seen in magnetic systems. Thus larger and more accurate simulations are needed to clarify this work.

4.2.1 Simulations of large systems

The extension of the simulations to larger systems was carried out in collaboration with I. Booth[8, 86]. Using the ground state calculations as a guides, two values of J where chosen for more detailed study. $J = 6.0$ yields a ground state of stripes with width $h = 4$, while $J = 8.9$ gives stripes of width $h = 8$. These two values were chosen because the lattice sizes which could be simulated were initially powers of two and hence these stripe widths would be commensurate with the lattice size (This size restriction was eventually relaxed in later versions of the program).

The specific heat as a function of temperature for $J = 6.0$ and $J = 8.9$ is shown in figure 4.5. In both graphs there are two peaks; for $J = 6.0$ there is a sharp peak at $T = 2.5$ followed by a broad peak or hump at $T = 5.0$ while for $J = 8.9$ there is a very sharp peak at $T = 4.8$ and a larger and broader peak at $T = 9.5$. The

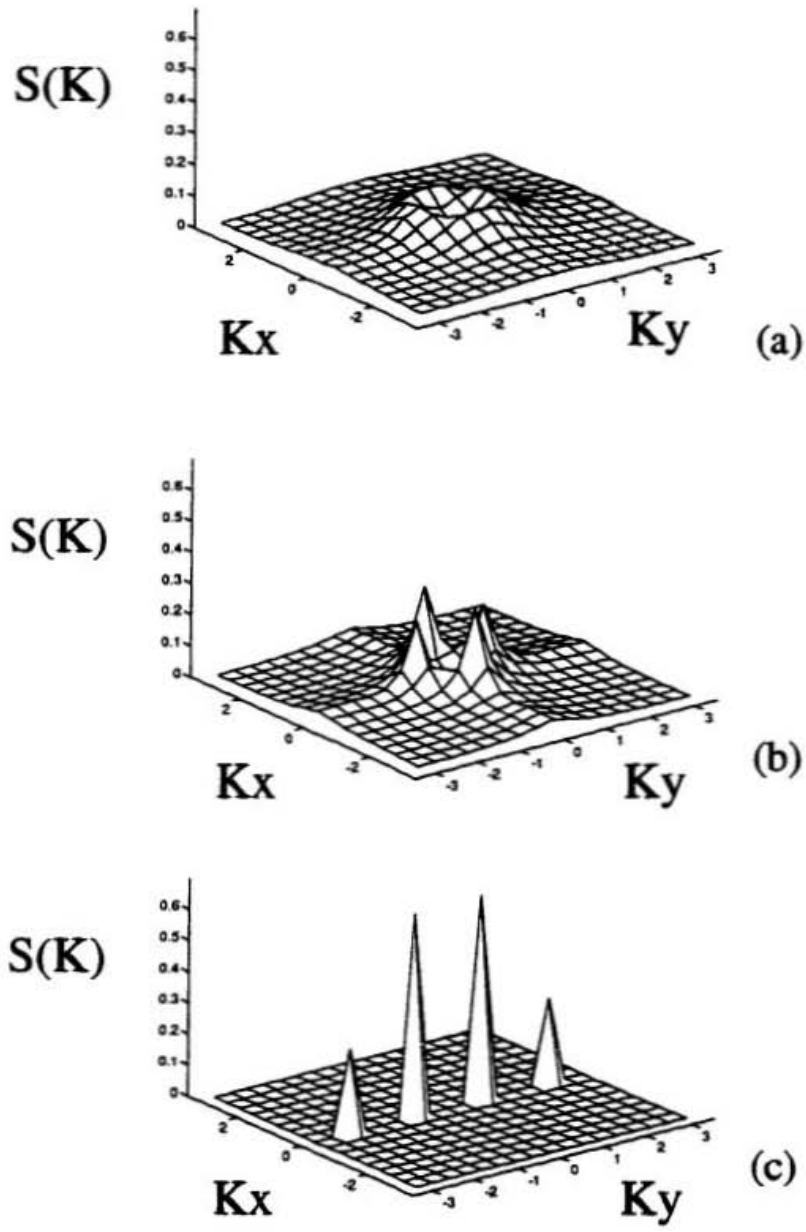

Figure 4.4: The structure factor for a 16×16 system at three temperatures. T=5.00 (a), T = 3.00 (b), and T=0.50 (c). Temperature is in units of g/k_B.

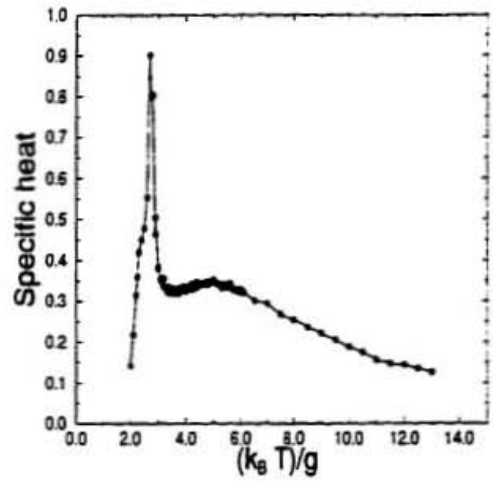

(a)

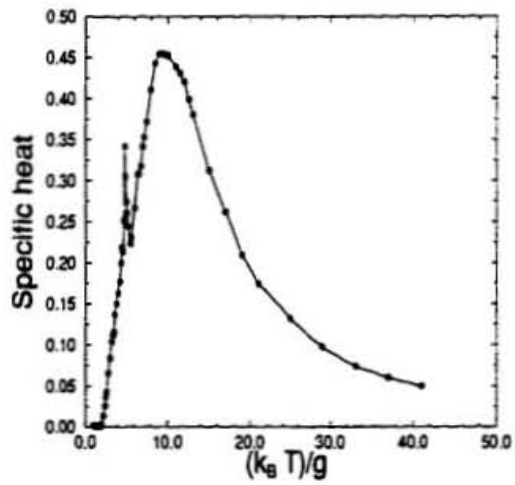

(b)

Figure 4.5: The specific heat for $J = 6.0$ on a 32×32 lattice (a) and $J = 8.9$ on a 64×64 lattice (b) as a function of temperature. Temperature is in units of g/k_B.

nature of the two peaks can be partially discerned by comparing typical configurations at various temperatures and matching them with the features in the specific heat. Figure 4.6 shows a series of such configurations for $J = 8.9$. At low temperature the. system is ordered in the ground state stripe phase with only small fluctuations at the boundaries. The first peak occurs at T_O (the O refers to fact that this is an orientational transition, as discussed below) and corresponds to the break up, not of the stripes, but of the orientational order of the stripes. Thus just above T_0, as shown in figure 4.6 the system is composed of extended domains where both the translational and orientational order of the low temperature phase are absent. The second peak at T_n (T_n is used in analogy to the Néel temperature in an antiferromagnetic) then corresponds to the disordering of these extended domains similar to that seen in the Ising model. This is seen in figure 4.6, where as the temperature is raised the average domain size and distribution of domain sizes appear very similar to those seen in the Ising model. It is useful to draw an analogy to the phases found in the study of liquid crystals. The low temperature phase of the dipolar system is similar to the smectic phase of liquid crystals. In the smectic phase in a liquid crystal, the liquid crystal has positional order and long-range orientational order[87]. In the dipolar model the system has long-range orientational order. The nature of the positional order has not been determined. Just above T_O one has a tetragonal phase which no longer possesses the orientational order. At higher temperature, the stripes disorder and one has the fully disordered phase. This analogy provides a well known, initial

basis for classifying the various phases and transitions. Therefore in the rest of this thesis. the various phases will be referenced using this analogy. One must keep in mind that in some cases a firm correspondence between the ordering observed in the dipolar system and the liquid crystal may not have been clearly established[87].

Figure 4.6: Typical configurations of a 64 by 64 system at various temperatures for $J = 8.9$. Starting in the upper left and moving across the top row the temperatures are $T = 3.50$, $T = 4.50$, $T = 5.50$. In the bottom row the temperatures are from left to right $T = 6.50$, $T = 9.00$, and $T = 11.0$. T_O in this system is approximately $T = 4.8$. Temperature is in units of g/k_B.

This explanation of the two peaks in the specific heat is consistent with the structure factor as measured for this larger system. Once again taking just the $J = 8.9$ system, plots of the structure factor, shown in figure 4.7, show that below T_O there are only peaks at those wave vectors associated with a single orientation of the stripes. Above T_O, but below T_n, the structure factor shows significant ordering at all wave vectors associated with stripes of width $h = 8$, regardless of the orientation. As the

temperature increases further the structure factor still shows residual structure which gradually disappears. These data were binned based on the magnitude of the wave vector, $|\vec{K}|$, and a plot of $S(|\vec{K}|)$ vs. $|\vec{K}|$ is shown in figure 4.8. It can be seen that both above and below T_O, the ordering in the system is associated with the same value of $|\vec{K}|$; ie. that which characterises stripes of width $h = 8$. Only at much higher temperatures are there significant contributions to the structure factor for other values of $|\vec{K}|$. If the system were completely disordered, there would, of course, be no peaks in $S(|\vec{K}|)$, as there would be no ordering at any wave vector. (In a finite system there would be a very broad, and shallow peak.) It is not clear if there is a sharp phase transition between the tetragonal and the disordered phase.

To study the orientation transition more closely an appropriate order parameter can be defined. In this case an order parameter is needed which is able to measure the orientation of the stripes despite the thermal fluctuations in the domain walls in the system. If n_h is the number of horizontal bonds separating oppositely aligned nearest neighbour spins and n_v is the number of vertical bonds separating oppositely aligned nearest neighbour spins, then an orientational order parameter can be defined as

$$O_{hv} = \frac{n_h - n_v}{n_h + n_v}. \tag{4.3}$$

If the stripes are preferentially oriented, then one of either n_h or n_v will be approximately zero and $|O_{hv}|$ will be approximately 1. If there is no preferred orientation then $n_h \approx n_v$ and $|O_{hv}|$ will be approximately 0. In figure 4.9, $\langle|O_{hv}|\rangle$ has been plotted for three system sizes at $J = 8.9$ as a function of temperature. $\langle|O_{hv}|\rangle$ is clearly

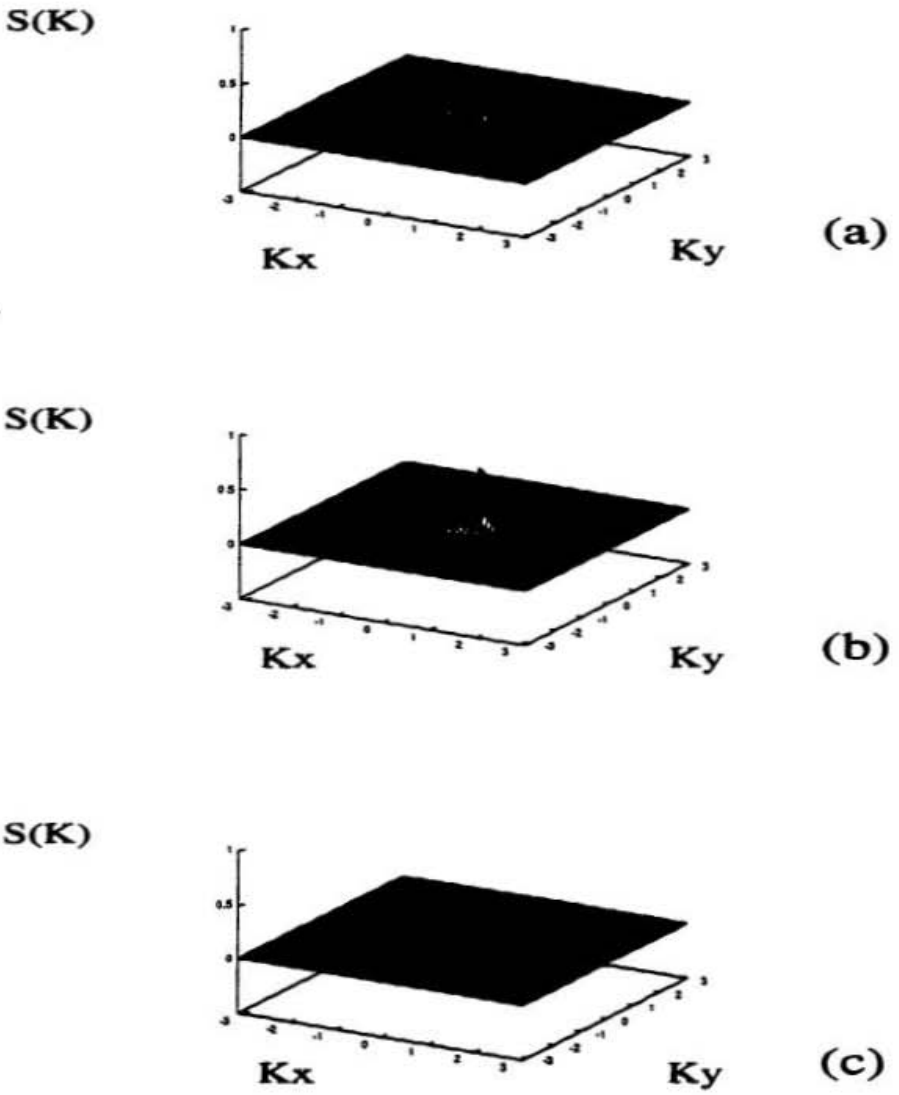

Figure 4.7: The structure factor for a 64×64 system with $J = 8.9$ at $T = 4.60$ just below T_O (a), $T = 5.11$ which is just above T_O (b), and $T = 10.0$ which is well above T_O (c). T_O in this system is approximately 4.8. Temperature is in units of g/k_B.

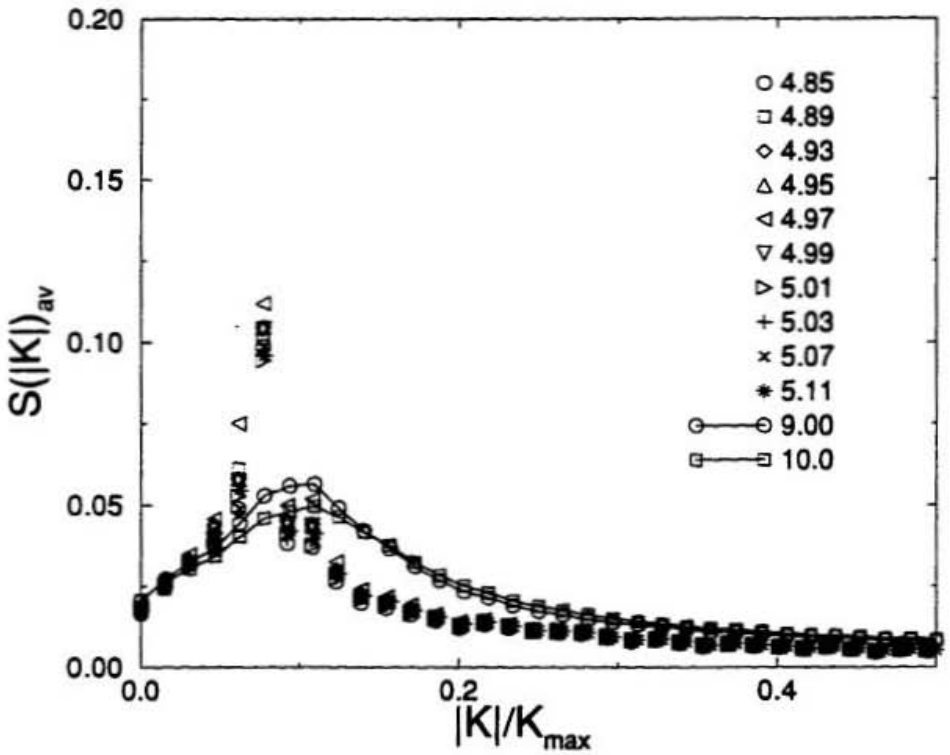

Figure 4.8: The structure factor at various temperatures binned based on the magnitude of the wave vector. The numbers in the legend indicate the temperature of the simulation. Temperature is in units of g/k_B.

1 at low temperatures and drops sharply to 0 (with finite size effects) at the same temperature as the sharp peak in the specific heat. These plots are consistent with a continuous transition from a phase with a distinguishable orientation to a phase with no net orientation.

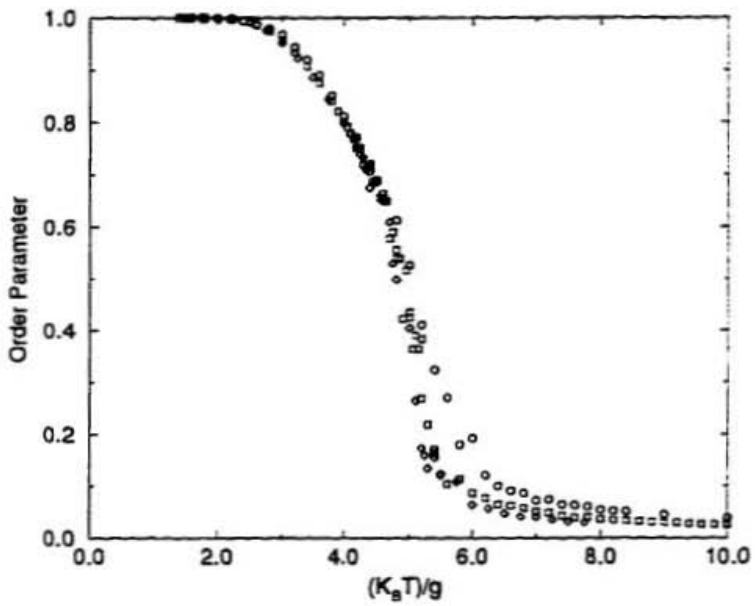

Figure 4.9: The orientational order parameter at $J = 8.9$ for system size $N = 32^2, 48^2, 64^2$ as a function of temperature. Temperature is in units of g/k_B.

4.2.2 Dislocations and disinclinations

The mechanism by which a stripe phase loses its orientational order is not well understood. There is speculation that the loss of orientational order is closely associated with the unbinding of topological defects[50]; the reasoning is as follows. In

the stripe phase on the square lattice there are two kinds of topological defects which are thought to be associated with the loss of orientational order: disinclinations and dislocations. A dislocation can be regarded as a bound pair of disinclinations. Examples of each are shown in figure 4.10. At low temperatures, disinclinations are bound in pairs. Above a transition at which the bound dislocation pairs unbind, one would observe no positional order, but long-range orientational order [50]. This is analogous to what is seen in the nematic phase in liquid crystals. The result of an unbinding of disinclinations would be the loss of the orientational order[50]. This would lead to the tetragonal phase in the case of the square lattice.

In the Monte Carlo simulations discussed above no evidence is found which indicates the existence of the nematic phase, as the transition appears to be from a low temperature smectic-like phase to a tetragonal phase at higher temperature. As of yet, no one has attempted to use Monte Carlo simulations to determine if either of the transitions occurs at the same temperature as the unbinding of the predicted bound pairs of disinclinations or dislocations. This is a very difficult measurement to make, largely due to the technical difficulties of efficiently identifying the topological defects.

4.2.3 Summary:Zero field

The theoretical analysis of the problem of a uniaxial dipolar system by Czech and Villain [47] predicted a depinning transition, where the magnetic superlattice

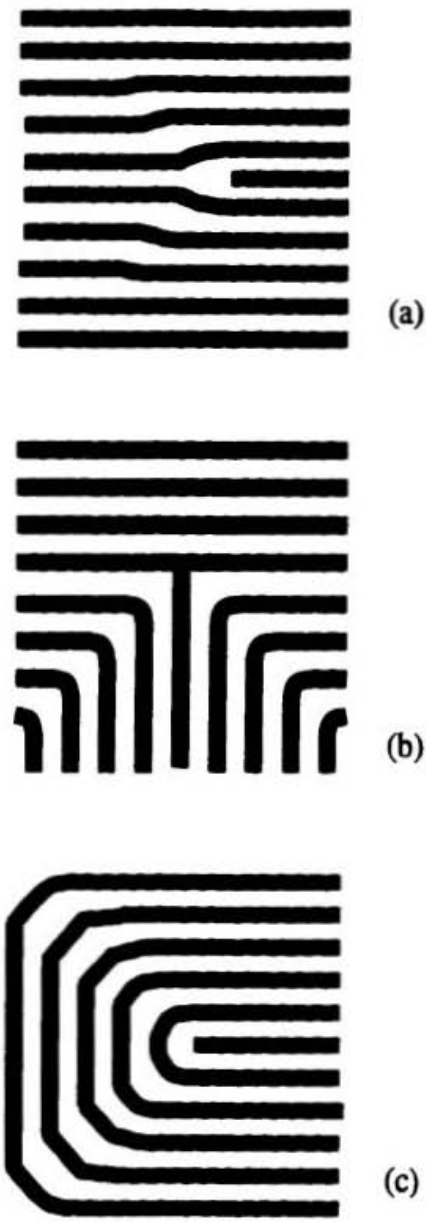

Figure 4.10: An example of a dislocation (a) and examples of the two types of disinclinations which can occur in the stripe phases (b) and (c). These examples are schematics. Black regions have magnetic moments along the positive $\hat{z}$ direction, while white regions have magnetic moments along the $-\hat{z}$ direction.

depins itself from the underlying lattice. It is feasible to associate this transition with the loss of orientational order found in the Monte Carlo simulations. There are, however, some difficulties in making this analogy. In particular Czech and Villain do not predict the complete loss of orientational and translational order seen in the Monte Carlo studies. As well, the dependence of the transition temperature on J in the simulations is non-trivial. In the analysis of Abanov *et al.*, done in the limit of a large, but finite anisotropy, they have the added complication of a reorientation transition. They predict a low temperature smectic phase which is similar to the oriented phase found in the Monte Carlo simulation, as well as a tetragonal phase. However while the Monte Carlo simulations seem to predict a continuous transition, Abanov *et al.* predict that the transition is either first order, or that there exists an Ising nematic phase, intermediate to the smectic and tetragonal phase. In the latter case the transition would proceed in a manner similar to that predicted for the melting of a two-dimensional lattice. There are limitations to making comparisons between this work and the Monte Carlo results. First, Abanov *et al.* treat the problem in the continuum limit and with finite anisotropy. Second, the Monte Carlo simulations are not sufficiently accurate to discount the possibility of the existence of a weak first order transition, nor are the simulations able to discount the possibility of a narrow region between the smectic and tetragonal phases where a nematic phase might be stable.

4.3 Finite field

The Monte Carlo analysis of the previous sections is now extended to include an applied field. The Monte Carlo simulations were done in collaboration with Jessica Arlett [10]. As in the case of zero field, it is not feasible to complete simulations for all possible values of J, so once again two particular values of J have been chosen for study. The values chosen are the same as those used in the zero field simulations: $J = 6.0$ and $J = 8.9$.

The magnetisation is shown in figure 4.11 as a function of temperature for several values of the applied field. The magnetisation saturates at low temperature to one of a few values. This is a result of the discrete nature of the lattice. In zero field the stripes of up and down spins are of equal width, hence the net magnetisation is zero at low temperature. As the field is increased, it eventually becomes energetically favourable for the stripes oriented parallel to the applied field to become thicker than those oriented anti-parallel to the field. The system also needs to maintain its periodicity due to the boundary conditions which have been imposed on the system. Therefore there are discrete jumps in the magnetisation corresponding to the parallel stripe width going from h to $h + 1$ and the anti-parallel stripe width going from h to $h - 1$. Once again the reader is warned that h has been used to refer to both the applied field in reduced units and to the characteristic domain size in the stripe and checkerboard phases. It will be clear from the context in which h is used, which quantity one is discussing.

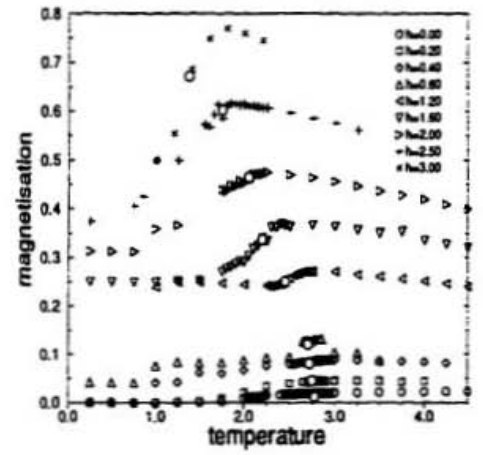

(a)

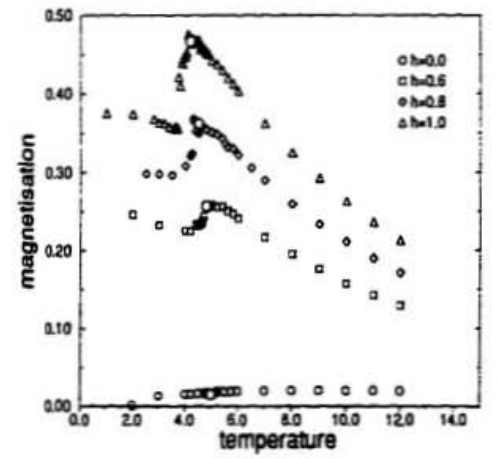

(b)

Figure 4.11: The magnetisation, for various values of the applied field as a function of temperature. $J = 6.0$ on a 32×32 lattice (a), $J = 8.9$ on a 64×64 lattice (b). The large circles indicate the location of the transition from the smectic phase to the tetragonal phase. Temperature is in units of g/k_B.

At low temperature the magnetisation remains almost constant. As the temperature is increased, the magnetisation rises quickly to a broad peak and then slowly drops. This behaviour can be understood by looking at the low energy fluctuations of the domain walls. The low energy fluctuations will consist of single spin flips somewhere along one of the domain walls. These will not occur in significant numbers until the temperature reaches a point at which the energy of the excitation is comparable to $k_B T$. In zero field the energy to flip a spin up and the energy to flip a spin down are equal. The numbers of such flips are also equal and on average they have no effect on the magnetisation. In a field, this degeneracy in energy is removed. Spin flips from anti-parallel to parallel to the field will begin to occur in significant numbers at lower temperature than spin flips in the opposite direction. Therefore the magnetisation will increase with temperature once the temperature reaches the activation energy of the anti-parallel to parallel spin flips. The magnetisation will continue to rise until the temperature reaches the activation energy for the parallel to anti-parallel flips. These spin flips will decrease the magnetisation.

As discussed above, the break up of the orientational order is believed to be precipitated by the formation of unbound disinclinations. As the field increases and the width of the minority stripes decreases it takes a smaller fluctuation to break these stripes. The breaking of a stripe forms a pair of unbound disinclinations. Thus increasing the field leads to a reduction in T_O. T_O approaches the limit of the temperature at which the anti-parallel to parallel spin flips are thermally activated. This

occurs because the spin flips can act as nucleation sites for the topological defects.

4.3.1 The orientational order parameter

In the case of zero field, an orientational transition from a smectic phase at low temperature to a tetragonal phase at higher temperatures was found. At finite field a similar transition is found by measuring the orientational order parameter defined in equation 4.3. $\langle |O_{hv}| \rangle$, the orientational order parameter, is shown in figure 4.12 for several values of the applied field, for the two chosen values of J. At the phase transition the stripes of the minority spins break up to form elongated islands, while the majority stripes remain until higher temperatures. In zero field both sets of stripes break up at the same temperature due to the symmetry of the system. The break up of one type of stripe is sufficient to destroy the long-range orientational order. The drop in $\langle |O_{hv}| \rangle$ in a finite field, particularly for large applied fields, is extremely sharp. There is also considerable hysteresis associated with the magnetisation and the average internal energy, which would indicate that the transition is first order. Although it is difficult to discern within the limits of the simulation, the results found are consistent with a first order transition at large values of the applied field, and with a weakly first order or a continuous transition in the limit as the applied field goes to zero.

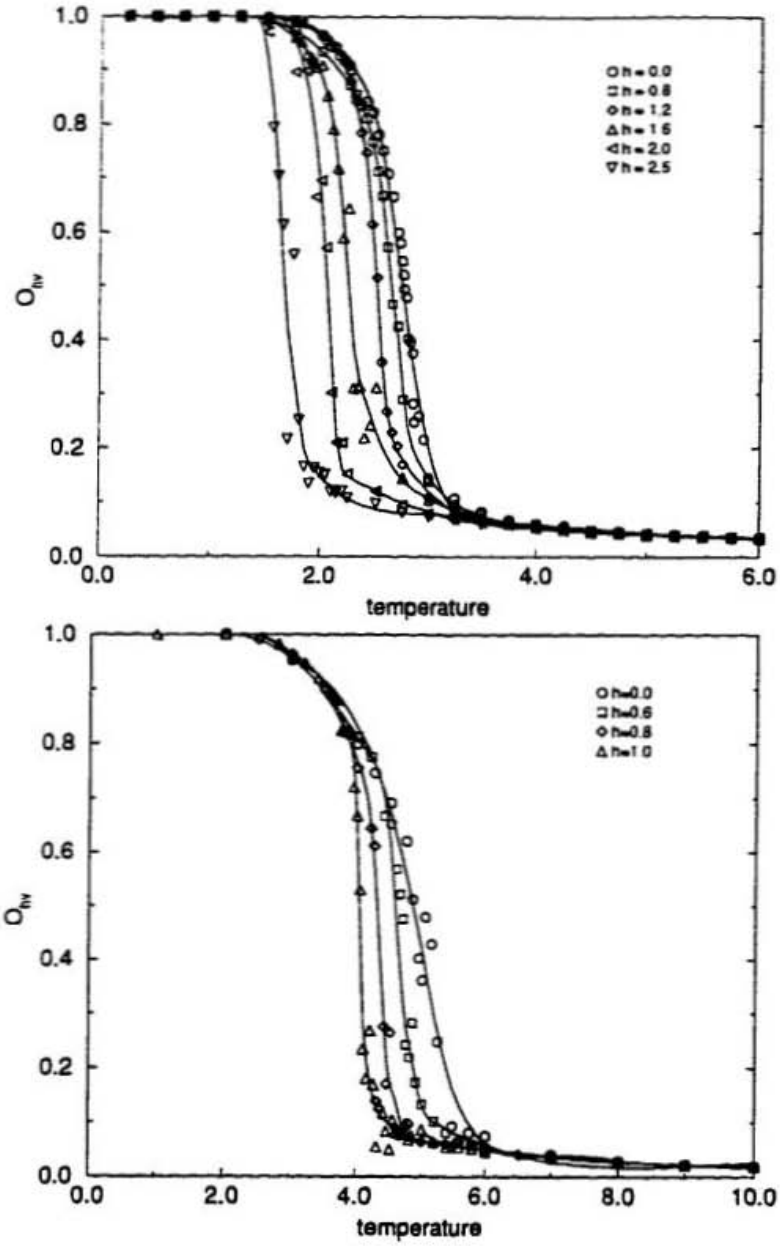

Figure 4.12: The orientational order parameter defined by equation 4.3 plotted as a function of temperature for several values of the applied field for $J/g = 6.0$ on a 32×32 lattice (a) and for $J/g = 8.9$ on a 64×64 lattice (b). The solid lines are guides to the eye only. Temperature is in units of g/k_B.

4.3.2 Domains in finite field

Above the orientational transition, the stripes of minority spins break up into elongated islands. It is possible to measure the degree of elongation of the islands as a function of both temperature and field. The eccentricity of a configuration can be defined as

$$e = \frac{1}{\sum_i n^i} \left| \frac{\sum_i n^i (n_h^i - n_v^i)}{n_h^i + n_v^i} \right| \tag{4.4}$$

where n_h^i and n_v^i are the number of horizontal and vertical bonds along the perimeter of the *ith* island of minority spins in a given configuration and n^i is the total number of spins in the *ith* island. In figure 4.13 the expectation value for e is shown for various applied fields as a function of temperature. In all cases e drops significantly at the temperature at which the system loses its orientational order. At high fields the drop appears to be discontinuous. Even above the transition the islands still retain a measurable eccentricity, which is larger for larger fields.

4.3.3 The phase diagram

The (h, T) phase diagram determined from the Monte Carlo simulations is shown in figure 4.14. The diagram includes a portion of the phase boundary between the smectic phase and the tetragonal phase. At low temperature the Monte Carlo simulations would not allow a determination of the phase behaviour. Points in the diagram were determined both from simulations in which T was slowly varied at constant field and simulations in which the temperature was held fixed and the field was varied.

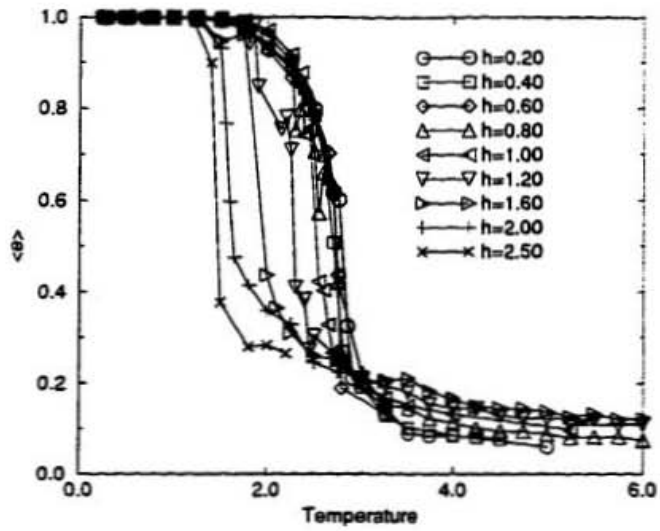

Figure 4.13: The eccentricity as a function of temperature for various values of the applied field on a 32×32 lattice with $J = 6.0$. Temperature is in units of g/k_B.

While the simulations were all done at positive values of h, the diagram has been extended to include negative values by assuming that the transition temperature is independent of the sign of h. This phase diagram differs from that predicted by Garel and Doniach[46] since there is no evidence of a bubble phase, and there is no sharp transition between the tetragonal and the fully disordered phase. Similarly, the phase diagram Abanov *et al.* [50], figure 4.1, predicts a phase transition between the tetragonal and disordered phase. Comparison to the phase diagram of Hurley and Singer[42] is more difficult as our Monte Carlo simulations are not able to describe the phase behaviour at low temperatures. Although there is no evidence of the coexistence regions predicted by Hurley and Singer, it is possible they might be seen at

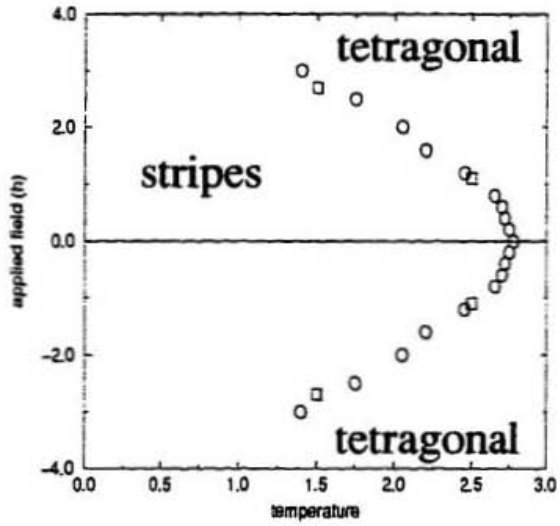

Figure 4.14: The phase diagram as a function of T and h showing the boundary between the smectic stripe phase and the tetragonal phase for $J = 6.00$ on a 32×32 lattice. Circles are from simulations done at constant field, and squares indicate results from simulations done at constant temperature. Temperature is in units of g/k_B.

temperatures lower than those which have been simulated.

4.4 Summary

Notwithstanding the problems associated with comparing the various predictions of Czech and Villain[47] and Abanov *et al.* [50] to the Monte Carlo results obtained, there are definite statements which can be made based on the results in zero field. First, the typical sharp order-disorder phase transition associated with the Ising model is absent in this model. In its place a broad peak is found in the specific heat and the detailed nature of the transition to the fully disordered phase is unclear. Between the low temperature ordered phase and the fully disordered phase, there exists a phase which lacks the orientational order of the low temperature phase, but is composed of well defined structures with a characteristic period. The transition from the smectic phase to the tetragonal phase appears to be continuous.

The Monte Carlo results indicate that, in an applied field as the temperature increases, the stripe (smectic) phase melts to an orientationally disordered (tetragonal) phased which consists of elongated islands. The transition can be characterised using a suitably defined order parameter, which measures the orientation of the system, as was done in the case of zero field. At the transition, this order parameter drops sharply to zero with a corresponding peak in the associated susceptibility. While the Monte Carlo data are not sufficient to determine the order of the transition from the smectic to the tetragonal phase, there is some evidence that it is first order for large

fields. but continuous or at most weakly first order in the limit as the applied field goes to zero. The tetragonal phase maps continuously to the paramagnetic phase with increasing field, without a well defined transition. In the tetragonal phase the islands retain their elongation. There is no evidence in these simulations of a well defined transition to a bubble or hexagonal phase, although it is possible that it exists at low temperature. This is a significant difference between the phase diagram found in this work and those predicted previously. One must bear in mind that the underlying symmetry plays a prominent role in the results found both in the smectic and in the tetragonal phase. This is a result of the lattice which is included in our Monte Carlo studies, but is often omitted in studies which treat the problem in terms of a continuum.

Chapter 5

The dipolar planar model

This chapter is a discussion of the dipolar planar model. As in the previous chapter the model is two-dimensional and the magnetic moments lie on the square lattice. In this chapter the magnetic moments are assumed to have two components. The magnetic moments can be thought of as vectors confined to lie in the plane of the film; ie., with only $\hat{x}$ and $\hat{y}$ components. Generally this would be due to some finite anisotropy, such as that due to crystal fields. However only the case of infinite anisotropy, which confines the magnet moments to the plane of the film, will be considered. In terms of the Hamiltonian given in equation 1.5, the system is also limited to the case of $J \equiv 0$, $\vec{h} \equiv 0$, and the anisotropy is $K = -\infty$. Because the system will now have an easy plane (hard $\hat{z}$ axis) the Hamiltonian of equation 1.5 can

be written in units of g as

$$\mathcal{H} = \left\{ \frac{1}{2} \sum_{\vec{R}_i \vec{R}_j} {}'\sigma^{\alpha}(\vec{R}_i)\Gamma^{\alpha\beta}(\vec{R}_{ij})\sigma^{\beta}(\vec{R}_j) \right\}, \tag{5.1}$$

where the anisotropy has been dropped, since $\sigma^z \equiv 0$.

This chapter contains two separate but related parts. The first part of the chapter is a classical linearised spin wave calculation of the low temperature properties of a finite sized system. The second part of the chapter consists of the results of Monte Carlo simulations, including those done at low temperature. The low temperature results of the two calculations are compared closely.

Comparing the results is very important because it is possible for the finite size of the systems used in the Monte Carlo simulations to lead to incorrect information concerning the ordering in the model. Such is the case in the two-dimensional XY model, which appears to order in a finite system, but does not order in the thermodynamic limit. Classical linearised spin wave calculations for the classical two-dimensional XY model predict a non-zero value for the order parameter, in a finite size system, at finite temperatures[54]. They also predict that in the limit as the system size goes to infinity the order parameter goes to zero for all temperatures. Monte Carlo simulations of the classical two-dimensional XY model, which must be done using finite size system, give non-zero values for the order parameter at finite temperature [88]. By comparing the order parameter at low temperature found using the Monte Carlo simulations, to that predicted by the classical spin wave calculations for a similar size system, one can show that the apparent ordering seen in the simulations of the classical 2-D XY

model is the result of the finite size of the system. Thus if one could simulate an infinite system, the ordering would not take place. Because of the possibility that the Monte Carlo simulations might lead to incorrect conclusions concerning the ordering in our model, it is important to analyse the results of the simulations in light of the classical linearised spin wave calculation.

5.1 The ground state

Despite the fact that the model is restricted to include only one interaction - the dipolar interaction - the nature of the ground state for this system is not trivial. It is well known that the ground state in this model is antiferromagnetic[89]. It is also continuously degenerate. Two particular ground state configurations are shown in figure 5.1. The other ground state spin configurations can be generated from either of these states by means of a complicated set of sublattice rotations. It is easier to characterise the states belonging to the ground state manifold if a simple gauge transformation of the spins is made. This transformation may be written as

$$S^x(\vec{r}) = (-1)^{n_y}\sigma^x(\vec{r}), \tag{5.2}$$

$$S^y(\vec{r}) = (-1)^{n_x}\sigma^y(\vec{r}). \tag{5.3}$$

Here the $\vec{\sigma}$'s are the untransformed spins and the $\vec{S}$'s are the transformed spins. n_x and n_y are the components of the displacement $\vec{r}$ in the x and y directions measured relative to an arbitrary origin in units of the lattice spacing. The ground states

shown in figure 5.1 are shown in terms of the gauge transformed spin variables in figure 5.2. Each configuration in the ground state manifold can be characterised by the orientation of the vector $\vec{V}$ defined as

$$\vec{V} = \frac{1}{N} \sum_{\vec{R}_i} \vec{S}(\vec{R}_i). \tag{5.4}$$

For any ground state configuration $|\vec{V}| = 1$, and the inverse is also true.

Zimmerman *et al.* [55] considered the problem of a classical dipolar planar model on the honeycomb lattice as a model for $FeCl_3$-graphite intercalated compounds within the mean-field approximation. They showed that the ground state in this model is highly degenerate, even though the Hamiltonian itself does not possess a similar symmetry. Using a mean field approach they predicted the existence of an ordered phase at low temperature and developed a phase diagram in the temperature–applied field plane. Henley [56] and later Prakash and Henley [57] considered an anisotropic nearest neighbour model where they chose the anisotropy to match the nearest neighbour portion of the dipolar interaction. Their model mimics the ground state degeneracy found in the dipolar models by Zimmerman *et al.* in the case of the honeycomb lattice, and they showed that a similar effect is seen on the square lattice. Prakash and Henley showed that spin fluctuations in their model lead to an effective potential in the free energy, and that this potential has a symmetry determined by the underlying lattice. They conclude that this potential is sufficient to induce ordering at low temperature and refer to the phenomenon as thermally induced magnetic ordering. As stated, Prakash and Henley[57] used a short range approximation to the

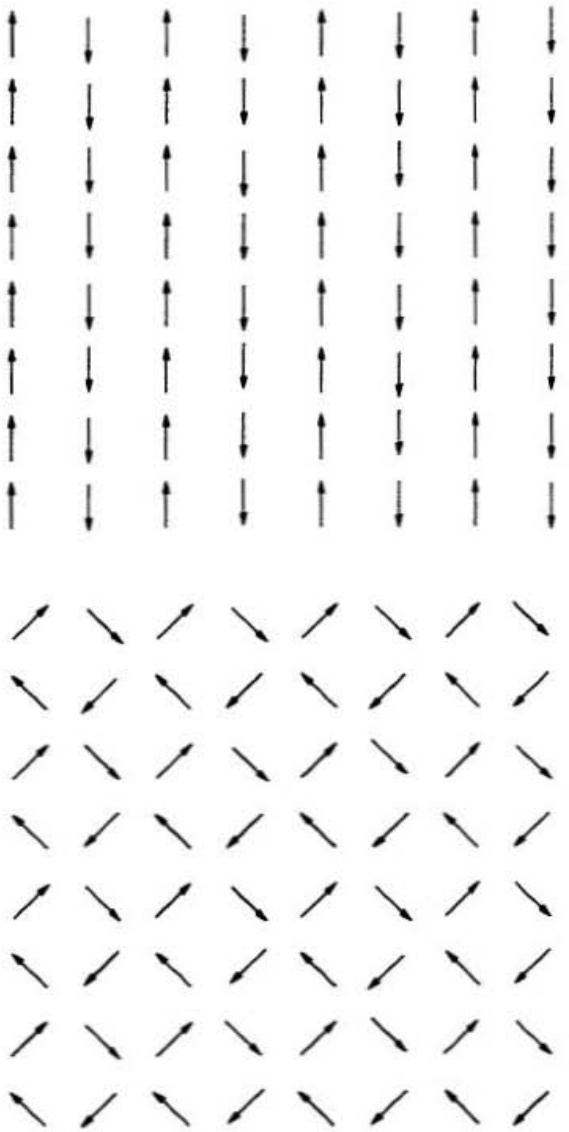

Figure 5.1: Two examples of ground states for the dipolar planar model.

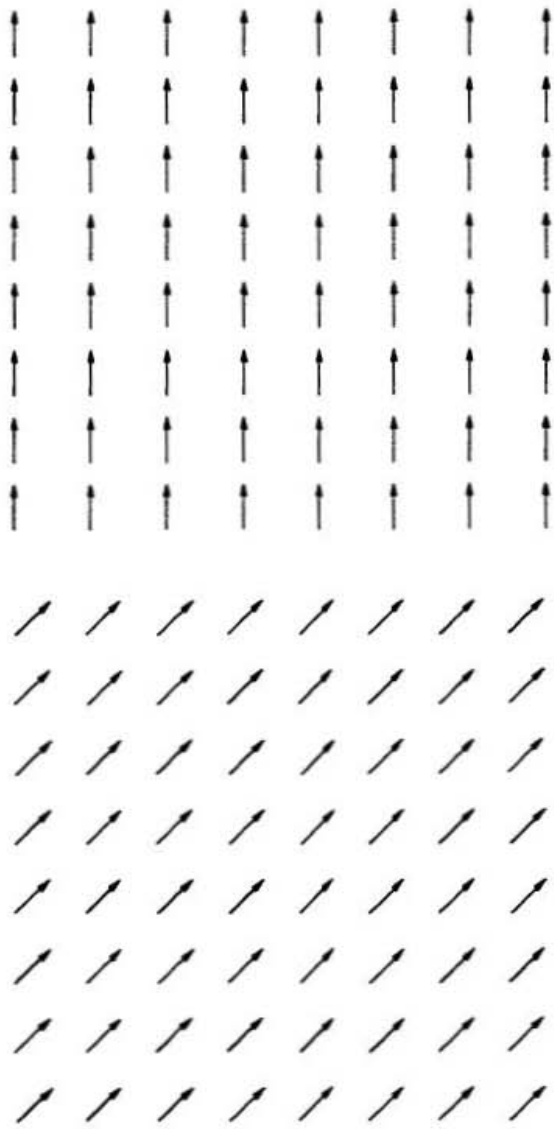

Figure 5.2: The ground state spin configurations corresponding to those in figure 5.1, but shown in terms of the gauge transformed spins.

dipolar interaction, and it was unclear how the results for their model would differ from one in which the full long-range nature of the dipolar interaction is included. Throughout this chapter comparisons will be drawn between the results obtained using the full dipolar interaction and those obtained from Prakash and Henley's short range approximation.

There are a number of papers which deal with a two-dimensional planar system with dipolar and ferromagnetic exchange interactions [60, 62, 67]. In all of these studies, the exchange interaction is assumed to be dominant and the ground state is therefore ferromagnetic. It is not useful to compare the results found here to those results. There have been classical spin wave studies on pure dipolar systems. Bajaj *et al.* [59] have done spin dynamics simulations using the short range approximations of Prakash and Henley. They have not, to the best of our knowledge, repeated the simulations with the full dipolar interaction. Bedanov[58] has looked at the problem of a two-dimensional dipolar planar model on the triangular lattice, and concluded that the system orders at low temperature. Corruccini and White [65], who studied the quantum mechanical model on the square lattice in the spin wave approximation, predict that the model does not order at low temperature. Pich and Schwabl [64] have treated a similar quantum mechanical model on the square lattice, and predict that the model will order at low temperature. While none of these papers deals with the model treated in this thesis, the conflicting predictions do serve to illustrate that considerable difficulties still exist when treating dipolar interactions, and these

subtleties can lead to completely contradictory answers to seemingly simple questions.

5.2 Low temperature behaviour

The low temperature behaviour of the dipolar planar system can be studied via a linearised spin wave calculation. A spin wave calculation is a version of a standard method of solid state physics[43], by which one parameterises the states of the system in terms of a set of variables which describes the states in terms of deviations from the ground state. Expanding the Hamiltonian about the ground state in terms of these variables, and taking the lowest order, non-zero term leads to a simplified approximation to the Hamiltonian which describes the low lying excitations of the system. For example, in a crystal one takes the positions of the ions in the ground state and expands the Hamiltonian in terms of small deviations about these positions. The result is a phonon spectrum for the crystal. For a magnetic system the orientations of the magnetic moments serve to parameterise the state of the system, and one can calculate a spin wave spectrum to lowest order in fluctuations in these orientations. Within this approximation, it is possible to calculate the free energy, the order parameter and many other thermodynamic quantities. In this thesis the magnetic system is treated classically and hence the spin wave analysis is also a classical calculation. Quantum-mechanical spin wave analyses of similar models have been performed previously[65, 64].

Among the benefits of calculating the classical spin wave modes of the system is

that these modes can be measured experimentally using inelastic neutron scattering[43]. Spin waves can also be detected in NMR studies by studying relaxation rates [43]. Unfortunately, relevant experiments are not yet available for comparison. Both techniques would allow a direct comparison between the predictions of theory and the results of experiments. It will be interesting to compare the results of the simulations presented in this thesis and these experimental results when they become available.

While the classical spin wave method is quite powerful it still, of course, has limitations. The method is valid only in the limit of low temperature, and excludes other possible low energy excitations which are of higher order. This can be very significant, as was seen in the history of the classical planar model. The theory of Mermin and Wagner indicated that the the classical planar model does not have long-range order at any non-zero temperature [33], hence that there is no order-disorder transition in this system. Spin wave calculations of the two-point correlation function in the classical planar model showed that it decayed with a power-law dependence on distance at low temperature [90]. High temperature series expansion [91] indicated that the two-point correlation function should decay exponentially with distance. The change in the behaviour of the correlation function indicates that there is a phase change in the system from a phase with power-law decay to one with an exponential decay in the correlation function. The work of Kosterlitz and Thouless[13, 53, 54], in which the significance of low energy vortex excitations was treated, led to the resolution of the apparent discrepancy.

Because of the controversy associated with the classical planar model. the existence of a continuous symmetry with respect to the rotation of the net magnetic moment is a well studied problem. In the classical planar model, which is a model with short range exchange interactions, the continuous symmetry leads to the existence of a gapless spin wave excitation. Gapless means that at some value of $\vec{q}$, the energy of the spin wave is zero. The gap generally refers to the minimum energy required to excite any of the spin wave modes, hence a gapless spin wave excitation requires no energy to be excited. Spin wave excitations have been shown to be sufficient to destroy any long-range order at any finite temperature in the classical planar model[33]. Thus there is no traditional order-disorder transition in this model. Zimmerman *et al.* [55] realized that the situation is somewhat more subtle in the case of a dipolar interaction. In the case of a dipolar system, the ground state is highly degenerate and there is a gapless spin wave excitation at $T = 0$. The dipolar Hamiltonian itself does not possess a similar symmetry. The question is then: Does one observe ordering in a planar system with only dipolar interactions? Another way of phrasing this question is, is there a thermally induced gap in the eigenspectrum which leads to long-range order, and does one observe a Kosterlitz-Thouless phase transition or not?

In order to properly describe the spin wave excitations, a superlattice with lattice spacing $2a$ and four spins per unit cell, as shown in figure 5.3, must first be defined. This is necessary because the ground state is an antiferromagnetic state. The calculation is done in terms of the gauge transformed spins, since then it is possible to define

the ground state in terms of the angle θ_0 which $\vec{V}$ makes with the x axis. The state of a spin is given by $\theta_\alpha(\vec{R})$, where $\vec{R}$ is the position of the unit cell and $\alpha = 0.1.2,3$ gives the position of the spin within the unit cell. The Hamiltonian can be written as a function of the state of the spins, $\mathcal{H}(\{\theta\})$, and then expanded in terms of fluctuations of those spins about any ground state. In mathematical terms the Hamiltonian is

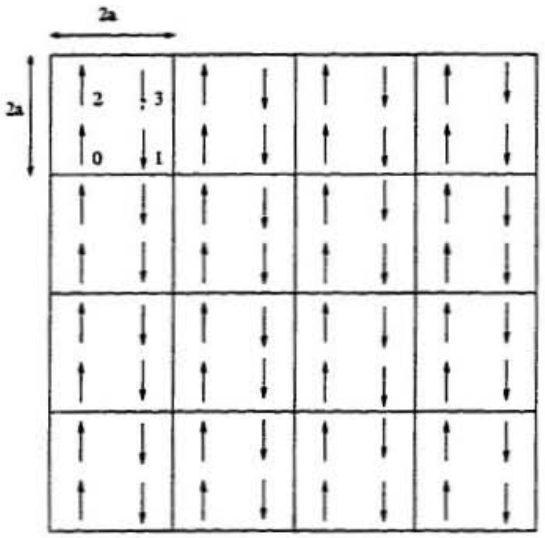

Figure 5.3: The unit cell used in the classical spin wave calculations. A unit cell is $2a \times 2a$, and contains 4 spins. This figure shows 16 unit cells. The labelling scheme used is indicated in the upper left unit cell.

expanded in terms of the fluctuations of the direction of the moments:

$$\begin{aligned}\mathcal{H}(\{\theta\}) &= \mathcal{H}_0 + \mathcal{H}_1 + \mathcal{H}_2 + \ldots \\ &= \mathcal{H}_0 + \sum_i \delta\theta_\alpha(\vec{R}_i)\frac{\partial}{\partial\theta_\alpha(\vec{R}_i)}\mathcal{H}|_{\theta_0} + \\ &\quad \frac{1}{2}\sum_{i,j}\delta\theta_\alpha(\vec{R}_i)\frac{\partial}{\partial\theta_\alpha(R_i)}\frac{\partial}{\partial\theta_\beta(\vec{R}_j)}\mathcal{H}|_{\theta_0}\delta\theta_\beta(\vec{R}_j) + \ldots, \qquad (5.5)\end{aligned}$$

where θ_0 defines the directions of the moments in the ground state about which

the Hamiltonian is expanded. Keeping only the lowest order terms in $\delta\theta_\alpha(\vec{R})$ the Hamiltonian can be written as

$$\mathcal{H} = E_0 + \frac{1}{2}\sum_{ij}\sum_{\alpha\beta}\delta\theta_\alpha(\vec{R}_i)G_{\alpha\beta}(\vec{R}_i - \vec{R}_j)\delta\theta_\beta(\vec{R}_j), \tag{5.6}$$

$$= E_0 + \sum_{\alpha\beta}\int_\Omega d\vec{q}\delta\theta_\alpha(\vec{q})G_{\alpha\beta}(\vec{q})\delta\theta_\beta(-\vec{q}), \tag{5.7}$$

where Ω is the first Brillouin zone. $G_{\alpha\beta}(\vec{R}_i - \vec{R}_j)$ is defined as

$$G_{\alpha\beta}(\vec{R}_i - \vec{R}_j) \equiv \frac{\partial}{\partial\theta_\alpha(R_i)}\frac{\partial}{\partial\theta_\beta(\vec{R}_j)}\mathcal{H}|_{\theta_0}. \tag{5.8}$$

$G_{\alpha\beta}(\vec{q})$ is quite complicated and is given in equation B.27. This expression for the Hamiltonian can be simplified by expressing the fluctuations in terms of the eigenvectors of $G_{\alpha\beta}(\vec{q})$, which are defined by the equation

$$\sum_\alpha G_{\alpha\beta}(\vec{q})\Phi^\omega_\alpha(\vec{q}) = \lambda_\omega(\vec{q})\Phi^\omega_\beta(\vec{q}) \tag{5.9}$$

where $\lambda_\omega(\vec{q})$ is the eigenvalue associated with the eigenvector $\Phi^\omega(\vec{q})$ and $\omega = 0, 1, 2, 3$. $\lambda_0(\vec{q})$ is chosen such that $\lim_{\vec{q}\to 0}\lambda_0(\vec{q}) = 0$. A detailed derivation is given in Appendix B. In figures 5.4 and 5.5, $\lambda_\omega(\vec{q})$ is plotted as a function of $\vec{q}$ for each branch of the eigenspectrum for $\theta_0 = 0$ and for $\theta_0 = \pi/5$, respectively, in the first Brillouin zone. These figures show how the long-range nature of the dipolar interaction affects the symmetry of the eigenspectra. They also illustrate how the axis about which the system orders can change the eigenspectra.

In figures 5.6 and 5.7, particular cuts through q-space are shown from the $\theta_0 = 0$ spectra to highlight some features of note. First one can see in both spectra that

as $\vec{q} \to 0$ there is one branch that goes to zero. This is a result of the continuously degenerate ground state, and for $\vec{q} = 0$ this is the mode associated with the rotation of $\vec{V}$. As well, one can see that in 5.7, which is a cut along the $q_x = q_y$ direction, that there is a branch in the spectrum which varies linearly with q_x as $\vec{q} \to 0$. This is a result of the of the non-analytic nature of $G_{\alpha\beta}$, which results from the long-range nature of the dipolar interaction.

The calculations of Prakash and Henley[57] were repeated by using a nearest neighbour interaction instead of the full dipolar interaction. Spectra equivalent to those shown in figures 5.6 and 5.7 were calculated using this interaction and are plotted in figures 5.8 and 5.9.

5.2.1 Spin wave stiffness

The excitation mode given by λ_0 is known as a soft mode and, in the limit of long wavelengths, the mode can be expressed as

$$\lim_{\vec{q}\to 0} \lambda_0(\vec{q}) = D(\hat{q})q^2. \tag{5.10}$$

$D(\hat{q})$ is known as the spin wave stiffness or rigidity. The name comes from Landau theory, where $D(\hat{q})$ plays the role analogous to the restoring force in response to a fluctuation away from the ground state. In figure 5.10 the spin wave stiffness is plotted as a function of the direction of the wave vector for two ordering angles; one for when the spins order parallel to the x-axis and the second for when the spins order about the direction at 45° to the x-axis. The corresponding results for the nearest-neighbour

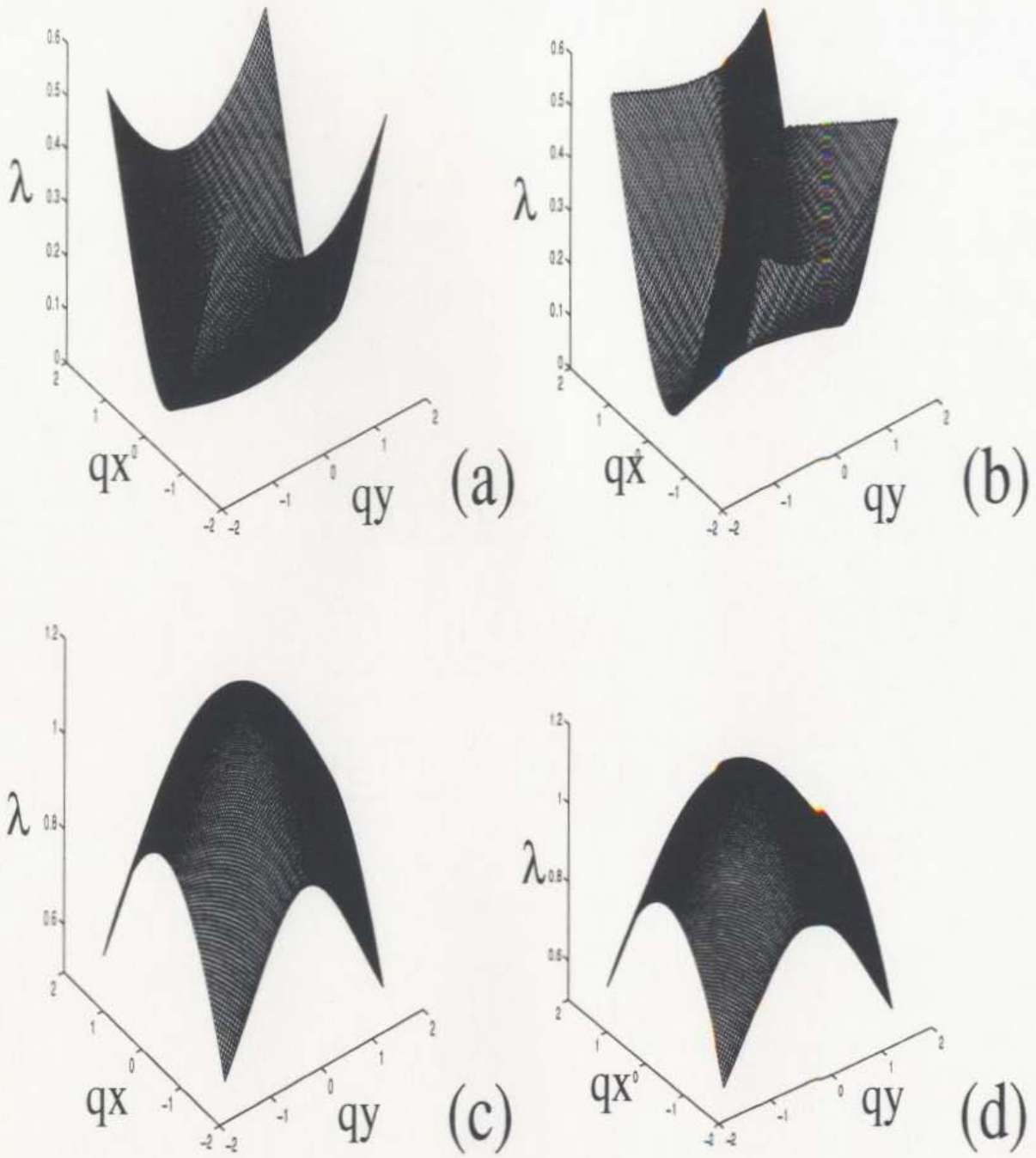

Figure 5.4: The full eigenspectra for $\theta_0 = 0$ using the full dipolar interaction. λ_0 is shown in (a).

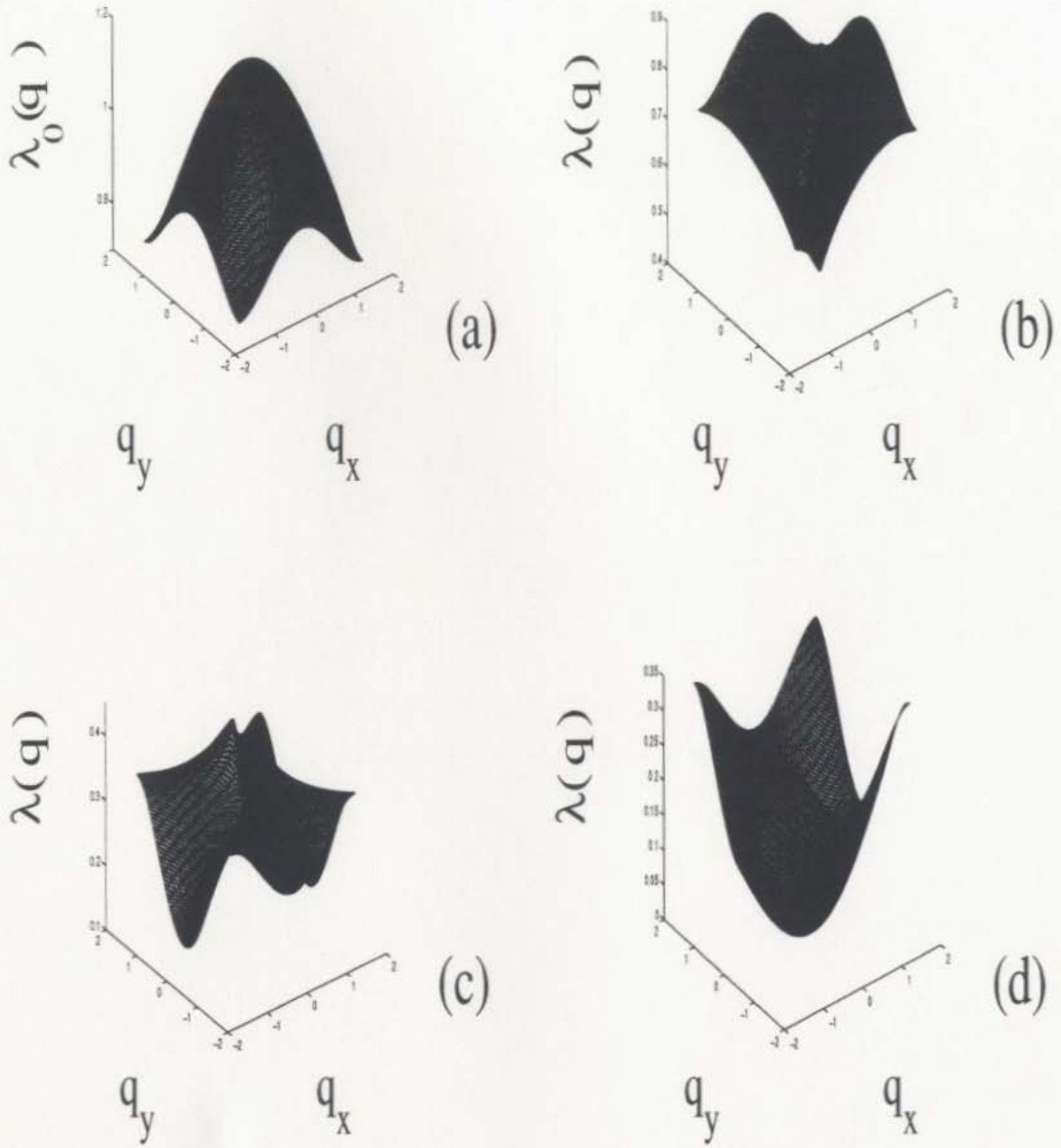

Figure 5.5: The full eigenspectra for $\theta_0 = \pi/5$ using the full dipolar interaction. λ_0 is shown in (a).

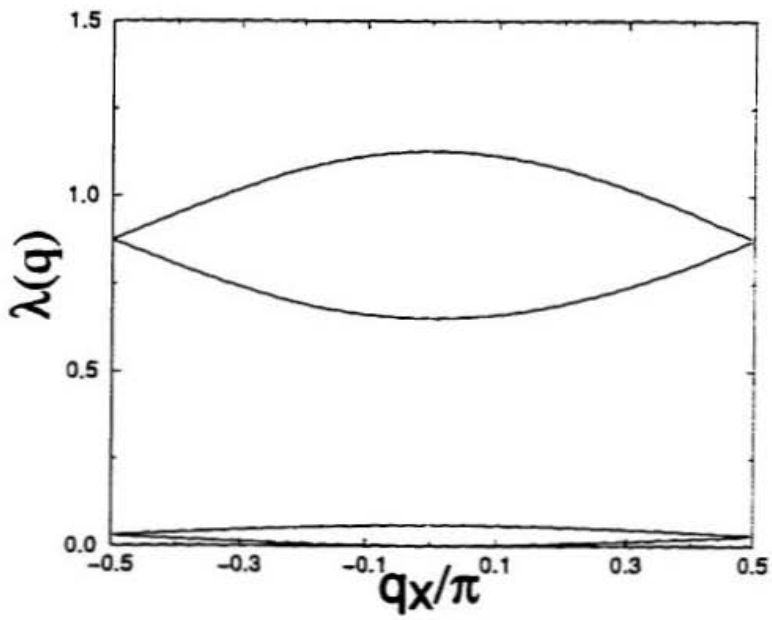

Figure 5.6: Eigenspectrum along the $q_y = 0$ direction using the full dipolar interaction for $\theta_0 = 0$.

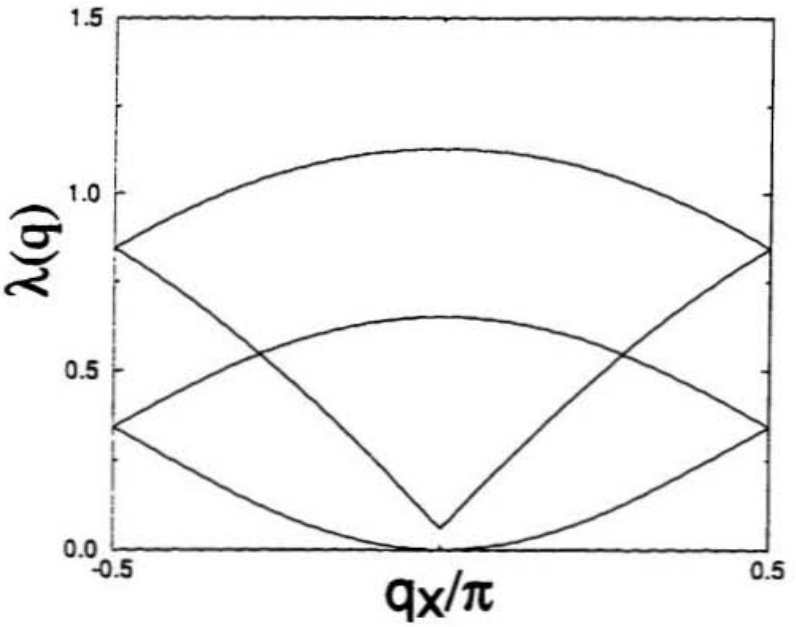

Figure 5.7: Eigenspectrum along the $q_x = q_y$ direction using the full dipolar interaction for $\theta_0 = 0$.

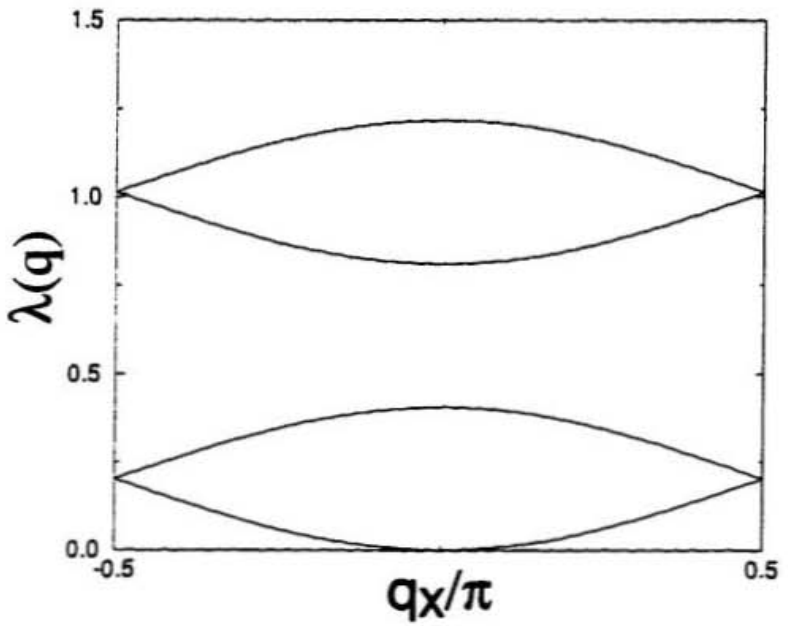

Figure 5.8: The eigenspectrum along the $q_y = 0$ direction for the nearest neighbour model of Prakash and Henley[57] for $\theta_0 = 0$.

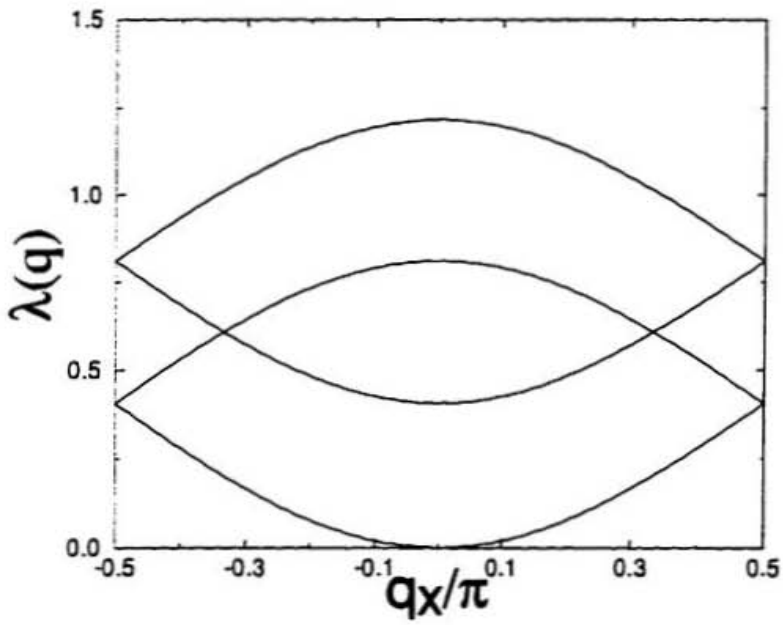

Figure 5.9: The eigenspectrum along the $q_x = q_y$ direction for the nearest neighbour model of Prakash and Henley[57] for $\theta_0 = 0$.

model of Prakash and Henley are shown in figure 5.10 as dashed lines for comparison. Note that while the results of Prakash and Henley are qualitatively similar to those described above, including the long-range nature of the dipolar interaction gives rise to a much larger variation in $D(\hat{q})$. On average $D(\hat{q})$ is smaller when the full dipolar interaction is included in the calculation. This will lead to softer modes, that is, modes which require less energy to excite, particularly near $\vec{q} = 0$ when the system has ordered along one of the axes.

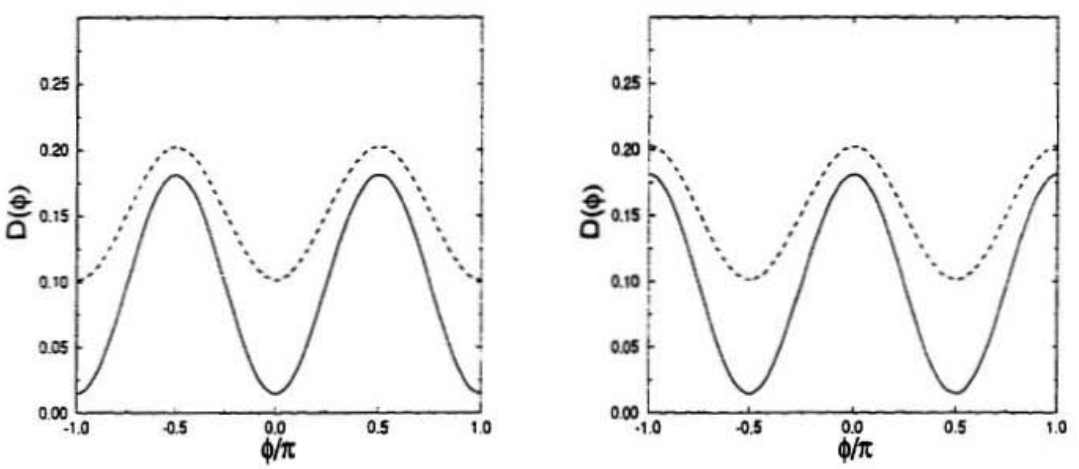

Figure 5.10: The spin wave stiffness $D(\hat{q})$ as a function of the direction of the wave vector, for spins ordered along the x-axis (left) and along the diagonal (45° to the x-axis) (right).

5.2.2 Free energy

Within the classical spin wave approximation one can calculate the free energy as

$$F = k_B T \ln Z \tag{5.11}$$

$$= k_B T \ln \prod_{\vec{q}}{}' \int_{-\infty}^{\infty} \exp\left(-\sum_{\vec{q}} \tilde{\phi}(\vec{q}) \tilde{G}(\vec{q}) \phi(\vec{q})\right), \tag{5.12}$$

$$= E_0 + \frac{N k_B T}{8\pi^2} \int_{\Omega} d\vec{q} \sum_{\omega} \ln\left[\lambda_{\omega}(\vec{q})\right] - \frac{N k_B T}{2} \ln\left(\frac{N k_B T}{8\pi}\right). \tag{5.13}$$

The first term is the ground state energy (in units of g) and is independent of the ordering angle θ_0. The second term in equation 5.13 will be dependent on the ordering angle through its dependence on the eigenspectrum. In figure 5.11 this term is plotted. in units of $gNk_BT/8\pi^2$, as a function of θ_0, along with the corresponding results for the nearest neighbour model of Prakash and Henley. One can see that there is a greater range in the correction to the free energy, implying that the thermal selection of the ordering angle is increased when the full dipolar interaction is included in the spin wave calculation.

5.2.3 Order parameter

It is also possible to calculate the order parameter within the classical spin wave approximation. The order parameter is defined as

$$\Psi = < |\vec{V}| >, \tag{5.14}$$

where $\vec{V}$ is defined in equation 5.4. To simplify the calculation the specific case of a system ordered about the positive x-axis is considered. The results would be the same if ordering about the negative x-axis or either the positive or the negative y-axis were considered. One finds

$$\Psi = \frac{1}{N} < S_x > \tag{5.15}$$

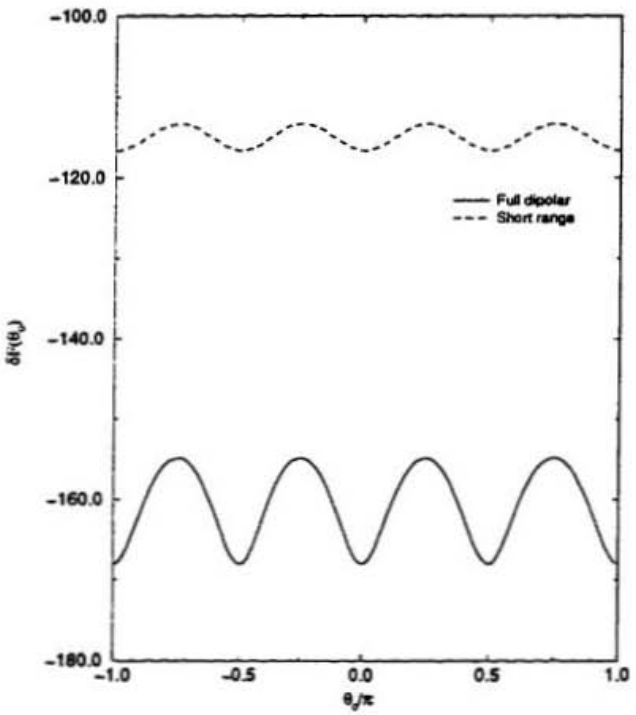

Figure 5.11: The angular dependent part of the correction to the free energy according to the classical linearised spin wave theory in units of $gNk_BT/(8\pi^2)$.

$$= 1 - \frac{1}{2N}\sum_{\vec{R}}\sum_{i=1}^{4}\langle\phi_i^2(\vec{R})\rangle \tag{5.16}$$

$$= 1 - \frac{1}{2N}\int d\vec{q}\sum_{\alpha=1}^{4}\frac{1}{\lambda_\alpha(\vec{q})}, \tag{5.17}$$

where the integral over $\vec{q}$ is only over the upper half of the Brillouin zone. The integral will diverge in the thermodynamic limit due to the soft mode for which $\lambda_0 \to 0$ as $\vec{q} \to 0$. This implies that in the thermodynamic limit the order parameter is zero for all non-zero temperatures and hence that there is no long-range order at any non-zero temperature in this approximation The details of the calculation are presented in Appendix B.

In a finite sized system the integral in equation 5.17 is replaced by a sum. The sum will be finite and the result can be compared to both the results of the short range approximation of Prakash and Henley and more importantly to the results of the Monte Carlo simulation. To calculate the order parameter for a finite size system $\tilde{D}$, defined as $D(\vec{q})$ averaged over the direction of $\vec{q}$, is substituted into equation 5.10. For small $\vec{q}$ this term will determine the $\vec{q}$ dependence of integrand in equation 5.17, and this dependence can be easily calculated once the integral has been converted to a sum. Once again the details of this calculation are relegated to Appendix B. Finally one can write the order parameter as

$$\Psi = 1 - \frac{T}{8\pi\tilde{D}}(\ln(N) + C), \tag{5.18}$$

where C is a constant to be determined, but is independent of N, and T, and $\tilde{D} = 5.154 \times 10^{-2}$ (Following Prakash and Henley would give $\tilde{D} = 0.1433$). Such a size

dependence can easily be checked using finite size analysis.

5.3 Monte Carlo results

Attention is now focused on the results of the Monte Carlo simulations, which will be interpreted in the light of the results of the linearised spin wave theory.

5.3.1 The order parameter

To begin, the order parameter is considered as a function of temperature. In figure 5.12 the magnetisation in terms of the gauge-transformed spins is plotted as a function of temperature for a number of system sizes. The system sizes vary from $N = 8 \times 8$ up to $N = 128 \times 128$. These results indicate that the system orders at low temperature. The associated magnetic susceptibility, defined as

$$\chi = \frac{1}{NT^2}\left[\langle|\vec{V}|^2\rangle - \langle|\vec{V}|\rangle^2\right], \tag{5.19}$$

also has a peak which corresponds to the sharp drop in the order parameter on warming. The susceptibility is plotted in figure 5.13. The specific heat, given by

$$C_v = \frac{1}{NT^2}\left[\langle|E|^2\rangle - \langle|E|\rangle^2\right], \tag{5.20}$$

where E is the internal energy of the system, which is plotted in figure 5.14. While the order parameter, susceptibility and the specific heat all indicate that the system orders, one must be cautious. The systems here are finite, but it is predictions in the

thermodynamic limit which are significant. It is possible for the finite system to order at a finite temperature, but for the system in the thermodynamic limit to remain disordered at all finite temperatures. This is the situation in the classical planar model, where in a finite system the magnetisation is non-zero at low temperatures, but is identically zero for all non-zero temperatures in the thermodynamic limit [88] as was shown in the classical spin wave calculation in the previous section.

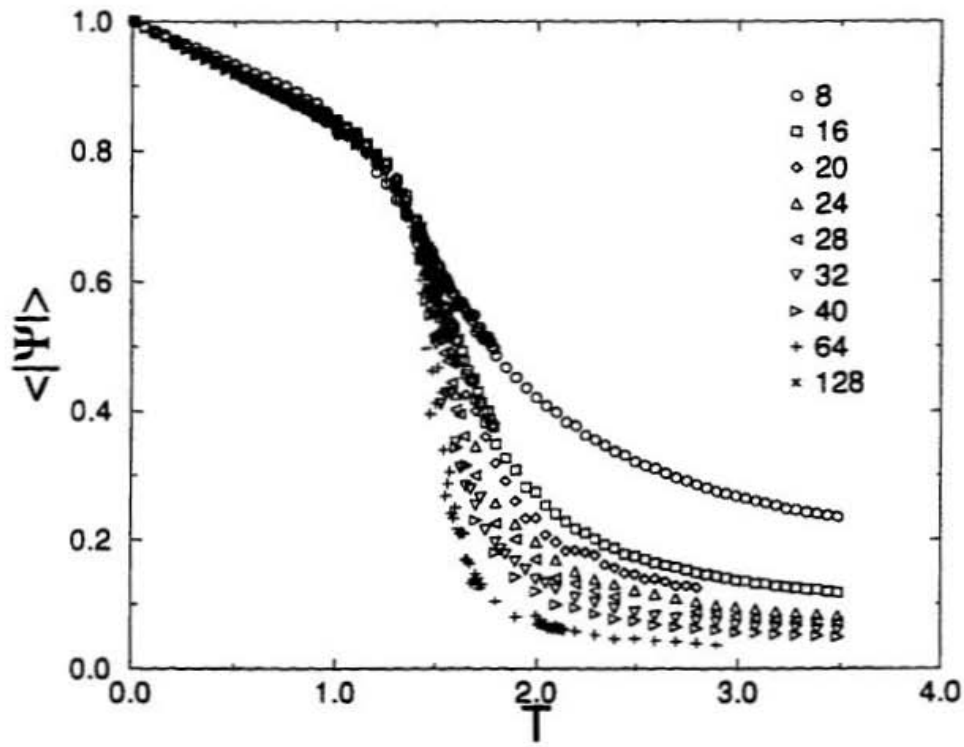

Figure 5.12: The order parameter for systems of various size as a function of temperature, as found using Monte Carlo simulation. The numbers in the legend refer to L, where the system size is $L \times L$. Temperature is in units of g/k_B.

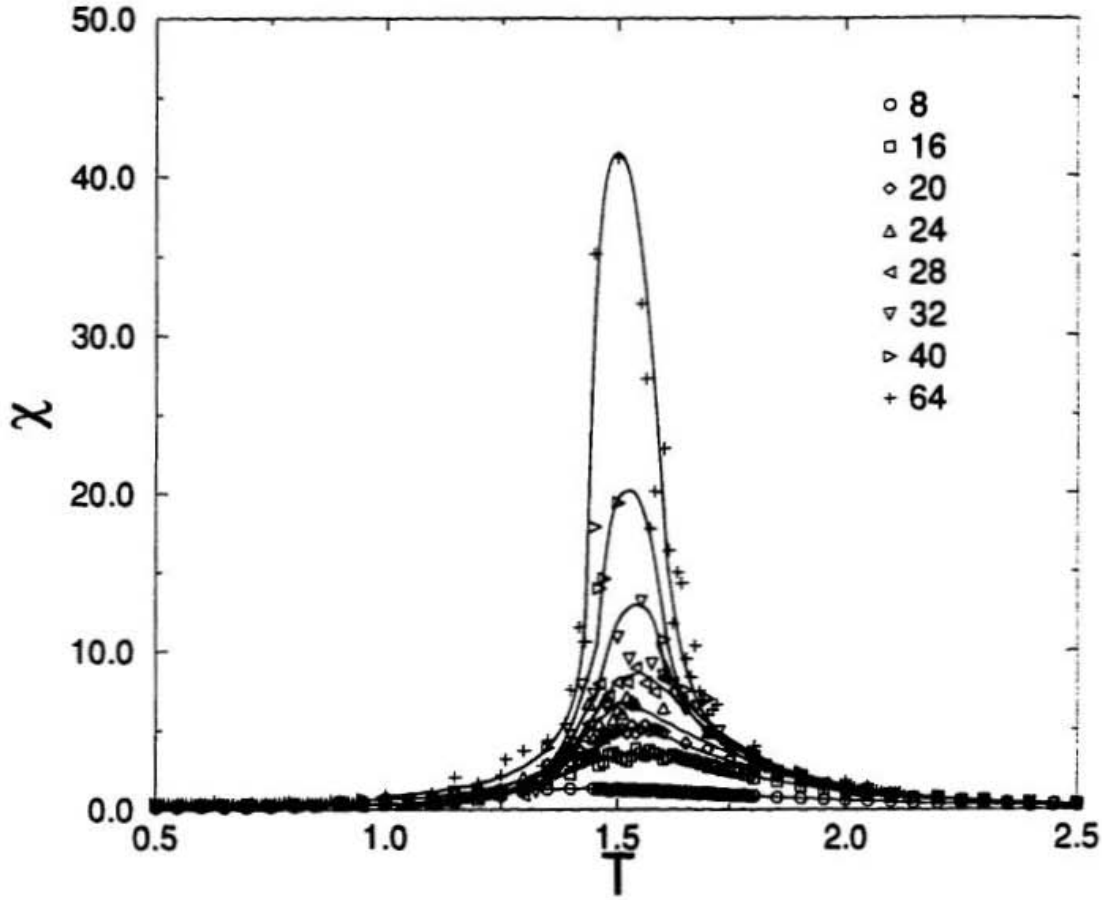

Figure 5.13: The susceptibility of the order parameter for various size systems as a function of temperature, as determined from Monte Carlo simulation. The numbers in the legend refer to L, where the system size is $L \times L$. The lines are guides to the eye. Temperature is in units of g/k_B.

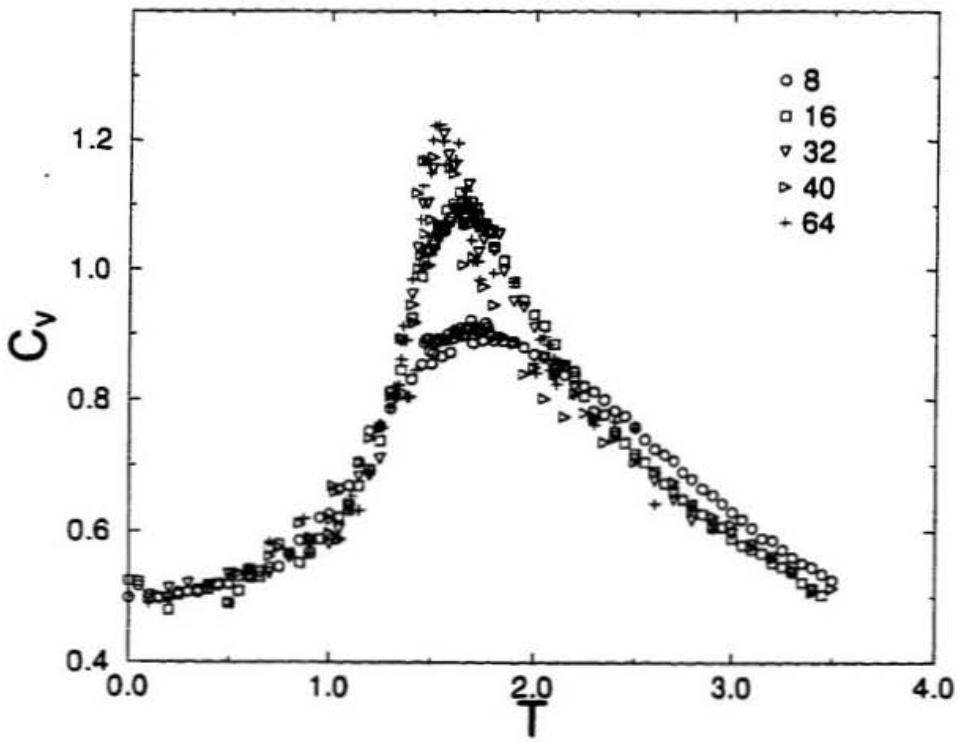

Figure 5.14: The specific heat for various size systems as determined by Monte Carlo simulation. The numbers in the legend refer to L, where the system size is $L \times L$. The lines are guides to the eye. Temperature is in units of g/k_B.

To determine if such is the case for this model, the size dependence of the order parameter must be considered. One can see in figure 5.15 that, at low temperature, the order parameter varies linearly with temperature. This feature is a consequence of the thermal excitation of the spin waves. A prediction for this slope was derived for the case of massless spin waves in equation 5.18. The slope is defined as

$$A(N) = \lim_{T \to 0} \left(\frac{1 - \Psi}{T} \right). \tag{5.21}$$

In the classical spin wave theory, $\lim_{N \to \infty} A(N) \approx 1/(8\pi \tilde{D}) \ln N$, where $\tilde{D}$ is as given above. Thus, in the thermodynamic limit, A diverges according to this theory. This is a direct result of the existence of the gapless branch in the linearised spin wave theory spectrum, and is the reason why the classical planar model does not exhibit an ordered state.

In figure 5.16, A is plotted as a function of $\ln N$. A was obtained by fitting equation 5.21 to the low temperature region of the order parameter as derived from Monte Carlo simulation. The line drawn in the figure is a least squares fit to the lowest four points. The classical spin wave theory predicts a linear dependence, but this theory is valid in the limit of large N. Fitting to the lowest four points gives the largest possible estimate for the slope. Even then the slope predicted by spin wave theory is two orders of magnitude larger than that of our fit in figure 5.16. As N increases, A deviates from this straight line and approaches a plateau. That A is independent of N for large N rather that depending linearly on N, suggests that the ordering observed in the simulations is not a finite size effect.

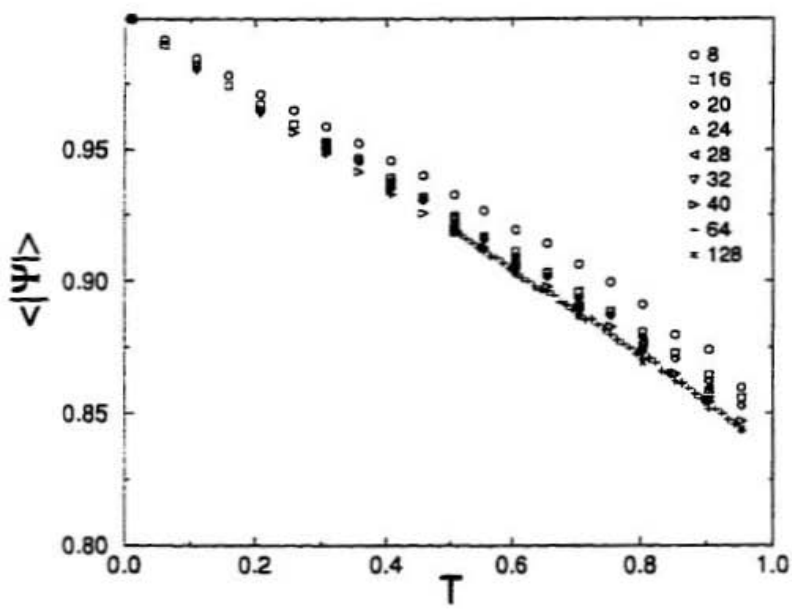

Figure 5.15: Expanded view of the low temperature region of figure 5.12. Temperature is in units of g/k_B.

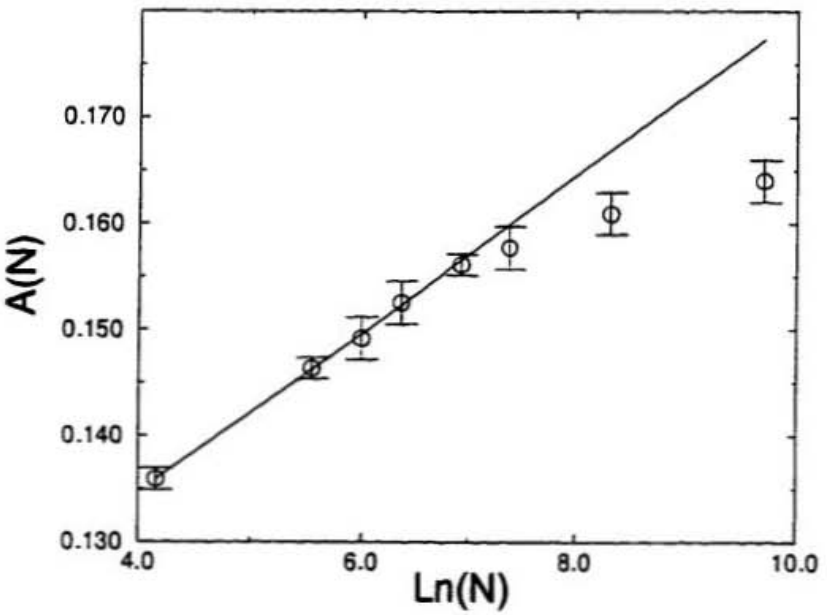

Figure 5.16: The variation of A as a function of $\ln N$.

The explanation of how this ordering comes about revolves around noting that the classical linearised spin wave theory predicts a gapless mode in the spin wave spectrum even at finite temperatures. At finite temperature the lack of a global invariance in the Hamiltonian leads to an effective anisotropy. This was evident in the angular dependence shown by the free energy in figure 5.11. To properly treat this anisotropy will require the treatment of higher order terms in the spin wave expansion of the Hamiltonian. This calculation is in progress[92]. It is expected that a self-consistent treatment will yield a gap in the renormalised spin wave spectrum at finite temperature. This gap will lead to a well defined finite value of A in the limit of $N \to \infty$. At present the Monte Carlo data would lead to a conservative estimate that in the limit as $N \to \infty$, $A(N) = 0.16 \pm 0.01$.

Henley suggested that the anisotropy can be considered in a manner similar to that used for studying a classical planar model with an anisotropy term of the form

$$h_4(S_x^4 + S_y^4), \tag{5.22}$$

added to the Hamiltonian. In the case of the dipolar model, h_4 can be thought of as a temperature dependent effective anisotropy. To gain some measure of the effects of this anisotropy one can define

$$P(T) \equiv \frac{1}{N}\langle S_x^4 + S_y^4 \rangle \tag{5.23}$$

which is the field conjugate to $h_4(T)$. In figure 5.17 $P(T)$ is plotted for a $N = 40 \times 40$ system for both the dipolar model and for a number of classical planar models with

different values of the h_4 term. If the net magnetisation is fixed along one of the axes then $P = 1$, while if the magnetisation is free to point in any direction $P = 0.75$. As one can see in figure 5.17, the classical XY model has $P = 0.75$ if $h_4 = 0$. For a non-zero h_4 $P(T) \to 1$ as $T \to 0$, since the introduction of the non-zero h_4 destroys the rotational invariance. For the dipolar model, with no explicit h_4 term in the Hamiltonian, one can see behaviour which is very similar to that in the classical planar model with $h_4 \approx 0.2$, but P for the dipolar planar and P for the classical XY model with $h_4 = 0.2$ are not identical.

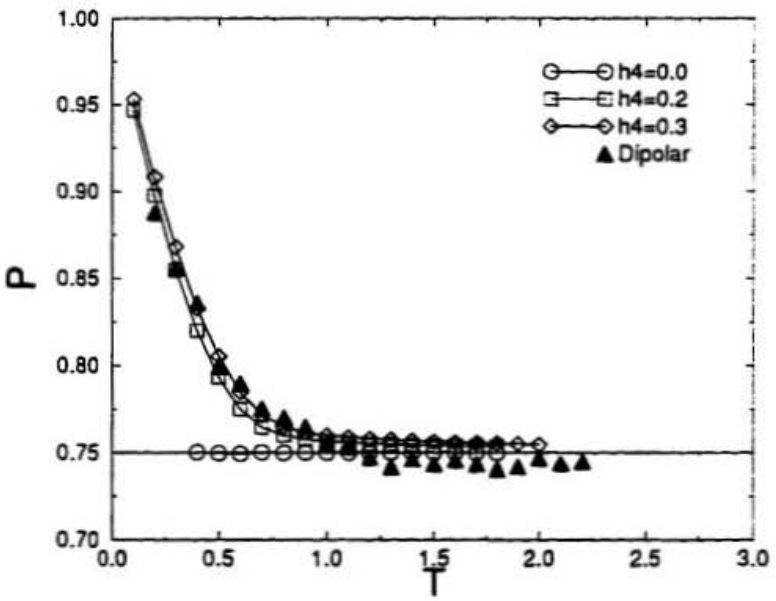

Figure 5.17: $P(T)$ for the classical planar model for three values of h_4, and for the dipolar planar model. Temperature is in units of g/k_B.

From the information available it is possible to determine the effective h_4 approx-

imately for a range of temperatures. Renormalisation arguments for the classical planar model indicate that any non-zero h_4 is a relevant variable below a certain temperature[90]. One can speculate that the arguments for the classical planar model with a four-fold anisotropy can be carried over to the dipolar model and hence the effective h_4 will be a relevant variable below a certain critical temperature. This would imply the existence of an order-disorder transition, which would agree with the Monte Carlo data.

5.3.2 Correlation function

The discussion of the effective anisotropy leads to an interesting question. If the effective anisotropy is very small near the transition, as it appears to be, then it is natural to ask to what extent the system acts like an isotropic system. The classical planar model, which is an isotropic model, does not have long-range order at any non-zero temperature and hence does not have a standard order-disorder transition as discussed above. In the case of the classical planar model with an anisotropic term like that in equation 5.22, José *et al.* [90] have shown using an RG calculation that the model exhibits a continuous transition to an ordered state for any non-zero value of h_4, with non-universal critical exponents. To determine the nature of the transition in the dipolar model, the two-point correlation function in two of the larger systems is considered ($L^2 = 1600$ and $L^2 = 4096$). The two-point correlation function is defined

as

$$C(\vec{r}) = \langle \vec{S}(0) \cdot \vec{S}(\vec{r}) \rangle - \langle \vec{S}(0) \rangle \langle \vec{S}(\vec{r}) \rangle. \tag{5.24}$$

In the classical planar model there is a Kosterlitz-Thouless transition. Near both the standard order-disorder transition and the Kosterlitz-Thouless transition the correlation function at high temperature has the same form, that being an exponential decay given by

$$C(\vec{r}) \approx \exp\left(\frac{-r}{\xi}\right). \tag{5.25}$$

The correlation length ξ in both models diverges at the critical temperature, albeit in different ways. In figure 5.18, the correlation function is plotted as a function of $|\vec{r}|$ for a number of temperatures well above T_c, in a 40×40 system. The data are consistent with the expected form for $5 << |\vec{r}| << 15$ lattice spacings. This is expected since the form given in 5.25 is not valid for very short distances and finite size effects will affect the function when $|\vec{r}|$ becomes close to half the system size ($L = 40$). The correlation length can be determined from the slope of the decay, and theoretically one could test to see if the correlation length diverges as predicted by K-T theory or as predicted for a standard continuous transition. Given that the data are for relatively small system sizes and that making this determination is very difficult, the data have not been subjected to that kind of mistreatment. Suffice to say the data are not sufficiently accurate to discount the possibility of either type of transition

On the other hand, the correlation function itself is expected to have different forms below the critical temperature. K-T theory predicts that the correlation func-

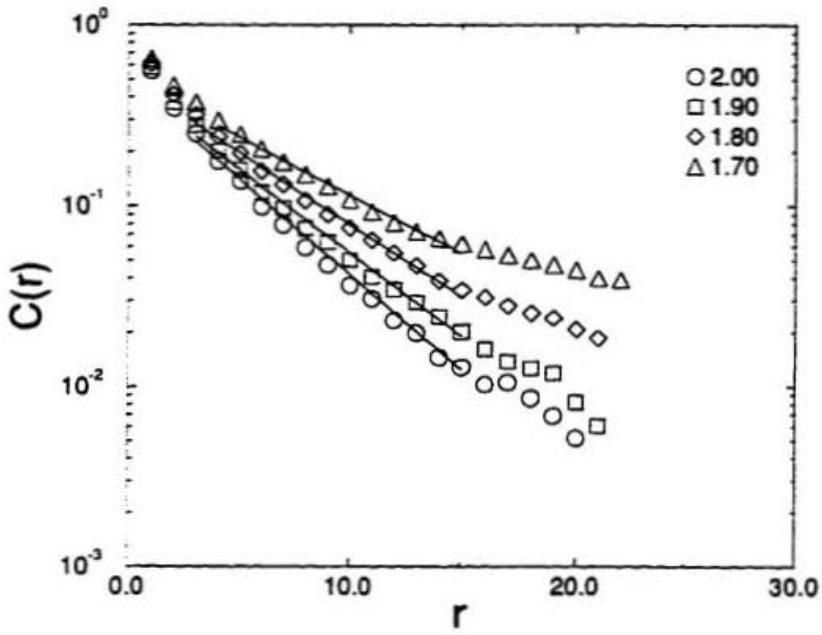

Figure 5.18: The correlation function for four temperatures above T_c as calculated from Monte Carlo simulation of a 40×40 system. Temperature is in units of g/k_B.

tion should decay with a power law dependence, with the power being temperature dependent, while below a standard transition the decay is exponential. In figures 5.19 and 5.20 the correlation function is plotted as a function of $|\vec{r}|$ for a number of temperatures well below T_c on semi-log and log-log scales respectively. As for the data above T_c, one can reasonably fit it to a straight line on the semi-log scale for moderate values of the distance. On the log-log scale it is not possible to get a linear fit in any appreciable range of $|\vec{r}|$. This is evidence that the transition is to an ordered state, and the anisotropic potential effects the ordering.

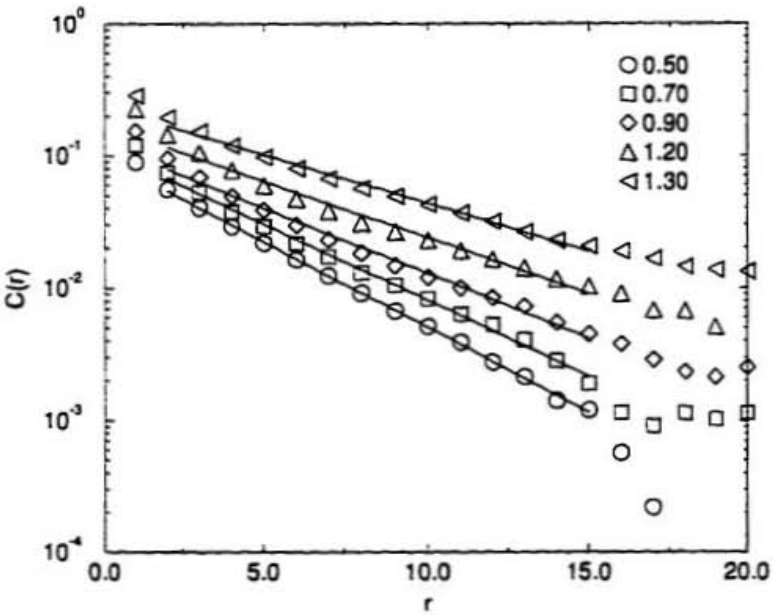

Figure 5.19: Correlation function below T_c on a semi-log plot for a system with $N = 40 \times 40$. Temperature is in units of g/k_B.

Although the data are not sufficiently accurate to determine the form of the di-

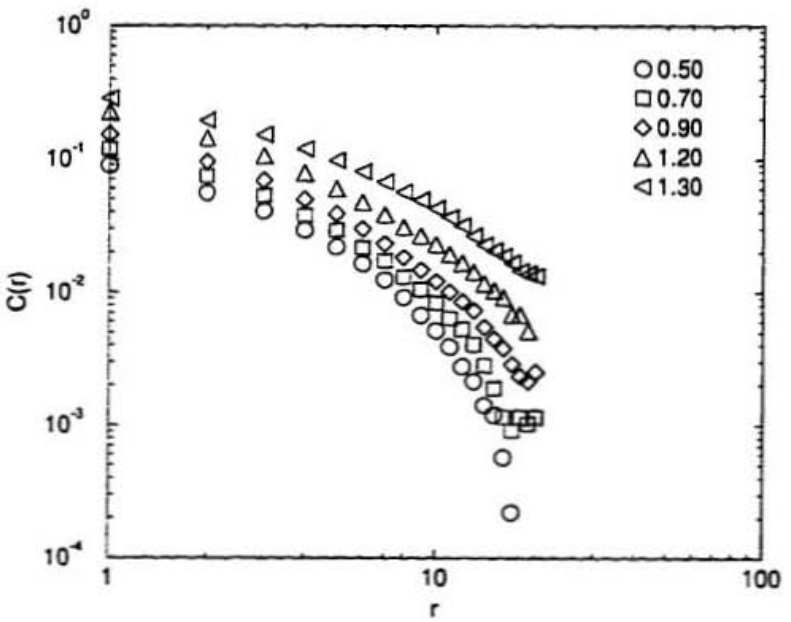

Figure 5.20: Correlation function below T_c on a log-log plot for a system with $N = 40 \times 40$. Temperature is in units of g/k_B.

vergence at the critical temperature, in figure 5.21 the correlation function is plotted as a function of temperature for two system sizes, $L = 40$ and 64. The peak at T_c with a rapid drop on either side is consistent with the expected behaviour of ordering with rotational anisotropy. No attempt has been made to apply finite size scaling techniques to this data to obtain quantitative results concerning the divergence.

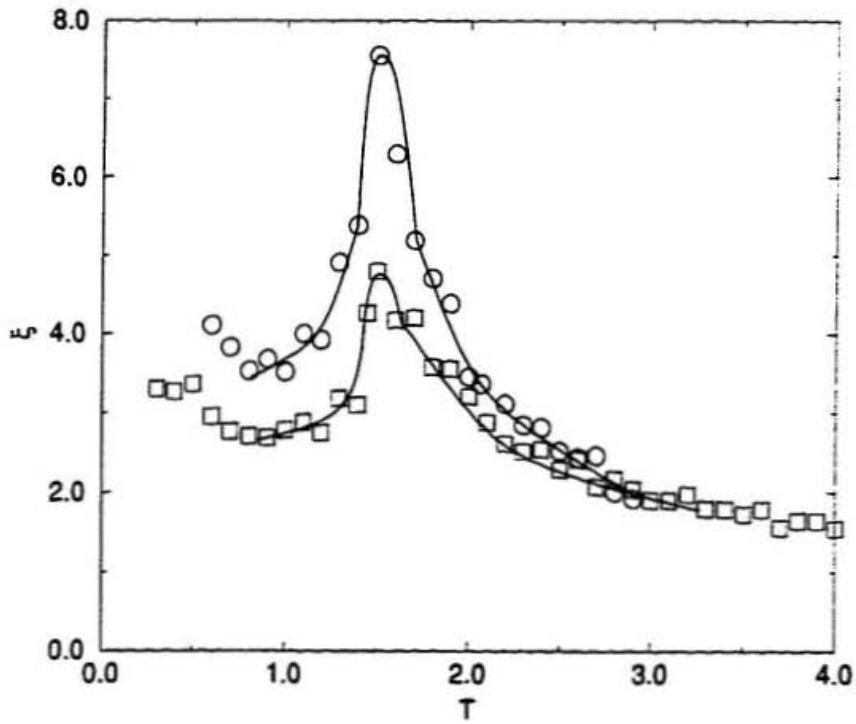

Figure 5.21: The correlation length as a function of temperature for $N = 40 \times 40$ (□) and $N = 64 \times 64$ (○). The lines are intended as guides to the eye. Temperature is in units of g/k_B.

5.4 Summary

In this chapter a dipolar planar model has been studied. The low temperature properties found using Monte Carlo simulation have been interpreted in the context of a classical linearised spin wave calculation. The Monte Carlo results differ substantially from the predictions of the spin wave calculation. A finite size analysis of the slope of the order parameter at low temperature clearly indicates that the dependence on system size is significantly less than that predicted by the classical linearised spin wave theory and that, for larger systems, the order parameter approaches a well defined value. This indicates that the system does exhibit an ordered phase at low temperature. This conjecture is supported by the analysis of the two-point correlation function which, when considered in light of the theory of José, implies that the thermally induced anisotropy leads to a standard continuous transition from a high temperature disordered phase directly to an ordered phase. By measuring the field conjugate to the effective anisotropy some estimate of the approximate size of the effective anisotropy was made. However in the region of the phase transition it was not possible to make an accurate estimate of the effective anisotropy.

In performing the classical spin wave calculation some features which were not present in the nearest neighbour model of Prakash and Henley [57] were identified. For example, the linear behaviour of the second branch of the spin wave spectra at small $\vec{q}$ is associated with the long-range nature of the dipolar interaction. Further analysis of the Monte Carlo results, in particular the low temperature dependence of

the order parameter and the two point correlation function. indicates that the model orders at low temperature along one of the in-plane axes and that the transition from the disordered phase to the ordered phase is a continuous transition.

Chapter 6

The dipolar Heisenberg model

6.1 Introduction

There have been a number of intriguing experimental results concerning dipolar thin films, as discussed previously in chapter 1. Two in particular are reported in the work of Pappas *et al.* [5], as well as that of Allenspach and Bischof [23] on Fe on the (100) surface of Cu. Both groups found that the system exhibited a reorientation transition at which the magnetisation switches from out-of-plane to in-plane as the temperature increases. This work has led to a number of other experiments with similar results which were discussed in the introduction [24, 25, 26, 27, 28, 29, 30, 31, 32].

The typical approach to treating this problem theoretically has been to start with a two-dimensional system in which the magnetic moments interact via a ferro-

magnetic exchange interaction, a perpendicular magnetic surface anisotropy, and a dipolar interaction. The relative strengths of the interactions are chosen to mimic the expected experimental parameters, so the exchange interaction and the MSA are typically much larger than the dipolar interaction. However, despite its small relative magnitude, the dipolar interaction plays an important role in determining the magnetic properties of these systems. Previous studies on two-dimensional systems have shown that including only a ferromagnetic exchange and a positive, perpendicular MSA, the system will order with a transition temperature determined by the ratio of the exchange interaction and the MSA. For $K/J > 0$, K being the strength of the MSA, there is a second order phase transition to the ferromagnetic state, with the moments ordered out-of-plane, which is in the Ising universality class. For $K/J < 0$ the system is similar to the classical XY model and exhibits a Kosterlitz-Thouless transition [93].

The addition of the dipolar interaction has three effects:

- 1. The anisotropic nature of the dipolar interaction is able to stabilise the in-plane ordered state as shown in chapter 5.

- 2. It allows for the possibility of a re-orientation transition.

- 3. It creates regions in phase space where the ground state is a perpendicular stripe phase as shown in chapter 3.

Systems which include the ferromagnetic exchange, the MSA and the dipolar inter-

action have recently been studied extensively using such methods as Renormalisation Group calculations[61, 94], mean field calculations[69, 71], Monte Carlo simulation [72, 73, 74], and spin wave analysis [31, 60, 66, 67]. However previous studies assumed that the lowest energy in-plane state and the lowest energy out-of-plane state were both ferromagnetic.

6.2 Dipolar dominated systems

In this chapter, a two-dimensional, magnetic system on the square lattice is simulated, with the magnetic moments being fully three-dimensional vectors. In contrast to the studies discussed above, the magnetic moments in these simulations interact via a dipolar interaction and a magnetic surface anisotropy, but there is no exchange interaction. Referring to the general Hamiltonian of equation 1.5, $J = 0$, and the properties of the system are studied as a function of K. In units of g, the Hamiltonian considered in this chapter is given by

$$\mathcal{H} = \left\{ \frac{1}{2} \sum_{\vec{R}_i, \vec{R}_j}{}' \sigma^{\alpha}(\vec{R}_i) \Gamma^{\alpha\beta}(\vec{R}_{ij}) \sigma^{\beta}(\vec{R}_j) - K \sum_{\vec{R}_i} (\sigma^z(\vec{R}_i))^2 \right\}. \tag{6.1}$$

The pure dipolar system is of interest because, while the exchange interaction is generally the dominant interaction in real systems, the dipolar interaction plays a crucial role in determining the phase behaviour and morphology of the magnetic ordering. That being the case, removing the extra interaction isolates the dipolar interaction somewhat and allows one to probe its effects more directly. A better

understanding of the dipolar system naturally aids in understanding the ferromagnetic system. Also, the pure dipolar system is a closer approximation to some of the (RE)$Ba_2Cu_3O_7$ compounds which do not have ferromagnetic ground states, than would an exchange dominated model [14, 15, 16, 17]. This model is also an important limiting case of the full Hamiltonian of equation 1.5, hence it is interesting in its own right.

6.2.1 The ground state

The ground state of the system is dependent on the value of K. For $K = 0$ it is the antiferromagnetic in-plane ground state described in chapter 5. This state can be characterised by the order parameter

$$M_{\parallel} = \frac{1}{N} \left\langle \left| \sum_{\vec{r}} (-1)^{r_y} \sigma^x(\vec{r})\hat{x} + (-1)^{r_x} \sigma^y(\vec{r})\hat{y} \right| \right\rangle . \tag{6.2}$$

For large K the ground state becomes the out-of-plane antiferromagnetic state. This state can be parameterised by the order parameter

$$M_{\perp} = \frac{1}{N} \left\langle \left| \sum_{\vec{r}} (-1)^{r_x + r_y} \sigma^z(\vec{r}) \right| \right\rangle . \tag{6.3}$$

These order parameters allow the characterisation of the magnetic order in terms of a homogeneous order parameter. $M_{\parallel}$ is identical to the order parameter defined for the planar model in chapter 5. Along with the definition of the order parameters we can define associated susceptibilities, $\chi_{\parallel}$ and $\chi_{\perp}$, as

$$\chi_{\parallel} = \frac{1}{T^2 N} \left[\langle M_{\parallel}^2 \rangle - \langle M_{\parallel} \rangle^2 \right] \tag{6.4}$$

and

$$\chi_{\perp} = \frac{1}{T^2 N}\left[\langle M_{\perp}^2\rangle - \langle M_{\perp}\rangle^2\right]. \tag{6.5}$$

One of the benefits of the antiferromagnetic ground state, from a computational point of view, is that convergence problems that arise in ferromagnetic ground states as a consequence of the long-range character of the dipolar interaction, are less severe when one is dealing with antiferromagnetic ground states. The limiting case of infinite anisotropy has already been treated in the two previous chapters. $K = +\infty$ is the uniaxial case which was discussed as a small part of chapter 3, while the model with $K = -\infty$ is simply the planar model of chapter 5.

At $T = 0$, the phase boundary between the two phases can be calculated by taking the dipolar energy for both the in-plane state, (E_{in}) and out-of-plane state (E_{out}) as calculated in chapter 3 and reference [22] and solving for the value of K where $E_{in} = E_{out} - NK$. The phase boundary at $T = 0$ is then found to be at $K = 2.44 \pm 0.01$.

6.2.2 Finite temperature

The results derived from the Monte Carlo simulations at finite temperature are quite intriguing. In figures 6.1, 6.2 and 6.3, both $M_{\parallel}$ and $M_{\perp}$ are plotted as functions of temperature for different values of K in a $N = 40 \times 40$ system.

In figure 6.1, $K = 0.50$ and the data indicate that there is a transition from the paramagnetic phase to an in-plane ordered phase. Thus, in figure 6.1, $M_{\parallel}$ goes

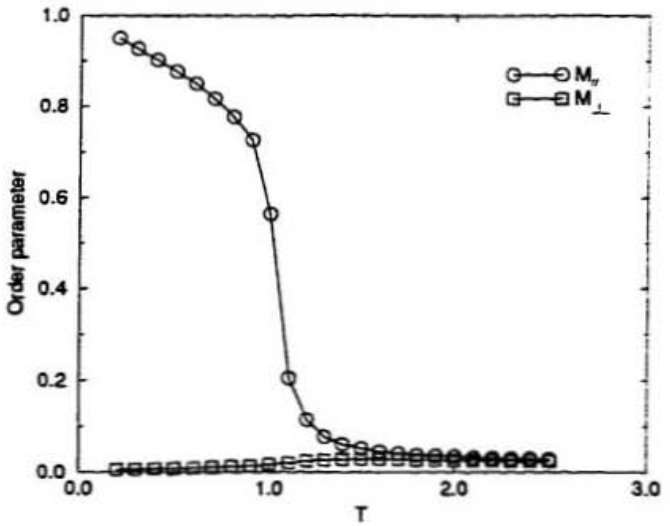

Figure 6.1: The order parameters defined in equations 6.3 and 6.2 as functions of temperature for $K = 0.5$ in a $N = 40 \times 40$ system. Temperature is in units of g/k_B.

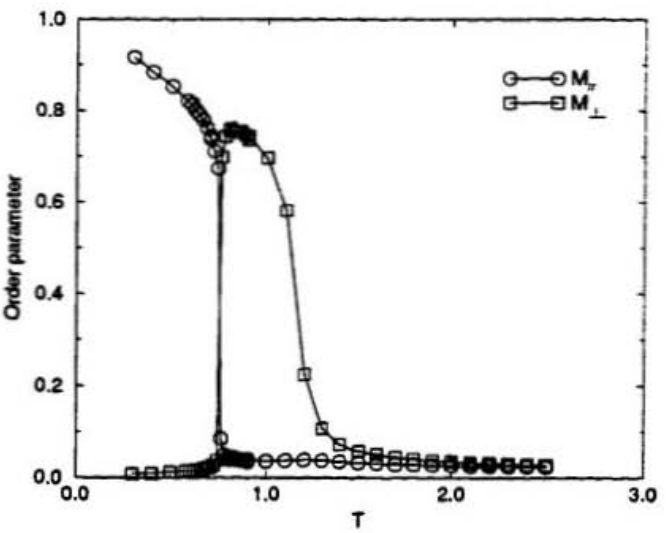

Figure 6.2: The order parameters defined in equations 6.3 and 6.2 as functions of temperature for $K = 1.50$ in a $N = 40 \times 40$ system. Temperature is in units of g/k_B.

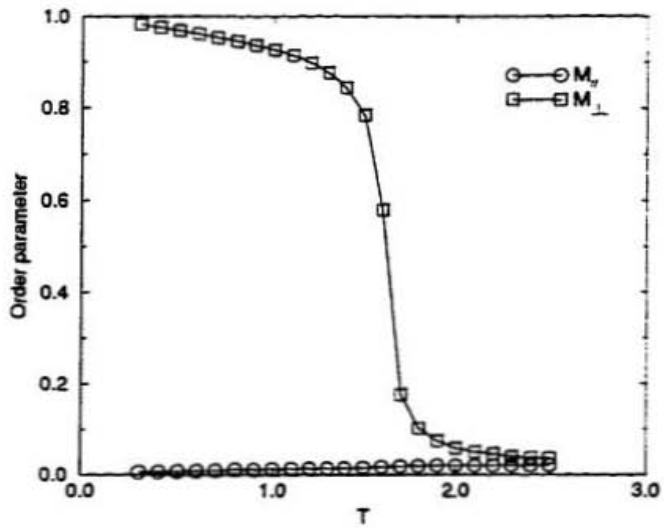

Figure 6.3: The order parameters defined in equations 6.3 and 6.2 as functions of temperature for $K = 3.00$ in a $N = 40 \times 40$ system. Temperature is in units of g/k_B.

sharply from effectively zero (with finite size effects preventing the average from being exactly zero) at high temperature to a finite value at non-zero temperature. Below this temperature it varies approximately linearly with temperature, and extrapolates to 1 at $T = 0$. This is a familiar result of spin wave excitations preventing complete ordering at finite T, which was discussed in depth in chapter 5 with respect to the planar model. $M_\perp$, on the other hand, remains effectively zero for all temperatures. The temperature dependence of the parallel susceptibility is shown in figure 6.4, and the specific heat is shown in figure 6.7. Both quantities have peaks which correspond to the drop in $M_\parallel$.

In figure 6.3, $K = 3.00$ and the data indicate that there is a transition from the

paramagnetic phase to an out-of-plane ordered phase. Thus we see exactly the same behaviour as was seen at $K = 0.5$, except that now it is $M_\perp$ which becomes non-zero at T_c while $M_\parallel$ remains zero at all temperatures. The temperature dependence of the perpendicular susceptibility is shown in figure 6.6. It is consistent with a continuous phase transition as is the specific heat which is shown in figure 6.9.

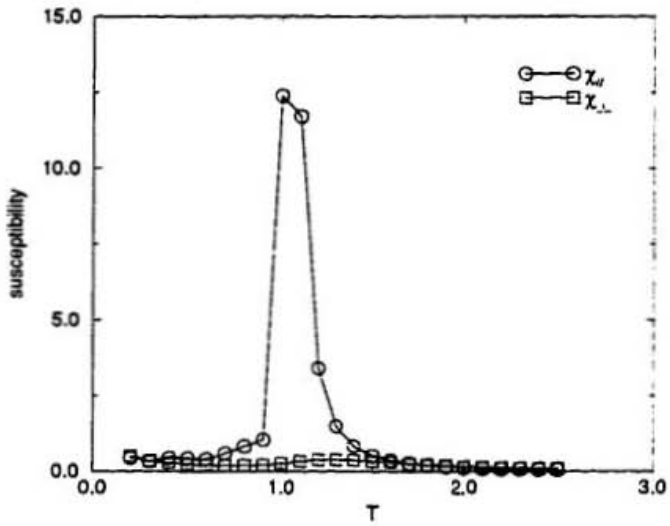

Figure 6.4: The susceptibility defined in equations 6.5 and 6.4 as a function of temperature for $K = 0.5$ in a $N = 40 \times 40$ system. Temperature is in units of g/k_B.

In figure 6.2, $K = 1.50$ and the behaviour of the two order parameters is now very different from that observed in figures 6.1 and 6.3. For this value of K the system starts out in the paramagnetic state at high temperature. As the temperature is lowered the system orders first in the out-of-plane state, so $M_\perp$ becomes non-zero while $M_\parallel$ remains zero. As the temperature is lowered further, the system then

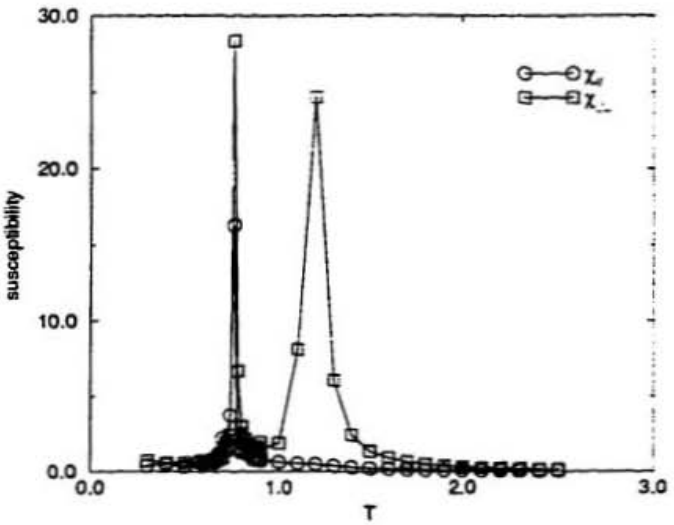

Figure 6.5: The susceptibility defined in equations 6.5 and 6.4 as a function of temperature for $K = 1.50$ in a $N = 40 \times 40$ system. Temperature is in units of g/k_B.

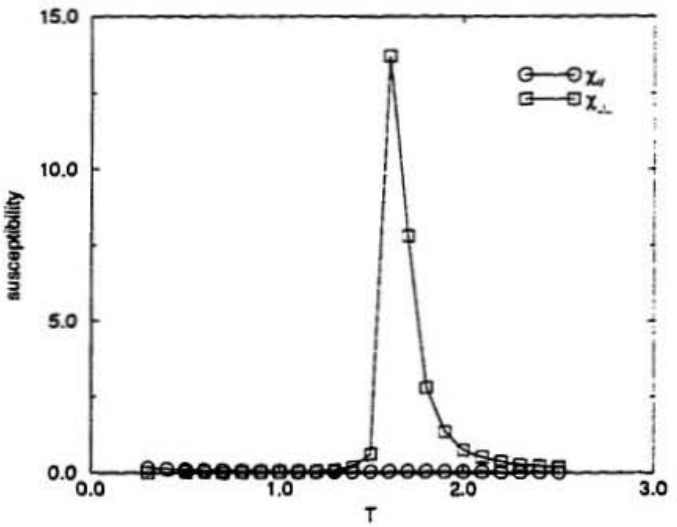

Figure 6.6: The susceptibility defined in equations 6.5 and 6.4 as a functions of temperature for $K = 3.00$ in a $N = 40 \times 40$ system. Temperature is in units of g/k_B.

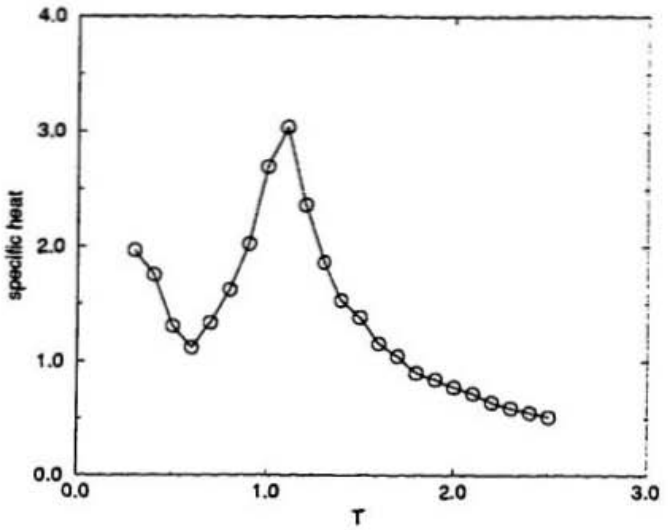

Figure 6.7: The specific heat as function of temperature for $K = 0.5$ in a $N = 40 \times 40$ system. Temperature is in units of g/k_B.

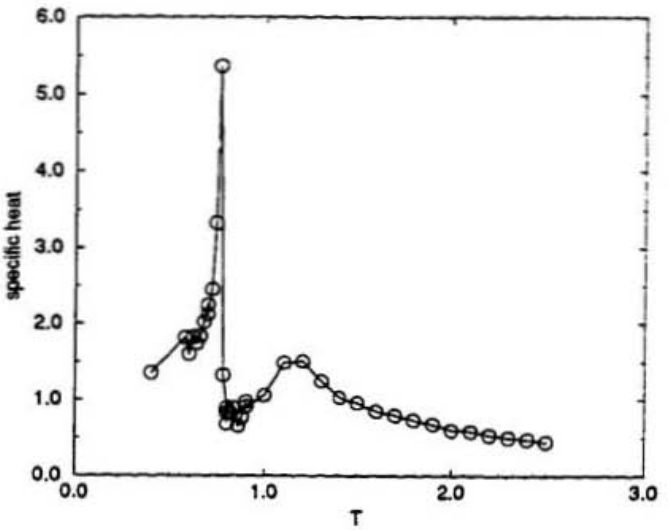

Figure 6.8: The specific heat as function of temperature for $K = 1.50$ in a $N = 40 \times 40$ system. Temperature is in units of g/k_B.

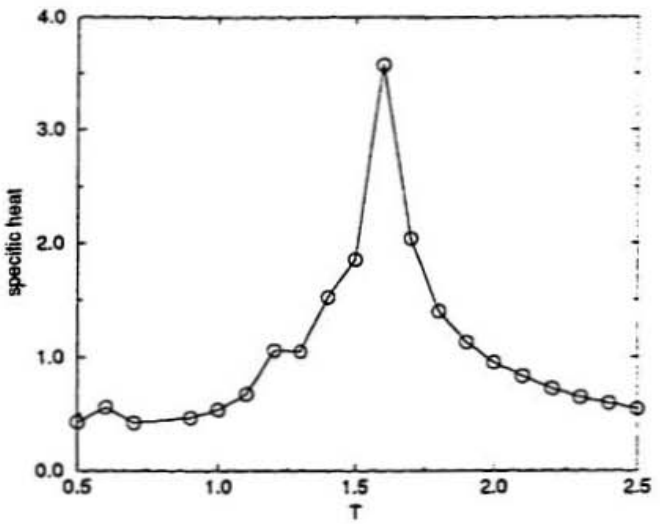

Figure 6.9: The specific heat as function of temperature for $K = 3.00$ in a $N = 40 \times 40$ system. Temperature is in units of g/k_B.

switches such that it orders in-plane; $M_{\parallel}$ becomes non-zero while $M_{\perp}$ effectively drops to zero. The temperature dependence of the specific heat is shown in figure 6.8, and the perpendicular and parallel susceptibilities are shown in figure 6.5.

In figure 6.10 samples of the configurations are shown at various temperatures, with $K = 1.50$, to illustrate the level of order present in the system. The upper configuration in figure 6.10 is from the paramagnetic phase, while the two lower configurations are from ordered phases. Thus in this system there are at least two transitions; one from the paramagnetic phase to the ordered phase shown in the middle configuration, and then a transition to the second ordered phase shown in the lowest configuration. This second transition is the reorientation transition which will

be discussed in more detail in the following sections.

In figures 6.11, 6.12 and 6.13 the order parameters have been plotted for the same values of K as in figures 6.1, 6.2 and 6.3 respectively, but for a number of different system sizes. In both figures 6.11 and 6.12 the finite size effects are consistent with what is expected for a continuous transition. This is not unexpected as in the two limiting cases discussed above, continuous transitions were also found [9, 11]. The transition from the paramagnetic state to the ordered state in figure 6.2 has the same finite size effects seen in figures 6.1 and 6.3. It is reasonable to conclude that this transition is the same as the order-disorder transition that is observed for the other choices of K. Thus the results indicate that an exchange interaction is not necessary for the existence of a reorientation transition.

6.2.3 A closer look at the reorientation transition

In figure 6.14, the two order parameters are shown in the region near the transition temperature. It is clear from this figure that the transition does not exhibit the finite size effects normally associated with a continuous transition. One does not observe a sharpening in the transition as the system size increases as is typically observed near a second order phase transition. At the reorientation transition there is a sharp drop in the average energy, with considerable hysteresis as the temperature is cycled through the transition by first increasing and then decreasing the temperature. This can be seen in figure 6.15. This is typical at a first order transition. Thus there is strong

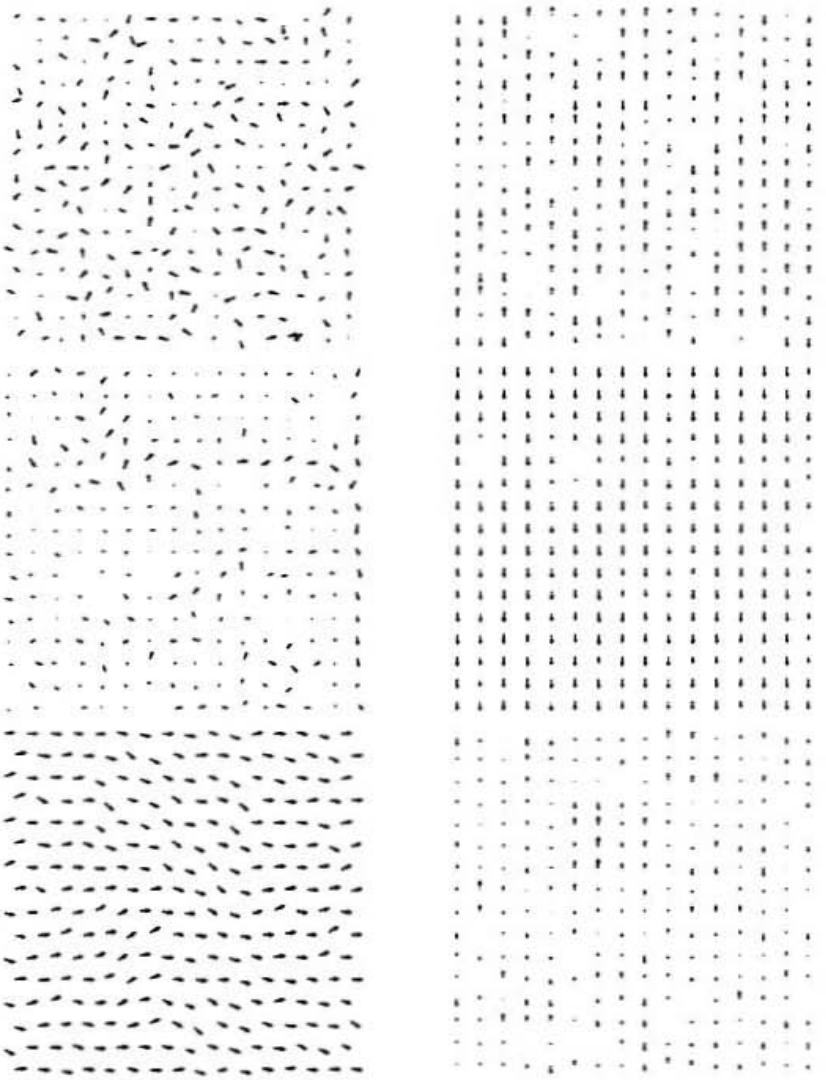

Figure 6.10: Examples of configurations in the three regions of the phase diagram with $K = 1.50$ and $L^2 = 256$. Figures on the left show the projection of the transformed system into the plane of the film, while the figures on the right show the transformed perpendicular components. $T = 2.00$ (upper), $T = 0.80$ (middle), and $T = 0.3$ (lower). Temperature is in units of g/k_B.

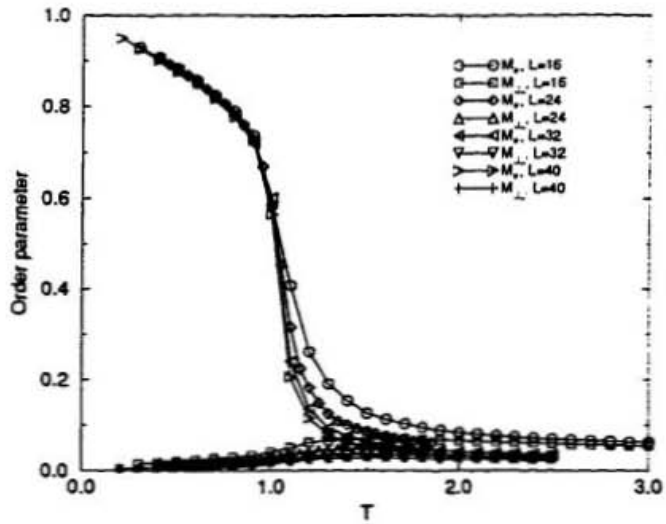

Figure 6.11: The order parameters defined in equations 6.3 and 6.2 as functions of temperature for $K = 0.5$ for various size systems. Temperature is in units of g/k_B.

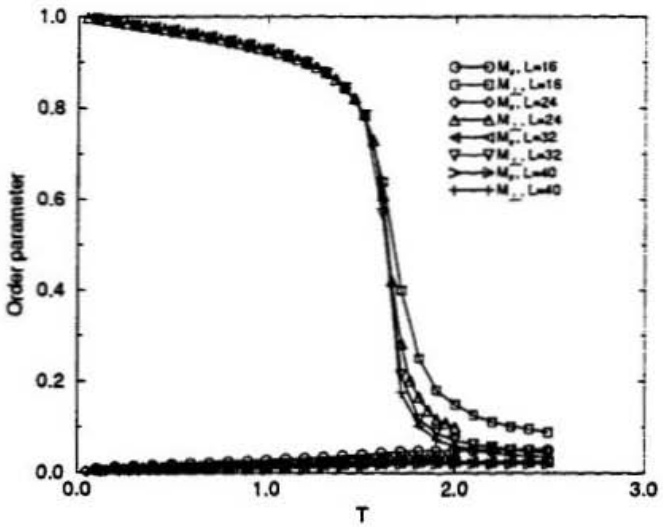

Figure 6.12: The order parameters defined in equations 6.3 and 6.2 as functions of temperature for $K = 1.50$ for various size systems. Temperature is in units of g/k_B.

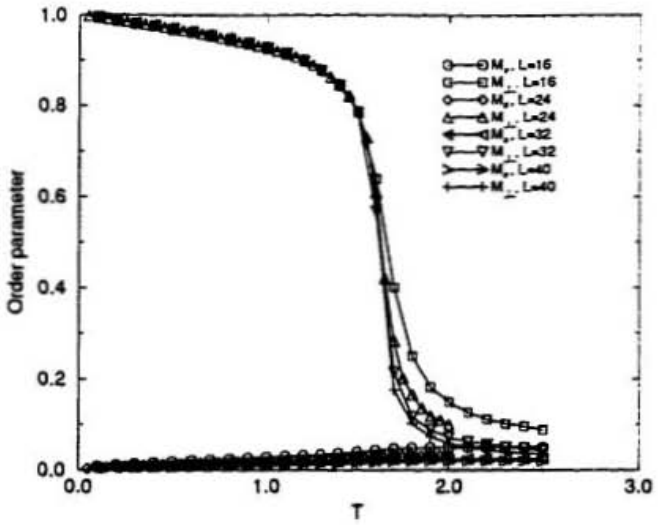

Figure 6.13: The order parameters defined in equations 6.3 and 6.2 as functions of temperature for $K = 3.00$ for various size systems. Temperature is in units of g/k_B.

evidence that the reorientation transition is a first order transition. This is consistent with the previously published results concerning the reorientation transition found in ferromagnetic exchange dominated systems [69]. This leads to a very interesting question concerning how the lines of first order transitions are related when the phase diagrams for both systems are combined. This question will be discussed in the next section.

It is important to note that the location of the reorientation transition can be difficult to determine. There is typically considerable hysteresis associated with a first order transition and that is evident in the results provided by the Monte Carlo simulation. For example, figure 6.16 shows the perpendicular order parameter and

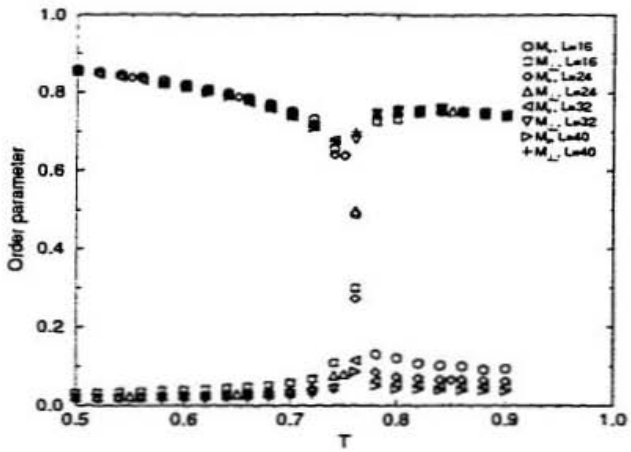

Figure 6.14: The order parameters from figure 6.12 in the region of the reorientation transition. All data shown were collected as the temperature was decreasing. Temperature is in units of g/k_B.

figure 6.15 shows the average internal energy as functions of temperature as calculated using both an increasing temperature and a decreasing temperature simulation. The normal practice is to use the final configuration of one simulation as the initial configuration of a simulation at a different temperature, using approximately the first 10% of the Monte Carlo steps to allow the system to reestablish equilibrium at the new temperature. The change in temperature is always small, either positive or negative. The meta-stability is most troublesome in the region where the reorientation transition temperature is very low, since thermally induced fluctuations are very weak. In this region successive simulations done with decreasing temperature often will not switch over to the in-plane state even at the lowest simulation temperatures. The reorientation can still be observed by starting in the in-plane ordered state and

performing a set of simulations at increasing temperatures.

6.2.4 Phase diagram

In figure 6.17 the results of the Monte Carlo simulations have been collected to form a phase diagram. It includes the results shown above as well as a large number of other simulations done at various values of K and on a number of different size systems. The phase diagram includes the two lines of continuous order-disorder transitions as well as the line of reorientation transitions. If the line of reorientation transitions is a line of first order transitions as it appears to be, then the point at which it meets the two lines of continuous transitions is, by definition, a tri-critical point. This point is indicated in figure 6.17 by a large triangle and is estimated to lie at $T = 0.90 \pm 0.05$ and $K = 1.30 \pm 0.05$.

The phase diagram shown in figure 6.17 is redrawn schematically in figure 6.18(a). Figure 6.18(b) is a schematic of the phase diagram predicted for an exchange dominated ferromagnet [69, 72, 94]. It is easy to see that while the two phase diagrams show certain similarities there are a number of fundamental differences. In particular, the role played by the in-plane phase and the role played by the out-of-plane phase in the reorientation transition have been reversed. In the model studied here the transition is from an in-plane state to an out-of-plane state as the temperature increases. In the ferromagnetic model the transition is from out-of-plane to in-plane as temperature is increased. Therefore the slope of the coexistence line is different in the two

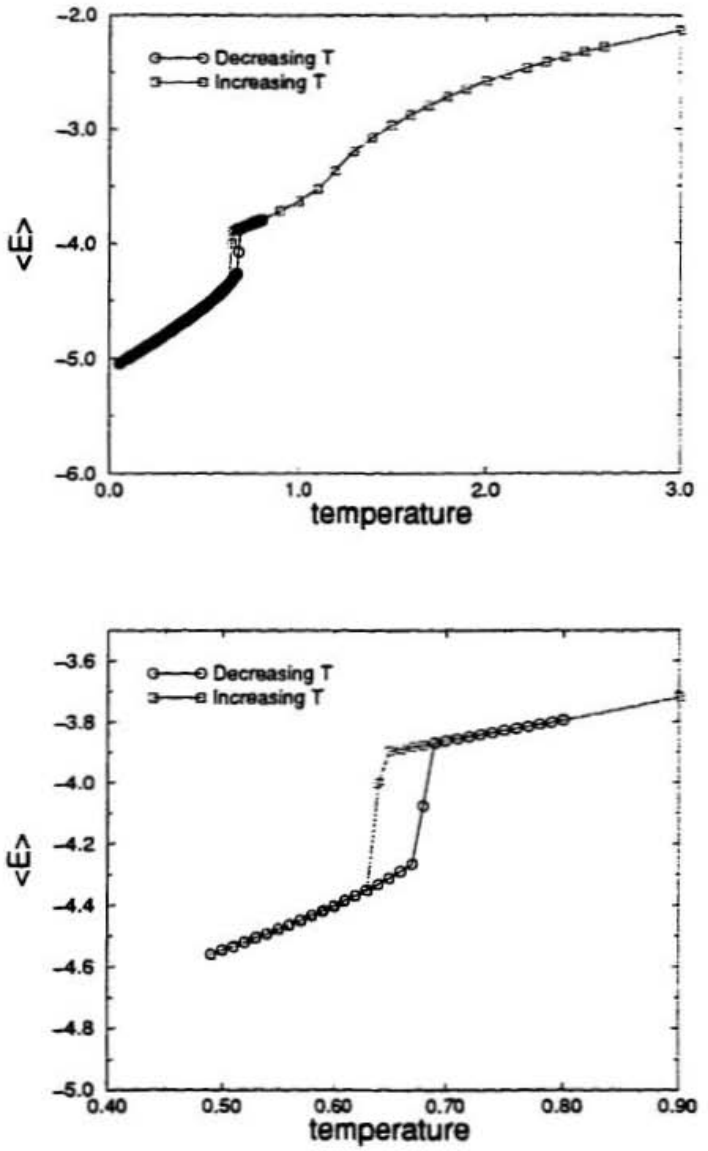

Figure 6.15: The average energy as calculated with decreasing temperature (o) and with increasing temperature (□) in a 40×40 system with $K = 1.70$. Figure (b) is an expanded view of the region near the reorientation transition showing the hysteresis. Temperature is in units of g/k_B.

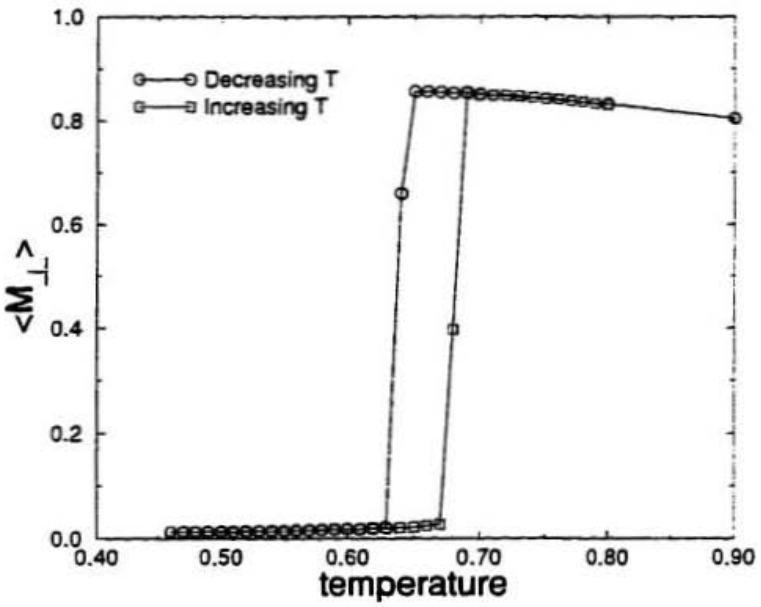

Figure 6.16: The average perpendicular order parameter as calculated with decreasing temperature (○) and with increasing temperature (□) in a 40×40 system with $K = 1.70$ in the region near the reorientation transition. Temperature is in units of g/k_B.

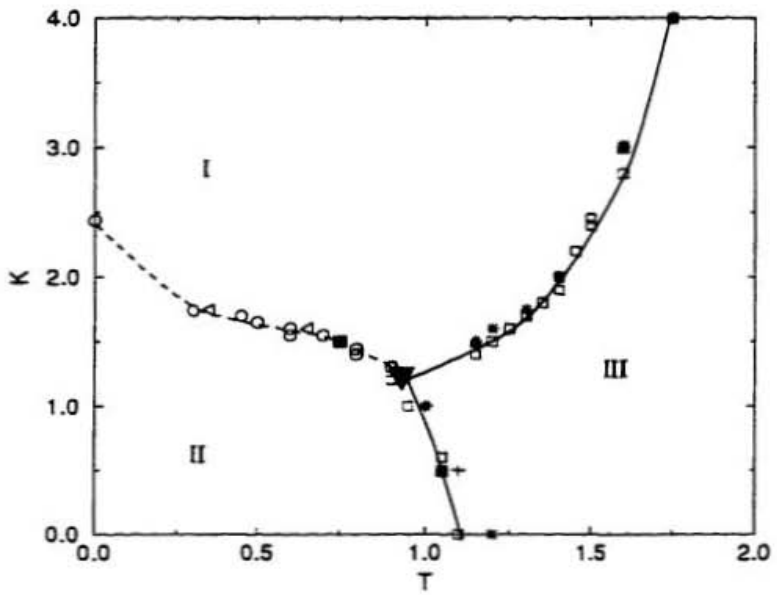

Figure 6.17: Phase diagram obtained from Monte Carlo simulation. Region I is ordered out-of-plane, region II is ordered in-plane, and region III is paramagnetic. The dashed line is a guide to the eye highlighting the line of first-order reorientation transitions between the two ordered states. The solid lines are guides to the eye highlighting the two lines of second order transitions from the paramagnetic state to one of the two ordered states. Points on each line are coded based on system size: $N = 16^2(\bigcirc, \square)$, $24^2(\diamond, \triangle)$, $32^2(\triangleleft, *)$, and $40^2(\triangleright, +)$. Temperature is in units of g/k_B.

models, being negative in the model studied here and positive in the ferromagnetic model. The two lines of first order transition belong to a first order surface in the T-K-J phase diagram. The nature of this surface is an unresolved problem, which is complicated by the existence of the stripe phases discussed in chapter 3. None of the previous studies considered the stripe phases in their analysis.

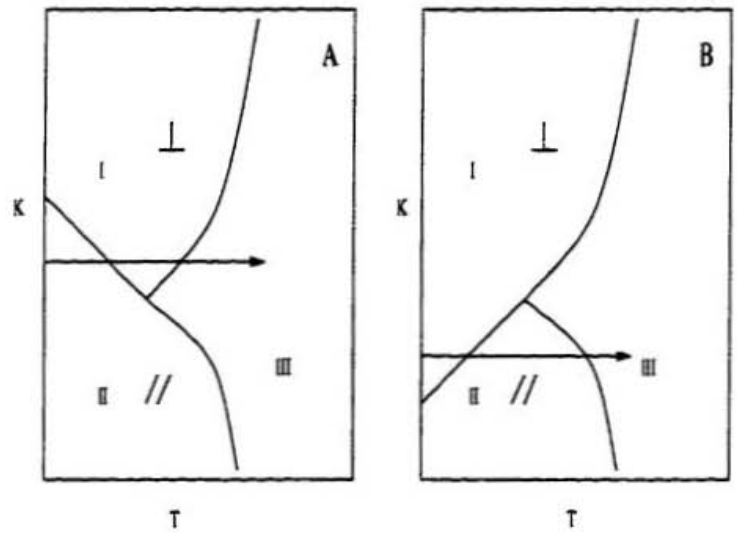

Figure 6.18: Schematic phase diagram for the dipolar model (a) and the ferromagnetic exchange model (b).

6.3 Summary

In summary, the phase diagram for a two-dimensional magnetic mono-layer with a dipolar interaction and a magnetic surface anisotropy has been determined as a function of K and temperature. The phase diagram contains three phases: a paramagnetic phase, an ordered phase with the moments in the plane of the film, and an

ordered phase with the moments perpendicular to the film. The three phases appear to coexist at a tri-critical point. This is the point where the line of reorientation transitions, which appear to be first order, meets the two lines of second order transitions. Comparison of this phase diagram to that predicted for a system with a dominant ferromagnetic exchange interaction shows some similarities, such as the existence of a first-order reorientation transition, but there are interesting differences. In particular the sign of the slope of the coexistence line between the two ordered phases is different, thus the role played by the lowest energy parallel phase and the lowest energy perpendicular phase in the reorientation transition are reversed. It will be interesting to see how the phase diagram changes as a function of J/g, when proper consideration of the stripe phases is included in the analysis.

Chapter 7

Conclusion

7.1 Summary of results

The goal of the studies upon which this thesis is based was to gain a better understanding of the magnetic properties of a model for a magnetic thin film. In particular, a major focus was on understanding the effects of the dipole-dipole interaction on the phase diagram.

For a system in which the magnetic moments are constrained to orient perpendicular to the system, ground state energy calculations were used to establish the ground states for a system with a short-range exchange interaction as well as a dipole-dipole interaction. It was shown that these ground states consist of stripe phases, with the stripe width growing exponentially with the ratio of the strength of the exchange interaction to the strength of the dipolar interaction in the limit of large stripe width.

This calculation helped clarify a discrepancy between the predicted ground states of calculations based on a continuum model and those based on calculations which retained the discrete nature of the system.

At finite temperature, the Monte Carlo study of the uniaxial model proved to be very illuminating. The simulations showed that there was no evidence of a sharp order-disorder transition, as is found in the Ising model of ferromagnetism. Instead, a broad peak is found in the specific heat, and the nature of the transition from the low temperature ordered phase to the fully disordered phase is not clear. It was also shown that there exists a phase intermediate to the fully disordered high temperature phase and the ordered low temperature phase. The low temperature phase consists of stripes which are orientationally ordered. This intermediate phase, called the tetragonal phase, consists of orientationally disordered stripes, The Monte Carlo results indicated that the transition from the stripe phase to the tetragonal phase is continuous in the absence of an applied field.

The addition of an applied field in the uniaxial model leads to a tetragonal phase which consists of elongated islands. The transition from the low temperature stripe phase to the tetragonal phase appears in the Monte Carlo results to be first order for large fields, but the results are not sufficient to determine if the transition is weakly first order or continuous for small fields. As in zero field, the tetragonal phase changes continuously to the fully disordered phase in an applied field. There is no evidence in this study for the existence of a hexagonal or bubble phase. It is possible that these

phases are stable in regions of phase space which our Monte Carlo simulations were not able to probe (eg., at very low temperatures in high fields).

The study of the dipolar planar model has shown that the finite size effects seen in order parameter, as calculated by the Monte Carlo simulation, can not be accounted for by a linearised spin wave calculation. This fact implies that the ordering observed in the simulations will persist in the limit $N \to \infty$. The analysis of the two-point correlation function indicates that there is a continuous transition from the fully disordered phase at high temperature to an ordered phase at low temperature. The low temperature ordered phase is stabilised by a thermally-induced effective anisotropy, the magnitude of which can be crudely estimated at low temperature by comparing the field conjugate to the effective anisotropy, to the equivalent field in the classical XY model. The spin wave analysis used in this thesis treated the full dipolar interaction, including its long-range nature. A number of features which are absent if one approximates the dipolar interaction with a nearest neighbour exchange interaction were highlighted by this analysis.

The final aspect of this thesis was a study of a dipolar Heisenberg model with a magnetic surface anisotropy. Using Monte Carlo simulation to map out the phase diagram as a function of temperature and the ratio of the strengths of the magnetic surface anisotropy and the dipole-dipole interaction, it was shown that this possesses a novel reorientation transition. The phase diagram contained three regions: an ordered region where the magnetic moments are oriented perpendicular to the film,

an ordered region where the magnetic moments are oriented parallel to the film. and a paramagnetic phase. Separating these regions are two lines of second order transitions and a single line of first order transitions. These lines all appear to meet at a tri-critical point.

7.2 Future work

While the study upon which this thesis is based was able to provide answers to a number of questions, there are many which remain to be resolved

In the uniaxial model it is still unclear what the exact mechanism is which leads to the transition from the smectic phase to the tetragonal phase. While it has been speculated that the transition can be understood in terms of the unbinding of topological defects[50, 38, 10], this has not been firmly established. There is also some question concerning the stability of the hexagonal or bubble phase which has been predicted to exist in an applied field at low temperature.

The linearised spin wave calculation, done as part of the study of the planar model, was unable to provide a suitable approximation scheme. A renormalised treatment of the spin waves which takes into account the higher order terms in the expansion may be able to account for these results and provide a more detailed understanding of the anisotropy which is present in the model[92]. The study of the dipolar planar model presented in this thesis is really just a starting point to understanding the nature of this system. The effect of the addition of an exchange interaction or an

applied field has not been addressed at all, and needs to be if one hopes to gain a full understanding of the model. It is also very important when one considers potential applications of magnetic thin films.

As stated in chapter 6, the study of the dipolar Heisenberg model presented in this thesis considers a region of phase space which is quite different from that of the other groups which have been studying similar models. The results presented here and the results of these other studies can be combined to define a larger phase diagram. So far only small pieces of this larger phase diagram are available and it is not completely clear how these pieces will fit together. As well, it is necessary to consider the results of chapters 3, 4, and 5 in forming the larger phase diagram as each provides a limiting case. In particular, the existence of the stripe phases has not yet been considered in any study of the dipolar Heisenberg model. No picture of this model will be complete without a thorough investigation of the stripe phases and their regions of stability in the phase diagram.

Bibliography

[1] R. Kretschmer and K. Binder, Z. Physik B. **34**, 375 (1979).

[2] N. M. Fujiki, K. De'Bell, and D. J. W. Geldart, Physical Review B. **36**, 8512 (1987).

[3] S. V. Maleev, Sov. Phys. JETP **43**, 1240 (1976).

[4] R. Allenspach, M. Stampanoni, and A. Bischof, Physical Review Letters **65**, 3344 (1990).

[5] D. P. Pappas, K.-P. Kämper, and H. Hopster, Physical Review Letters **64**, 3179 (1990).

[6] A. B. MacIsaac, J. P. Whitehead, M. C. Robinson, and K. De'Bell, Physica B. **194–196**, 223 (1994).

[7] A. B. MacIsaac and J. P. Whitehead, in *Proceedings of Supercomputing Symposium '94, Toronto, Ontario*, edited by D. J. W. Ross (University of Toronto, Toronto, 1994).

[8] I. N. Booth, A. B. MacIsaac, K. De'Bell, and J. P. Whitehead, Physical Review Letters **75**, 950 (1995).

[9] A. B. MacIsaac, J. P. Whitehead, M. C. Robinson, and K. De'Bell, Physical Review B **51**, 16033 (1995).

[10] J. Arlett, J. P. Whitehead, A. B. MacIsaac, and K. De'Bell, to appear in Physical Review B (1996).

[11] K. De'Bell, A. B. MacIsaac, I. N. Booth, and J. P. Whitehead, Physical Review B (1996).

[12] A. B. MacIsaac, J. P. Whitehead, K. De'Bell, and P. H. Poole, to appear in Physical Review Letters (1996).

[13] J. M. Kosterlitz and D. J. Thouless, in *Progress in Low Temperature Physics*, edited by D. F. Brewer (North-Holland Publishing Company, Amsterdam, 1978), Vol. VIIB, pp. 371–433.

[14] B. W. Lee *et al.*, Physical Review B. **37**, 2368 (1988).

[15] A. I. Goldman *et al.*, Physical Review B **36**, 7234 (1987).

[16] R. N. Shelton *et al.*, Physica B **148**, 285 (1987).

[17] H. Zhang *et al.*, Physical Review B **41**, 11229 (1990).

[18] J. W. Lynn and W.-H. Li, J. Appl. Phys. **64**, 6065 (1988).

[19] P. Fischer *et al.*, Physica C **152**. 145 (1988).

[20] A. B. MacIsaac, Master's thesis, Memorial University, 1992.

[21] J. P. Whitehead, K. De'Bell, and A. B. MacIsaac, in *Proceedings of Quantum Field Theory and Collective Phenomena, Perugia, Italy, May, 1992*. edited by S. D. Lillo, F. Khanna, G. Semenoff, and P. Sodano (World Scientific, Singapore, 1993).

[22] A. B. MacIsaac, J. P. Whitehead, K. De'Bell, and K. S. Narayanan, Physical Review B. **46**, 6387 (1992).

[23] R. Allenspach and A. Bischof, Physical Review Letters **69**, 3385 (1992).

[24] D. Kerkmann, D. Pescia, and R. Allenspach, Physical Review Letters **68**, 686 (1992).

[25] Z. Q. Qiu, J. Pearson, and S. D. Bader, Physical Review Letters **70**, 1006 (1993).

[26] B. Scholz, R. A. Brand, and W. Keune, Physical Review B **50**, 2537 (1994).

[27] G. V. Sayko, S. Utochkin, and A. K. Zvezdin, Journal of Magnetism and Magnetic Materials **113**, 194 (1992).

[28] F. Baudelet *et al.*, Physical Review B **51**, 12563 (1995).

[29] F. H. Salas and D. Weller, Journal of Magnetism and Magnetic Materials **128**, 209 (1993).

[30] M. Speckmann, H. P. Oepen, and H. Ibach, Physical Review Letters **75**, 2035 (1995).

[31] J. A. C. Bland *et al.*, Journal of Physics: Condensed Matter **7**, 6467 (1995).

[32] H. Fritzsche, J. Kohlhepp, H. J. Elmers, and U. Gradmann, Physical Review B **49**, 15665 (1994).

[33] N. D. Mermin and H. Wagner, Physical Review Letters **17**, 1133 (1966).

[34] Y. Yafet and E. M. Gyorgy, Physical Review B. **38**, 9145 (1988).

[35] B. Kaplan and G. A. Gehring, Journal of Magnetism and Magnetic Materials **128**, 111 (1993).

[36] C. M. Knobler, Advances in Chemical Physics **77**, 397 (1990).

[37] R. M. Weis and H. M. McConnell, Nature **310**, 47 (1984).

[38] M. Seul and R. Wolfe, Physical Review Letters **68**, 2460 (1992).

[39] C. Roland and M. Grant, Physical Review Letters **63**, 551 (1989).

[40] C. Roland and R. Desai, Physical Review B. **42**, 6658 (1990).

[41] C. Sagui and R. Desai, Physical Review E **49**, 2225 (1994).

[42] M. M. Hurley and S. J. Singer, Journal of Physical Chemistry **96**, 1938 (1992).

[43] C. Kittel, *Introduction to Solid State Physics* (John Wiley and Sons, New York, 1986).

[44] N. W. Ashcroft and N. D. Mermin, *Solid State Physics* (Holt, Rinehart and Winston, Orlando, 1976).

[45] N. Goldenfeld, *Lectures on Phase Transitions and the Renormalization Group*, 1st ed. (Addison-Wesley Publishing Company, Reading, 1993).

[46] T. Garel and S. Doniach, Physical Review B. **26**, 325 (1982).

[47] R. Czech and J. Villain, J. Phys.:Condens. Matter **1**, 619 (1989).

[48] M. B. Taylor and B. L. Gyffory, J. Phys. : Condens. Matter **5**, 4527 (1993).

[49] G. A. Gehring and M. Keskin, J. Phys.: Condens. Matt. **5**, L581 (1993).

[50] A. Abanov, V. Kalatsky, V. Pokrovsky, and W. Saslow, Physical Review B **51**, 1023 (1995).

[51] M. M. Hurley and S. J. Singer, Journal of Physical Chemistry **96**, 1951 (1992).

[52] M. M. Hurley and S. J. Singer, Physical Review B **46**, 5783 (1992).

[53] J. M. Kosterlitz and D. J. Thouless, J. Phys. C: Solid State Phys. **6**, 1181 (1973).

[54] J. M. Kosterlitz, J. Phys. C: Solid State Phys. **7**, 1046 (1974).

[55] G. Zimmerman, A. K. Ibrahim, and F. Y. Wu, Physical Review B **37**, 2059 (1988).

[56] C. L. Henley, Physical Review Letters **62**, 2056 (1989).

[57] S. Prakash and C. L. Henley, Physical Review B. **42**, 6574 (1990).

[58] V. M. Bedanov, J. Phys.:Condens. Matter **4**, 75 (1992).

[59] K. M. S. Bajaj, R. Mehrotra, D. Kumar, and V. Soni, Europhysics Letters **27**, 153 (1994).

[60] Y. Yafet, J. Kwo, and E. Gyorgy, Physical Review B **33**, 6519 (1986).

[61] D. Pescia and V. L. Pokrovsky, Physical Review Letters **65**, 2599 (1990).

[62] P. Poloti, A. Rettori, M. G. Pini, and D. Pescia, Europhysics Letters **28**, 71 (1994).

[63] A. M. Polyakov, Physics Letters **59**, 79 (1975).

[64] C. Pich and F. Schwabl, Physical Review B **47**, 7957 (1993).

[65] L. R. Corruccini and S. J. White, Physical Review B **47**, 773 (1993).

[66] R. L. Stamps and B. Hillebrands, Physical Review B **44**, 12417 (1991).

[67] P. Bruno, Physical Review B **43**, 6015 (1991).

[68] A. Moschel and K. D. Usadel, Physical Review B **49**, 12868 (1994).

[69] A. Moschel and K. D. Usadel, Physical Review B **51**, 16111 (1990).

[70] A. Moschel and K. D. Usadel, Journal of Magnetism and Magnetic Materials **140–144**, 649 (1995).

[71] X. Hu and Y. Kawazoe, Physical Review B **51**, 311 (1995).

[72] S. Chui, Physical Review B **50**, 12559 (1990).

[73] A. Hucht, A. Moschel, and K. D. Usadel, Journal of Magnetism and Magnetic Materials **148**, (1995).

[74] A. Hucht and K. D. Usadel, preprint (1995).

[75] K. Binder and D. W. Heermann, *Monte Carlo Simulation in Statistical Physics*, second corrected edition ed. (Springer-Verlag, Berlin, 1993).

[76] K. Binder, in *Monte Carlo Methods in Statistical Physics*, edited by K. Binder (Springer-Verlag, Berlin, 1979), pp. 1–46.

[77] M. N. Barber, in *Phase Transitions and Critical Phenomena*, edited by C. Domb and J. L. Lebowitz (Academic Press, New York, 1983), Vol. 8.

[78] V. Privman, *Finite Size Scaling and Numerical Simulation of Statistical Systems*, 1st ed. (World Scientific Publishing Co. Pte. Ltd., Singapore, 1990).

[79] K. Binder and D. Stauffer, in *Applications of the Monte Carlo Method in statistical physics*, edited by K. Binder (Springer-Verlag, Berlin, 1984), pp. 1–36.

[80] R. W. Swendsen, J.-S. Wang, and A. M. Ferrenberg, in *Topics in Applied Physics:The Monte Carlo Method in Condensed Matter Physics*, edited by K. Binder (Springer-Verlag, Berlin, 1992), Vol. 71, pp. 75–91.

[81] K. Binder, in *Phase Transitions and Critical Phenomena*, edited by C. Domb and M. S. Green (Academic Press, New York, 1976), Vol. 5b, pp. 37–44.

[82] N. Metropolis *et al.*, J. Chem. Phys. **27**, 1087 (1953).

[83] E. Ising, Z. Physik **31**, 253 (1925).

[84] L. Onsager, Physical Review **65**, 117 (1944).

[85] J. P. Whitehead and K. De'Bell, Journal of Physics: Condensed Matter **6**, L731 (1994).

[86] I. N. Booth, Master's thesis, Memorial University, 1995.

[87] D. R. Nelson and B. I. Halperin, Physical Review B **19**, 2457 (1979).

[88] J. Tobochnik and G. V. Chester, Physical Review B **20**, 3761 (1979).

[89] A. B. MacIsaac, I. N. Booth, K. De'Bell, and J. P. Whitehead, submitted for publication to Physical Review B (1996).

[90] J. V. José, L. Kadanoff, S. Kirkpatrick, and D. R. Nelson, Physical Review B **16**, 1217 (1977).

[91] H. E. Stanley and T. A. Kaplan, Physical Review Letters **17**, 913 (1966).

[92] J. P. Whitehead, to be published (1996).

[93] M. Bander and D. L. Mills, Physical Review B. **38**, 12015 (1988).

[94] K. Ried, Y. Millev, M. Fähnle, and H. Kronmüller, Physical Review B **51**, 15229 (1995).

[95] K. De'Bell and J. Whitehead, J. Phys.:Condens. Matter **3**, 2431 (1991).

Appendix A

The energy of stripe and checkerboard phases

In this appendix the dipolar contributions to the energy of the stripe and the checkerboard phases are calculated as functions of the characteristic domain size h.

For the stripe phases the characteristic size is the thickness of the stripe. If the magnetic moments are uniaxial and perpendicular to the plane of the film, then the dipolar energy can be written as

$$E = \sum_{\vec{R}_n \neq \vec{R}_m} \frac{\sigma(\vec{R}_m)\sigma(\vec{R}_n)}{R_{mn}^3}, \tag{A.1}$$

which is a simplification of equation 1.5. $R_{mn} = \vec{R}_m - \vec{R}_n$ and all displacements are scaled by the lattice constant a. The stripe phases are translationally invariant along the $\hat{y}$ direction and are periodic with modulation length $\Lambda = 2h$ in the $\hat{x}$ direction. Given the symmetry of the stripe phases, the sum over all spins $\vec{R}_n$ can be replaced

by a sum over the spins in a single strip of width h and a sum over all superlattice vectors $\vec{G}$ of the stripe phase. Therefore the energy can be rewritten as

$$E = \sum_{\vec{R}_m}{}' \sum_{n=1}^{h} \sum_{\vec{G}} \frac{\sigma(\vec{r}_n + \vec{G})\sigma(\vec{R}_m)}{|\vec{r}_{mn} + \vec{G}|^3} , \tag{A.2}$$

where the vector $\vec{r}_n = (n)\hat{x}$ and is confined to a single strip. The prime on the sum over $\vec{R}_m$ is a reminder that the case when $\vec{R}_m$ and $\vec{r}_n - \vec{G}$ refer to the same spin is excluded. Given the periodicity of the square lattice, as well as the symmetry of the stripe phases, $\vec{G}$ has been defined such that

$$\vec{G} = g_1 h\hat{x} + g_2\hat{y}. \tag{A.3}$$

The symmetry of the stripe phases also means that $\sigma(\vec{R}_m) = -\sigma(\vec{R}_m + h\hat{x})$ with $\sigma(0) \equiv 1$.

The system will be made up of $\frac{N}{h}$ equivalent spins, where N is the total number of spins in the system. Equation A.2 can then be written as

$$E = \frac{N}{h} \sum_{m=1}^{h} \sum_{n=1}^{h}{}' \sum_{\vec{G}} \frac{\sigma(\vec{G} + n\hat{x})\sigma(m\hat{x})}{|\vec{r}_{mn} + \vec{G}|^3} , \tag{A.4}$$

with $\vec{r}_{mn} = (m - n)\hat{x}$. Equation A.4 naturally breaks into two parts. The first part contains the interaction between spins where $\vec{r}_{mn} = 0$. The second part contains all other interactions. Therefore one can write

$$E = \frac{N}{h}\left(h \sum_{\vec{G}\neq 0} \frac{(-1)^{g_1}}{|\vec{G}|^3} + \sum_{m=1}^{h} \sum_{n=1}^{h}{}' \sum_{\vec{G}} \frac{(-1)^{g_1}}{|\vec{r}_{mn} + \vec{G}|^3} \right) , \tag{A.5}$$

where the prime means that the term $m = n$ is excluded from the sum.

The evaluation of the terms appearing in the above expression is complicated by the long-range character of the dipolar interaction and is best accomplished by a variation of the Ewald summation technique described in earlier work [2. 95]. This allows one to express the above summation in terms of a combination of rapidly convergent series.

Consider the second of the two terms that appear in equation A.5. In order to evaluate this sum, the integral representation

$$\frac{1}{R^3} = \frac{4}{\sqrt{\pi}} \int_0^\infty d\rho \, \rho^2 e^{-R^2\rho^2}, \tag{A.6}$$

is used and the sum is written in two parts as

$$\sum_{\vec{G}} \frac{(-1)^{g_1}}{|\vec{r}_{mn} + \vec{G}|^3} = \frac{4}{\sqrt{\pi}} \sum_{\vec{G}} (-1)^{g_1} \int_0^\infty d\rho \, \rho^2 e^{-|\vec{r}_{mn}-\vec{G}|^2\rho^2} \tag{A.7}$$

$$= \frac{4}{\sqrt{\pi}} \sum_{\vec{G}} (-1)^{g_1} \left(\int_0^\eta d\rho \, \rho^2 e^{-|\vec{r}_{mn}-\vec{G}|^2\rho^2} + \int_\eta^\infty d\rho \, \rho^2 e^{-|\vec{r}_{mn}-\vec{G}|^2\rho^2} \right). \tag{A.8}$$

where η is an arbitrary constant. The second integral appearing in equation A.8 can be readily evaluated as

$$\int_\eta^\infty d\rho \, \rho^2 e^{-|\vec{r}_{mn}-\vec{G}|^2\rho^2} = \frac{F_1\left(\eta \left|\vec{r}_{mn} + \vec{G}\right|\right)}{\left|\vec{r}_{mn} + \vec{G}\right|^3}, \tag{A.9}$$

where $F_1(x)$ is given by

$$F_1(x) = \frac{1}{2} x e^{-x^2} + \frac{\sqrt{\pi}}{4} \mathrm{erfc(x)}\,, \tag{A.10}$$

to yield a rapidly convergent series

$$\sum_{\vec{G}} (-1)^{g_1} \frac{4}{\sqrt{\pi}} \int_\eta^\infty d\rho \, \rho^2 e^{-|\vec{r}_{mn}-\vec{G}|^2\rho^2} = \frac{4}{\sqrt{\pi}} \sum_{\vec{G}} (-1)^{g_1} \frac{F_1\left(\eta \left|\vec{r}_{mn} + \vec{G}\right|\right)}{\left|\vec{r}_{mn} + \vec{G}\right|^3}. \tag{A.11}$$

The first sum appearing in equation A.8 can also be made rapidly convergent by converting the sum over superlattice vectors to a sum over the corresponding reciprocal lattice vectors to give

$$\begin{aligned}\sum_{\vec{G}}(-1)^{g_1}\frac{4}{\sqrt{\pi}}\int_0^{\eta}d\rho\,\rho^2 e^{-|\vec{r}_{mn}+\vec{G}|^2\rho^2} &= \frac{4\sqrt{\pi}}{h}\sum_{\vec{Q}}e^{i\vec{Q}\cdot\vec{r}_{mn}}\int_{\frac{1}{\eta}}^{\infty}\frac{d\rho}{\rho^2}e^{-\rho^2|\vec{Q}|^2/4}\\ &= \frac{4\sqrt{\pi}}{h}\sum_{\vec{Q}}\frac{|\vec{Q}|}{2}F_2\left(\frac{|\vec{Q}|}{2\eta}\right)e^{i\vec{Q}\cdot\vec{r}_{mn}}\,, \quad \text{(A.12)}\end{aligned}$$

where $F_2(x)$ has been defined as

$$F_2(x) = \frac{e^{-x^2}}{x} - \sqrt{\pi}\,\mathrm{erfc}(x), \quad \text{(A.13)}$$

and the vector $\vec{Q}$ is given by

$$\vec{Q} = 2\pi\left(\frac{l_1 - 1/2}{h}\hat{x} + l_2\hat{y}\right)\,, \quad \text{(A.14)}$$

where l_1 and l_2 are integers.

The first term appearing in equation A.5 can be evaluated in a similar manner

$$\begin{aligned}\sum_{\vec{G}\neq 0}\frac{(-1)^{g_1}}{|\vec{G}|^3} &= \sum_{\vec{G}\neq 0}(-1)^{g_1}\frac{4}{\sqrt{\pi}}\int_0^{\infty}d\rho\,\rho^2 e^{-|\vec{G}|^2\rho^2},\\ &= \sum_{\vec{G}\neq 0}(-1)^{g_1}\frac{4}{\sqrt{\pi}}\left(\int_0^{\eta}d\rho\,\rho^2 e^{-|\vec{G}|^2\rho^2} + \int_{\eta}^{\infty}d\rho\,\rho^2 e^{-|\vec{G}|^2\rho^2}\right), \quad \text{(A.15)}\end{aligned}$$

where, as in the previous case, the integral has been divided into two parts to improve the convergence properties of the summation.

The second term in equation A.15 can be readily evaluated to give

$$\sum_{\vec{G}\neq 0}\frac{(-1)^{g_1}4}{\sqrt{\pi}}\int_{\eta}^{\infty}d\rho\,\rho^2 e^{-|\vec{G}|^2\rho^2} = \frac{4}{\sqrt{\pi}}\sum_{\vec{G}\neq 0}(-1)^{g_1}\frac{F_1(\eta|\vec{G}|)}{|\vec{G}|^3}\,, \quad \text{(A.16)}$$

where the function $F_1(x)$ was defined earlier by equation A.10. The first term in equation A.15 can be evaluated by transforming the sum over lattice vectors to one over reciprocal lattice vectors to give

$$\sum_{\vec{G}\neq 0}(-1)^{g_1}\frac{4}{\sqrt{\pi}}\int_0^{\eta} d\rho\,\rho^2 e^{-|\vec{G}|^2\rho^2} = \frac{4}{\sqrt{\pi}}\left[\frac{\pi}{h}\sum_{\vec{Q}}\int_{\frac{1}{\eta}}^{\infty}\frac{d\rho}{\rho^2}e^{-\rho^2|\vec{Q}|^2/4} - \frac{\eta^3}{3}\right], \qquad (A.17)$$

where the reciprocal lattice vector $\vec{Q}$ is given by equation A.14.

This integral can be readily evaluated to give

$$\sum_{\vec{G}\neq 0}(-1)^{g_1}\frac{4}{\sqrt{\pi}}\int_0^{\eta} d\rho\,\rho^2 e^{-|\vec{G}|^2\rho^2} = \frac{4}{\sqrt{\pi}}\left[\frac{\pi}{h}\sum_{\vec{Q}}\frac{|\vec{Q}|}{2}F_2\left(\frac{|\vec{Q}|}{2\eta}\right) - \frac{\eta^3}{3}\right]. \qquad (A.18)$$

Combining terms one has that

$$\begin{aligned}\frac{E}{N} &= \frac{4}{\sqrt{\pi}}\left(\sum_{\vec{G}\neq 0}(-1)^{g_1}\frac{F_1(\eta|\vec{G}|)}{|\vec{G}|^3} + \frac{1}{h}\sum_{\vec{G}}\sum_{m=1}^{h}\sum_{n=1}^{h}{}'(-1)^{g_1}\frac{F_1(\eta|\vec{r}_{mn}+\vec{G}|)}{|\vec{r}_{mn}+\vec{G}|^3}\right)\\ &+ \frac{4\sqrt{\pi}}{h}\sum_{\vec{Q}}\frac{|\vec{Q}|}{2}F_2(\frac{|\vec{Q}|}{2\eta})\left(1+\frac{1}{h}\sum_{m=1}^{h}\sum_{n=1}^{h}{}'e^{i\vec{Q}\cdot\vec{r}_{mn}}\right) - \frac{4\eta^3}{3\sqrt{\pi}}. \qquad (A.19)\end{aligned}$$

A similar calculation can be carried out for the checkerboard phases. One begins again with equation A.1. The characteristic domain is now a square of size h by h. Hence the system now possesses periodicity in both the $\hat{x}$ and $\hat{y}$ directions with a modulation length $\Lambda = 2h$. Therefore the sum over all spins n can be replaced by a sum over all spins in a single square of size $h \times h$ and a sum over all superlattice vectors $\vec{G}$.

$$E = \sum_{\vec{R}_m}{}'\sum_{n=1}^{h^2}\sum_{\vec{G}}\frac{\sigma(\vec{r}_n+\vec{G})\sigma(\vec{r}_m)}{|\vec{r}_{mn}+\vec{G}|^3}. \qquad (A.20)$$

Here the vector $\vec{r}_n$ is confined to lie in a single square of spins. For the checkerboard

phases the superlattice vector $\vec{G}$ is defined as

$$\vec{G} = g_1 h\hat{x} + g_2 h\hat{y}, \tag{A.21}$$

and the symmetry of the system is such that

$$\sigma(\vec{r}) = (-1)^{g_1+g_2}\sigma(\vec{r}+\vec{G}). \tag{A.22}$$

The system is now made up of $\frac{N}{h^2}$ equivalent sites and one can write equation A.20 as

$$E = \frac{N}{h^2}\sum_{m=1}^{h^2}\sum_{n=1}^{h^2}{}'\sum_{\vec{G}}\frac{\sigma(\vec{r}_n+\vec{G})\sigma(\vec{r}_m)}{|\vec{r}_{mn}+\vec{G}|^3}, \tag{A.23}$$

where both $\vec{r}_n$ and $\vec{r}_m$ are confined to lie within the single square of spins. Using equation A.22, equation A.23 can be written as

$$E = \frac{N}{h^2}\left(h^2\sum_{\vec{G}\neq 0}\frac{(-1)^{g_1+g_2}}{|\vec{G}|^3} + \sum_{m=1}^{h^2}\sum_{n=1}^{h^2}{}'\sum_{\vec{G}}\frac{(-1)^{g_1+g_2}}{|\vec{r}_{mn}+\vec{G}|^3}\right), \tag{A.24}$$

where the prime means that the term $m = n$ is excluded from the sum. The calculation proceeds exactly as for the stripe phases and hence only the conclusion is quoted here.

$$\begin{aligned}\frac{E}{N} &= \frac{4}{\sqrt{\pi}}\left(\sum_{\vec{G}\neq 0}(-1)^{g_1+g_2}\frac{F_1(\eta|\vec{G}|)}{|\vec{G}|^3} + \frac{1}{h^2}\sum_{\vec{G}}\sum_{m=1}^{h^2}\sum_{n=1}^{h^2}{}'(-1)^{g_1+g_2}\frac{F_1(\eta|\vec{r}_{mn}+\vec{G}|)}{|\vec{r}_{mn}+\vec{G}|^3}\right)\\ &+ \frac{4\sqrt{\pi}}{h^2}\sum_{\vec{Q}}\frac{|\vec{Q}|}{2}F_2\left(\frac{|\vec{Q}|}{2\eta}\right)\left(1+\frac{1}{h^2}\sum_{m=1}^{h^2}\sum_{n=1}^{h^2}{}'e^{i\vec{Q}\cdot\vec{r}_{mn}}\right) - \frac{4\eta^3}{3\sqrt{\pi}}.\end{aligned} \tag{A.25}$$

In this result the definitions of the functions F_1 and F_2 are as given before for the stripe phase calculation, but the vectors $\vec{G}$ are as given in equation A.21 and $\vec{Q}$ is now given by

$$\vec{Q} = 2\pi\left(\frac{l_1 - 1/2}{h}\hat{x} + \frac{l_2 - 1/2}{h}\hat{y}\right), \tag{A.26}$$

where l_1 and l_2 are integers.

Appendix B

Spin wave expansion for the dipolar planar model

B.1 The Hamiltonian

In this appendix the dipolar Hamiltonian is expanded to leading order in fluctuations about the ground state. One begins with the dipolar contribution to the Hamiltonian in units of μ_{eff}^2/a^3;

$$\mathcal{H} = \frac{1}{2} \sum_{\vec{r}_n, \vec{r}_m}{}' \sigma^{\alpha}(\vec{r}_n) \Gamma^{\alpha\beta}(\vec{r}_{nm}) \sigma^{\beta}(\vec{r}_m). \tag{B.1}$$

In this expression

$$\vec{r}_n = n_x \hat{x} + n_y \hat{y}, \tag{B.2}$$

where $n_x, n_y = 0, \pm 1, \pm 2 \ldots$ define the square lattice and all distances and displacements have been scaled by the lattice constant a.

$$\Gamma^{\alpha\beta}(\vec{r}_{nm}) = \lim_{\vec{r}\to 0} \frac{\partial}{\partial r^\alpha} \frac{\partial}{\partial r^\alpha} \frac{1}{|\vec{r}_{nm} - \vec{r}|} \tag{B.3}$$

is the dipole-dipole interaction between moments separated by $\vec{r}_{nm} = \vec{r}_n - \vec{r}_m$. The sum is a double sum over all lattice points in the system, excluding $n = m$, as indicated by the prime on the sum. The Hamiltonian is then rewritten in terms of the unit cell defined in figure B.1 using the notation

$$\sigma_u^\alpha(\vec{R}_n) = \sigma^\alpha(\vec{R}_n + \vec{r}_u), \tag{B.4}$$

$$\Gamma_{uvnm}^{\alpha\beta} = \Gamma^{\alpha\beta}(\vec{R}_{nm} + \vec{r}_{uv}), \tag{B.5}$$

where $\vec{R}_n$ is now a vector which indicates the position of the origin for a unit cell rather than a lattice point and is defined by

$$\vec{R}_n = 2n_x\hat{x} + 2n_y\hat{y} \tag{B.6}$$

with $n_x, n_y = 0, \pm 1, \pm 2 \ldots$. As shown in figure B.1 the vectors, $\vec{r}_u$, define the four sites in the unit cell with

$$\vec{r}_1 = 0\hat{x} + 0\hat{y} \tag{B.7}$$

$$\vec{r}_2 = 1\hat{x} + 0\hat{y} \tag{B.8}$$

$$\vec{r}_3 = 0\hat{x} + 1\hat{y} \tag{B.9}$$

$$\vec{r}_4 = 1\hat{x} + 1\hat{y}. \tag{B.10}$$

The Hamiltonian can then be written as

$$\mathcal{H} = \sum_{\vec{R}_n, \vec{R}_m} \sum_{u,v=1}^{4\prime} \sigma_u^{\alpha}(\vec{R}_n) \Gamma_{uvnm}^{\alpha\beta} \sigma_v^{\beta}(\vec{R}_m). \tag{B.11}$$

The sums over $\vec{R}_n$ and $\vec{R}_m$ are sums over all unit cells as given by equation B.6, while the sums over u and v are over spins within a unit cell. The prime on the sum now indicates that for $n = m$ one must exclude terms with $u = v$. Note that terms with $n = m$, but $u \neq v$ are included in the sums.

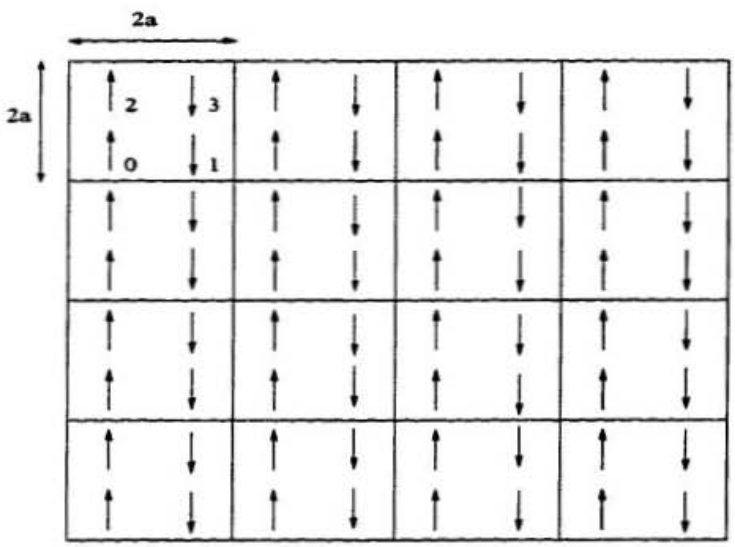

Figure B.1: The unit cell used in the spin wave calculations. A unit cell is $2a \times 2a$, and contains 4 spins. This figure shows 16 unit cells. The labelling scheme used is indicated in the upper left unit cell.

The ground state can now be characterised by a single variable using the transformation given below in equations B.12 and B.13, which are applied to the magnetic moments

$$\tilde{\sigma}^z(\vec{r}) \;=\; (-1)^{n_y} \sigma^z(\vec{r}), \tag{B.12}$$

$$\tilde{\sigma}^y(\vec{r}) \;=\; (-1)^{n_x}\sigma^y(\vec{r}). \tag{B.13}$$

The Hamiltonian can then written as

$$\mathcal{H} = \sum_{u,v=1}^{4}\sum_{n,m}{}'\tilde{\sigma}^{\alpha}_{u}(\vec{R}_n)A^{\alpha\beta}_{uv}\Gamma^{\alpha\beta}_{uvnm}\tilde{\sigma}^{\beta}_{v}(\vec{R}_m), \tag{B.14}$$

where $A^{\alpha\beta}_{uv}$ is given by

$$A^{\alpha\beta}_{uv} = (-1)^{|\vec{r}_u - \vec{r}^{\,\alpha}_u|}(-1)^{|\vec{r}_v - \vec{r}^{\,\beta}_v|}, \tag{B.15}$$

which is just a convenient manner of representing the inverse of the transform (it is also the transform itself, since $A^{\alpha\beta}_{uv}$ is its own inverse). After the transformation, the spin state can be specified by an angle $\theta(\vec{R}_n + \vec{r}_u) \equiv \theta_{n,u}$, such that

$$\tilde{\sigma}^x_u(\vec{R}_n) \;=\; \cos(\theta_{n,u}) \tag{B.16}$$

$$\tilde{\sigma}^y_u(\vec{R}_n) \;=\; \sin(\theta_{n,u}), \tag{B.17}$$

As stated previously in the text, all ground states will be characterised by an angle, θ_0, which is the angle the ordered spins make with the x-axis. Next the angle $\theta_{n,u}$ made by the spin at $\vec{R}_n + \vec{r}_u$ is perturbed by some small amount $\delta\theta_{n,u}$; so that $\theta_{n,u} \to \theta_0 + \delta\theta_{i,k}$. The Hamiltonian is expanded in terms of these fluctuations, giving

$$\mathcal{H} \;=\; \mathcal{H}_0 + \mathcal{H}_1 + \mathcal{H}_2 + \ldots \tag{B.18}$$

$$\;=\; E_0 + \sum_i\sum_{k=1}^{4}\delta\theta_{i,k}\frac{\partial}{\partial\theta_{i,k}}\mathcal{H}|_{\theta_0} + \frac{1}{2}\sum_{i,j}\sum_{l',k'=1}^{4}\delta\theta_{i,l}{}'\frac{\partial}{\partial\theta_{i,k}}\frac{\partial}{\partial\theta_{j,l}}\mathcal{H}|_{\theta_0}\delta\theta_{j,l} + \ldots \tag{B.19}$$

E_0 is the ground state energy, while $\mathcal{H}_1$ is zero by definition and defines the set of angles θ_0 associated with the ground state configurations. $\mathcal{H}_2$ gives the lowest order

correction to the Hamiltonian in terms of the fluctuations. After taking the two derivatives and evaluating the result at $\theta_{i,k} = \theta_0$, $\mathcal{H}_2$ can be written as

$$\mathcal{H}_2 = \sum_{i,j}\sum_{l',k'=1}^{4} \delta\theta_{i,l'} \left\{ -\delta_{l',k'}\delta_{i,j} \sum_{k=1}^{4}\sum_{m}(1-\delta_{j,m}\delta_{k,k'}) \sum_{\alpha\beta} B^{\alpha\beta} A^{\alpha\beta}_{k',k} \Gamma^{\alpha\beta}_{k',kjm} + (1-\delta_{i,j}\delta_{l',k'}) \sum_{\alpha\beta} C^{\alpha\beta} A^{\alpha\beta}_{k',l'} \Gamma^{\alpha\beta}_{k',l',ji} \right\} \delta\theta_{j,k'}, \tag{B.20}$$

where B and C are defined as

$$B = \begin{pmatrix} \cos^2(\theta_0) & \sin(\theta_0) \\ \sin(\theta_0) & \sin^2(\theta_0) \end{pmatrix},$$

$$C = \begin{pmatrix} \sin^2(\theta_0) & -\sin(\theta_0) \\ -\sin(\theta_0) & \cos^2(\theta_0) \end{pmatrix}.$$

Next, one Fourier transforms the fluctuations in the magnetic moments, such that

$$\delta\theta_k(\vec{q}) = \sum_{\vec{R}} \delta\theta_k(\vec{R}) e^{-i\vec{q}\cdot\vec{R}}, \tag{B.21}$$

while the inverse transform gives

$$\delta\theta_k(\vec{R}) = \frac{1}{\pi^2}\int_{\Omega_B} d\vec{q}; \delta\theta_k(\vec{q}) e^{i\vec{q}\cdot\vec{R}}, \tag{B.22}$$

where the integral is over the first Brillouin zone. The first Brillouin zone is a square with $-\frac{\pi}{2} > q_\alpha > \frac{\pi}{2}$. Two useful results are

$$\frac{1}{\pi^2}\int_{\Omega_B} e^{i\vec{q}\cdot(\vec{R}-\vec{R}')} = \delta(\vec{R}-\vec{R}'), \tag{B.23}$$

$$\sum_{\vec{R}} e^{i(\vec{q}-\vec{q}')\cdot\vec{R}} = \pi^2 \sum_{\vec{Q}} \delta(\vec{q}-\vec{q}'+\vec{Q}), \tag{B.24}$$

where $\vec{Q}$ is a reciprocal lattice vector. After substituting equation B.22 into equation B.20. and simplifying one can write the Hamiltonian as

$$\mathcal{H} = E_0 + \sum_{u,v} \int_{\Omega_B} d\vec{q}\delta\theta_u(\vec{q})G_{uv}(\vec{q})\delta\theta_v(-\vec{q}), \tag{B.25}$$

which is equivalent to equation 5.7 quoted in the main text. $G_{uv}(\vec{q})$ can be written as

$$\begin{aligned} G_{uv}(\vec{q}) &= -\delta_{uv}\frac{1}{\pi^2}\sum_{\alpha\beta}\sum_{k=1}^{4}\sum_{\vec{R}}(1-\delta(\vec{R})\delta_{uk})A_{uk}^{\alpha\beta}B^{\alpha\beta}\Gamma_{uk}^{\alpha\beta}(\vec{R}) + \\ &\quad \frac{1}{\pi^2}\sum_{\alpha\beta}\sum_{\vec{R}}(1-\delta(\vec{R})\delta_{uv})A_{vu}^{\alpha\beta}C^{\alpha\beta}\Gamma_{vu}^{\alpha\beta}(\vec{R})e^{-i\vec{q}\cdot\vec{R}}. \end{aligned} \tag{B.26}$$

To simplify later calculations and to highlight features of the various terms, the q-dependent and q-independent parts of $G_{uv}(\vec{q})$ are separated:

$$G_{uv}(\vec{q}) = \delta_{uv}\mathcal{A}_u + \gamma_{uv}(\vec{q}), \tag{B.27}$$

where

$$\mathcal{A}_u \equiv -\frac{1}{\pi^2}\sum_{\alpha\beta}\sum_{k=1}^{4}A_{uk}^{\alpha\beta}B^{\alpha\beta}\Delta_{uk}^{\alpha\beta}(0), \tag{B.28}$$

$$\gamma_{uv}(\vec{q}) \equiv \frac{1}{\pi^2}\sum_{\alpha\beta}A_{uv}^{\alpha\beta}C^{\alpha\beta}\Delta_{uv}^{\alpha\beta}(\vec{q}), \tag{B.29}$$

$$\Delta_{uv}^{\alpha\beta}(\vec{q}) \equiv \sum_{\vec{R}}(1-\delta(\vec{R})\delta_{uv})\Gamma_{uv}^{\alpha\beta}(\vec{R})e^{-i\vec{q}\cdot\vec{R}}. \tag{B.30}$$

To calculate $\Delta_{uv}^{\alpha\beta}(\vec{q})$ the standard methods of Ewald summations are applied as has been explained previously in Appendix A and in earlier work [22]. The result for $u \neq v$ gives

$$\Delta_{uv}^{\alpha\beta}(\vec{q}) = \frac{4}{\sqrt{\pi}}\sum_{\vec{R}}\frac{\left(R^\alpha + r_{uv}^\alpha\right)\left(R^\beta + r_{uv}^\beta\right)}{\left|\vec{R}+\vec{r}_{uv}\right|^5}e^{-i\vec{q}\cdot\vec{R}}\Gamma\left(\frac{5}{2};\eta^2\left|\vec{R}+\vec{r}_{uv}\right|\right)$$

$$-\delta_{\alpha\beta}\frac{2}{\sqrt{\pi}}\sum_{\vec{R}}\frac{e^{-i\vec{q}\cdot\vec{R}}}{\left|\vec{R}+\vec{r}_{uv}\right|^3}\Gamma\left(\frac{3}{2};\eta^2\left|\vec{R}+\vec{r}_{uv}\right|^2\right)$$
$$-\frac{\sqrt{\pi}}{2}\sum_{\vec{R}\neq 0}\frac{\left(q^\alpha+\frac{\pi\vec{R}^\alpha}{2}\right)\left(q^\beta+\frac{\pi\vec{R}^\beta}{2}\right)}{\left|\vec{q}+\frac{\pi\vec{R}}{2}\right|}e^{-i(\vec{q}+\frac{\pi\vec{R}}{2})\cdot\vec{r}_{uv}}\Gamma\left(\frac{1}{2};\frac{\left|\vec{q}+\frac{\pi\vec{R}}{2}\right|^2}{4\eta^2}\right)$$
$$-\frac{\pi}{2}\frac{q^\alpha q^\beta}{|\vec{q}|}e^{i\vec{q}\cdot\vec{r}_{uv}}\mathrm{erfc}\left(\frac{|\vec{q}|}{2\eta}\right), \qquad \text{(B.31)}$$

while for $u = v$

$$\begin{aligned}\Delta_{uu}^{\alpha\beta}(\vec{q}) &= \frac{4}{\sqrt{\pi}}\sum_{\vec{R}}\frac{\left(R^\alpha R^\beta\right)}{\left|\vec{R}\right|^5}e^{-i\vec{q}\cdot\vec{R}}\Gamma\left(\frac{5}{2};\eta^2\left|\vec{R}\right|\right)\\ &-\delta_{\alpha\beta}\frac{2}{\sqrt{\pi}}\sum_{\vec{R}}\frac{e^{-i\vec{q}\cdot\vec{R}}}{\left|\vec{R}\right|^3}\Gamma\left(\frac{3}{2};\eta^2\left|\vec{R}\right|^2\right)\\ &-\frac{\sqrt{\pi}}{2}\sum_{\vec{R}\neq 0}\frac{\left(q^\alpha+\frac{\pi\vec{R}^\alpha}{2}\right)\left(q^\beta+\frac{\pi\vec{R}^\beta}{2}\right)}{\left|\vec{q}+\frac{\pi\vec{R}}{2}\right|}\Gamma\left(\frac{1}{2};\frac{\left|\vec{q}+\frac{\pi\vec{R}}{2}\right|^2}{4\eta^2}\right)\\ &+\delta_{\alpha\beta}\frac{4\eta^{-3}}{3\sqrt{\pi}}-\frac{\pi}{2}\frac{q^\alpha q^\beta}{|\vec{q}|}\mathrm{erfc}\left(\frac{|\vec{q}|}{2\eta}\right), \qquad \text{(B.32)}\end{aligned}$$

where $\Gamma(x;y)$ is the incomplete Gamma function and erfc(x) is the complementary error function. In this form it is possible to efficiently calculate $\Delta_{uu}^{\alpha\beta}(\vec{q})$, and hence the Hamiltonian.

B.2 Partition function

This is a calculation of the partition function of the dipolar systems in the spin wave approximation for a system of finite size, $N = 2L \times 2L$ (L^2 units cells and $4L^2$ spins). By definition the partition function is given by

$$Z = \sum_{\text{all states}} \exp\left(\frac{-\mathcal{H}}{k_B T}\right). \qquad \text{(B.33)}$$

In the spin wave approximation one can write this as

$$Z_{sw} = \left(\prod_{\vec{R}} \int_{-\infty}^{\infty} d\overline{\phi}\left(\vec{R}\right) \right) \exp\left(-H_{sw}\left[\overline{\phi}\left(\vec{R}\right)\right] \right), \tag{B.34}$$

with

$$H_{sw}\left[\overline{\phi}\left(\vec{R}\right)\right] = \frac{1}{k_B T} \sum_{\vec{R},\vec{R}'} \overline{\phi}(\vec{R}) \hat{G}\left(\vec{R} - \vec{R}'\right) \overline{\phi}(\vec{R}'). \tag{B.35}$$

$\left[\overline{\phi}\left(\vec{R}\right)\right]$ specifies the set of orientations of all the spins in the system after being transformed by the transform given in equations B.12 and B.13. To simplify the expressions the following notation is adopted. $\overline{\phi}(\vec{R}) = (\phi_1, \phi_2, \phi_3, \phi_4)$ is a four component vector which gives the orientation of the moments in the unit cell with origin at $\vec{R}$. Matrices will be denoted with either a $\hat{}$ or $\tilde{}$, where the $\tilde{}$ will signify a diagonal matrix. Any four component vector will be signified by the $\bar{}$ over line. The following substitutions are now made:

$$\phi_\alpha\left(\vec{R}\right) = \frac{1}{\sqrt{N}} \sum_{\vec{q}} \phi_\alpha(\vec{q})\, e^{i\vec{q}\cdot\vec{R}} \tag{B.36}$$

$$\phi_\alpha(\vec{q}) = \frac{1}{\sqrt{N}} \sum_{\vec{R}} \phi_\alpha\left(\vec{R}\right) e^{-i\vec{q}\cdot\vec{R}}. \tag{B.37}$$

After Fourier transformation the Hamiltonian can be represented by

$$H_{sw}\left[\phi\left(\vec{q}\right)\right] = \sum_{\vec{q}} \overline{\phi}(\vec{q})^t \hat{G}\left(\vec{q}\right) \overline{\phi}(-\vec{q}). \tag{B.38}$$

The temperature dependence of is now contained in $\hat{G}\left(\vec{q}\right)$. The partition function can now be written as

$$Z_{sw} = \left(\prod_{\vec{q}}{}' \int_{\infty}^{-\infty} d\overline{\phi}\left(\vec{q}\right) \right) \exp\left(-H_{sw}\left[\phi\left(\vec{q}\right)\right] \right), \tag{B.39}$$

In changing from integrals over $\phi\left(\vec{R}\right)$ to integrals over $\phi\left(\vec{q}\right)$, the integration has changed from being over real fields to an integration over complex fields and hence might appear to have increased the degrees of freedom from $4L^2$ to $8L^2$. This is not the case, since by symmetry $\phi\left(\vec{q}\right) = \phi^*\left(-\vec{q}\right)$. To adjust for this change the integrations are only over $d\phi\left(\vec{q}\right)$, where $\vec{q}$ lies in the upper half of the Brillouin zone (the half above $q_y = 0$). Bear in mind that at this point the sums over $\vec{q}$ still run over the entire Brillouin zone.

The next step is to diagonalise $\hat{G}\left(\vec{q}\right)$ by changing the basis such that

$$\overline{\phi}(\vec{q})^t \hat{G}\left(\vec{q}\right) \overline{\phi}(-\vec{q}) = \overline{\phi}(\vec{q})^t \hat{P}^t \hat{P} \hat{G}\left(\vec{q}\right) \hat{P}^t \hat{P} \overline{\phi}(-\vec{q}). \tag{B.40}$$

The matrix $\hat{P}$ is chosen such that

$$\tilde{G}\left(\vec{q}\right) = \hat{P} \hat{G}\left(\vec{q}\right) \hat{P}^t \tag{B.41}$$

is diagonal and hence $\hat{P}\overline{\phi}(-\vec{q})$ are the eigenvectors of $\hat{G}\left(\vec{q}\right)$. One defines $\overline{\psi} = \hat{P}\overline{\phi}$ (Note that the components of $\overline{\psi}$ will be numbered $0 \rightarrow 3$). Equation B.38 can be rewritten as

$$\begin{aligned} H_{sw}\left[\phi\left(\vec{q}\right)\right] &= \sum_{\vec{q}} \overline{\psi}(\vec{q})^t \tilde{G}\left(\vec{q}\right) \overline{\psi}(-\vec{q}) && \text{(B.42)} \\ &= \sum_{\vec{q}} \sum_{\alpha=0}^{3} \lambda_\alpha\left(\vec{q}\right) |\psi_\alpha(\vec{q})|^2 && \text{(B.43)} \\ &= 2 \sum_{\vec{q}}{}' \sum_{\alpha=0}^{3} \lambda_\alpha\left(\vec{q}\right) |\psi_\alpha(\vec{q})|^2. && \text{(B.44)} \end{aligned}$$

where the λ_α are the eigenvalues of $\tilde{G}$. The sum over $\vec{q}$ is now over the upper half of the Brillouin zone, with the factor of 2 accounting for the bottom half.

One can now substitute equation B.44 into equation B.34 to yield

$$Z_{sw} = \prod_{\vec{q}}{}' \int_{-\infty}^{\infty} d\vec{\phi}\,(\vec{q}) \exp\left(-2\sum_{\alpha=0}^{3} \lambda_\alpha\,(\vec{q})\,|\psi_\alpha(\vec{q})|^2\right) \tag{B.45}$$

$$= \prod_{\vec{q}}{}' \int_{-\infty}^{\infty} d\vec{\phi}\,(\vec{q}) \prod_{\alpha=0}^{3} \exp\left(-2\lambda_\alpha\,(\vec{q})\,|\psi_\alpha(\vec{q})|^2\right) \tag{B.46}$$

$$= \prod_{\vec{q}}{}' \int_{-\infty}^{\infty} d\vec{\psi}\,(\vec{q})\,J\,(\vec{q}) \prod_{\alpha=0}^{3} \exp\left(-2\lambda_\alpha\,(\vec{q})\,|\psi_\alpha(\vec{q})|^2\right) \tag{B.47}$$

$$= \prod_{\vec{q}}{}' J\,(\vec{q}) \prod_{\alpha=0}^{3} \int_{-\infty}^{\infty} d\psi_\alpha\,(\vec{q}) \exp\left(-2\lambda_\alpha\,(\vec{q})\,|\psi_\alpha(\vec{q})|^2\right), \tag{B.48}$$

where $J\,(\vec{q})$ is the Jacobian. One must be careful here as the integration over $d\psi_\alpha\,(\vec{q})$ is over the complex plane. Hence one has that

$$\int d\psi_\alpha \exp\left(-2\lambda_\alpha|\psi_\alpha^2|\right) = \int_0^{2\pi} d\theta \int_0^{\infty} d|\psi_\alpha| \exp\left(-2\lambda_\alpha|\psi_\alpha|^2\right) \tag{B.49}$$

$$= 2\pi\left(\frac{1}{4\lambda_\alpha}\right) \tag{B.50}$$

$$= \left(\frac{\pi}{2\lambda_\alpha}\right), \tag{B.51}$$

and the final result is that

$$Z_{sw} = \prod_{\vec{q}}{}' J\,(\vec{q}) \prod_{\alpha} \frac{\pi}{2\lambda_\alpha} \tag{B.52}$$

$$= \prod_{\vec{q}}{}' \frac{\pi^4 J\,(\vec{q})}{16 \prod_\alpha \lambda_\alpha}. \tag{B.53}$$

From equation B.53 one can calculate the free energy, which is given by

$$F = K_B T \ln(Z) \tag{B.54}$$

$$= E_0 + \frac{N k_B T}{8\pi^2} \int_{\Omega_B} d\vec{q}\,\ln\left(detG(\vec{q})\right) - \frac{N k_B T}{8\pi^2} \ln\left(\frac{N k_B T}{8\pi}\right) \tag{B.55}$$

$$= E_0 + \frac{N k_B T}{8\pi^2} \int_{\Omega_B} d\vec{q} \sum_{\omega} \ln\left(\lambda_\omega(\vec{q})\right) - \frac{N k_B T}{8\pi^2} \ln\left(\frac{N k_B T}{8\pi}\right) \tag{B.56}$$

B.3 The order parameter

Now the order parameter, as defined in equation 5.14, is calculated within the spin wave approximation for a finite system of size $N = 2L \times 2L$. Without loss of generality it can be assumed that the system orders along the $\hat{y}$ direction and hence the order parameter can be written as,

$$\Psi = \frac{1}{4L^2}\left\langle \sum_{\vec{R}} \sum_{i=1}^{4} \cos\left(\phi_i\left(\vec{R}\right)\right)\right\rangle \tag{B.57}$$

$$= \frac{1}{4L^2}\sum_{\vec{R}} \sum_{i=1}^{4} \left\langle \cos\left(\phi_i\left(\vec{R}\right)\right)\right\rangle \tag{B.58}$$

$$\approx \frac{1}{4L^2}\sum_{\vec{R}} \sum_{i=1}^{4} \left\langle 1 - \frac{1}{2}\phi_i^2\left(\vec{R}\right) + \ldots\right\rangle \tag{B.59}$$

$$= \frac{1}{4L^2}\sum_{\vec{R}} \sum_{i=1}^{4} \langle 1\rangle - \frac{1}{8L^2}\sum_{\vec{R}} \sum_{i=1}^{4} \left\langle \phi_i^2\left(\vec{R}\right)\right\rangle + \mathcal{O}\left(\left\langle \phi_i^4\right\rangle\right) \tag{B.60}$$

$$\approx 1 - \frac{1}{8L^2}\sum_{\vec{R}} \sum_{i=1}^{4} \left\langle \phi_i^2\left(\vec{R}\right)\right\rangle \tag{B.61}$$

It has been assumed that the fluctuations about the ground state are small and one need only calculate terms of order ϕ_i^2. The second term in equation B.61 can be written as

$$TA(N) \equiv \frac{1}{8L^2}\sum_{\vec{R}} \sum_{i=1}^{4} \left\langle \phi_i^2\left(\vec{R}\right)\right\rangle \tag{B.62}$$

$$= \frac{1}{8L^2}\frac{1}{\mathcal{Z}}\sum_{\vec{R}} \sum_{i=1}^{4} \left[\left(\prod_{\vec{R}'}\prod_{j=1}^{4} \int d\phi_j\left(\vec{R}'\right)\right)\phi_i^2\left(\vec{R}\right) e^{(-H_{sw})}\right], \tag{B.63}$$

where $A(N)$ is defined with considerable foresight, and T is temperature. H_{sw} is the spin wave approximation to the Hamiltonian as given by equation B.38. Continuing

by Fourier transform one gets for this second term

$$TA(N) = \tag{B.64}$$

$$= \frac{1}{8L^2}\frac{1}{\mathcal{Z}}\sum_{\vec{R}}\sum_{i=1}^{4}\left[\left(\prod_{\vec{q}}{}'\prod_{j=1}^{4}\int d\phi_j(\vec{q})\right)\frac{1}{\sqrt{N}}\sum_{\vec{q}}\phi_i(\vec{q})e^{i\vec{q}\cdot\vec{R}}\frac{1}{\sqrt{N}}\sum_{\vec{q}}\phi_i(\vec{q})e^{i\vec{q}\cdot\vec{R}}\right.$$
$$\left.\exp\left(-\sum_{\vec{q}}\overline{\phi}^t(\vec{q})\hat{G}\overline{\phi}(\vec{q})\right)\right] \tag{B.65}$$

$$= \frac{1}{8L^2}\frac{1}{\mathcal{Z}}\sum_{\vec{R}}\sum_{i=1}^{4}\left[\left(\prod_{\vec{q}}{}'\prod_{j=1}^{4}\int d\phi_j(\vec{q})\right)\frac{1}{N}\sum_{\vec{q},\vec{q}'}\phi_i(\vec{q})\phi_i(\vec{q}')e^{i(\vec{q}-\vec{q}')\cdot\vec{R}}\right.$$
$$\left.\exp\left(-\sum_{\vec{q}}\overline{\phi}^t(\vec{q})\hat{G}\overline{\phi}(\vec{q})\right)\right] \tag{B.66}$$

$$= \frac{1}{8L^2}\frac{1}{\mathcal{Z}}\sum_{i=1}^{4}\left[\left(\prod_{\vec{q}}{}'\prod_{j=1}^{4}\int d\phi_j(\vec{q})\right)\frac{1}{N}\sum_{\vec{q},\vec{q}'}\phi_i(\vec{q})\phi_i(\vec{q}')\sum_{\vec{R}}e^{i(\vec{q}-\vec{q}')\cdot\vec{R}}\right.$$
$$\left.\exp\left(-\sum_{\vec{q}}\overline{\phi}^t(\vec{q})\hat{G}\overline{\phi}(\vec{q})\right)\right] \tag{B.67}$$

$$= \frac{1}{8L^2}\frac{1}{\mathcal{Z}}\sum_{i=1}^{4}\left[\left(\prod_{\vec{q}}{}'\prod_{j=1}^{4}\int d\phi_j(\vec{q})\right)\frac{1}{N}\sum_{\vec{q},\vec{q}'}\phi_i(\vec{q})\phi_i(\vec{q}')N\delta_{\vec{q},\vec{q}'}\right.$$
$$\left.\left(e^{-\sum_{\vec{q}}\overline{\phi}^t(\vec{q})\hat{G}\overline{\phi}(\vec{q})}\right)\right] \tag{B.68}$$

$$= \frac{1}{8L^2}\frac{1}{\mathcal{Z}}\sum_{i=1}^{4}\left[\left(\prod_{\vec{q}}{}'\prod_{j=1}^{4}\int d\phi_j(\vec{q})\right)\sum_{\vec{q}}|\phi_i(\vec{q})|^2\left(e^{-\sum_{\vec{q}}\overline{\phi}^t(\vec{q})\hat{G}\overline{\phi}(\vec{q})}\right)\right] \tag{B.69}$$

$$= \frac{1}{8L^2}\frac{1}{\mathcal{Z}}\sum_{i=1}^{4}\left[\left(\prod_{\vec{q}}{}'\prod_{j=1}^{4}\int d\phi_j(\vec{q})\right)\sum_{\vec{q}}{}'2|\phi_i(\vec{q})|^2\left(e^{-2\sum_{\vec{q}}{}'\overline{\phi}^t(\vec{q})\hat{G}\overline{\phi}(\vec{q})}\right)\right] \tag{B.70}$$

$$= \frac{1}{4L^2}\frac{1}{\mathcal{Z}}\sum_{i=1}^{4}\left[\prod_{\vec{q}}{}'\prod_{j=1}^{4}\int d\phi_j(\vec{q})\sum_{\vec{q}}{}'|\phi_i(\vec{q})|^2e^{-2\overline{\phi}^t(\vec{q})\hat{G}\overline{\phi}(\vec{q})}\right], \tag{B.71}$$

where the sums have been adjusted to run over only the upper half of the Brillouin zone, with the appropriate factor of 2 to compensate. Now one writes the partition function out in full so that one has

$$TA(N) = \frac{1}{4L^2}\frac{\left[\prod_{\vec{q}}{}'\prod_{j=1}^{4}\int d\phi_j(\vec{q})\sum_{\vec{q}}{}'|\overline{\phi}(\vec{q})|^2\left(e^{-2\overline{\phi}^t(\vec{q})\hat{G}\overline{\phi}(\vec{q})}\right)\right]}{\left[\prod_{\vec{q}}{}'\prod_{j=1}^{4}\int d\phi_j(\vec{q})\left(e^{-2\overline{\phi}^t(\vec{q})\hat{G}\overline{\phi}(\vec{q})}\right)\right]}. \tag{B.72}$$

When $\vec{q}' \neq \vec{q}$, certain terms in the sum in the numerator and denominator are identical and will cancel. One is then left with

$$TA(N) = \frac{1}{4L^2}\sum_{\vec{q}}{}' \frac{\left[\int d\overline{\phi}\,(\vec{q})\,|\overline{\phi}(\vec{q})|^2 e^{-2\overline{\phi}^t(\vec{q})\hat{G}\overline{\phi}(\vec{q})}\right]}{\left[\int d\overline{\phi}\,(\vec{q})\,e^{-2\overline{\phi}^t(\vec{q})\hat{G}\overline{\phi}(\vec{q})}\right]}. \tag{B.73}$$

One can diagonalise the matrix as in the previous section such that

$$\overline{\psi} = \hat{P}\overline{\phi} \tag{B.74}$$

$$\tilde{G} = \hat{P}\hat{G}\hat{P}^t, \tag{B.75}$$

where as before $\tilde{G}$ is diagonal with eigenvalues λ_α and the eigenvectors are given by v_α. This gives

$$TA(N) = \frac{1}{4L^2}\sum_{\vec{q}}{}' \frac{\left[\int d\overline{\psi}\,(\vec{q})\,J\,(\vec{q})\,|\hat{P}^{-1}\overline{\psi}(\vec{q})|^2\left(e^{-2\overline{\psi}^t(\vec{q})\tilde{G}\overline{\psi}(\vec{q})}\right)\right]}{\left[\int d\overline{\psi}\,(\vec{q})\,J\,(\vec{q})\left(e^{-2\overline{\psi}^t(\vec{q})\tilde{G}\overline{\psi}(\vec{q})}\right)\right]}. \tag{B.76}$$

The Jacobians in the denominator and numerator are independent of the coordinates and hence can come outside the integrals and then cancel. The matrix $\hat{P}^{-1}$ is the inverse of $\hat{P}$. Because $\tilde{G}$ is a diagonal matrix one can simplify equation B.76 as

$$TA(N) = \frac{1}{4L^2}\sum_{\vec{q}}{}' \frac{\int d\overline{\psi}\,(\vec{q})\,|\hat{P}^{-1}\overline{\psi}(\vec{q})|^2 \exp\left(-2\sum_\alpha \lambda_\alpha \overline{\psi}_\alpha^2\right)}{\int d\overline{\psi}\,(\vec{q})\exp\left(-2\sum_\alpha \lambda_\alpha \overline{\psi}_\alpha^2\right)} \tag{B.77}$$

$$= \frac{1}{4L^2}\sum_{\vec{q}}{}' \frac{\int d\overline{\psi}\,(\vec{q})\,|\hat{P}^{-1}\overline{\psi}(\vec{q})|^2 \prod_{\alpha=0}^{3}\exp\left(-2\lambda_\alpha \overline{\psi}_\alpha^2\right)}{\int d\overline{\psi}\,(\vec{q})\prod_{\alpha=0}^{3}\exp\left(-2\lambda_\alpha \overline{\psi}_\alpha^2\right)}. \tag{B.78}$$

Examination of the term $|\hat{P}^{-1}\overline{\psi}(\vec{q})|^2$ shows that the even terms upon expansion (odd terms are zero by symmetry) are just $|\psi_1|^2 + |\psi_2|^2 + |\psi_3|^2 + |\psi_4|^2$. Hence

$$\frac{1}{4L^2}\sum_{\vec{q}}{}' \frac{\int d\overline{\psi}\,(\vec{q})\,|\overline{\psi}|^2\prod_{\alpha=0}^{3} e^{-\lambda_\alpha|\psi_\alpha|^2}}{\int d\overline{\psi}\,(\vec{q})\prod_{\alpha=0}^{3} e^{-\lambda_\alpha|\psi_\alpha|^2}} = \frac{1}{4L^2}\sum_{\vec{q}}{}' \sum_{\alpha=0}^{3}\frac{\int d\psi_\alpha\,(\vec{q})\,|\psi_\alpha|^2 e^{-\lambda_\alpha|\psi_\alpha|^2}}{\int d\psi_\alpha\,(\vec{q})\,e^{-\lambda_\alpha|\psi_\alpha|^2}} \tag{B.79}$$

Now the integral in the denominator is identical to that seen in the calculation of the partition function and the result is given in equation B.51. It is important to recall that this integral is over all space in the complex plane. Taking the integral in the denominator one has

$$\int d\psi_\alpha |\psi_\alpha|^2 e^{-2\lambda|\psi_\alpha|^2} = \int_0^{2\pi} d\theta \int_0^\infty |\psi_\alpha| d|\psi_\alpha| |\psi_\alpha|^2 e^{-2\lambda_\alpha|\psi_\alpha|^2} \tag{B.80}$$

$$= 2\pi \int_0^\infty d|\psi_\alpha| |\psi_\alpha|^3 e^{-2\lambda_\alpha|\psi_\alpha|^2} \tag{B.81}$$

$$= 2\pi \frac{1}{8\lambda_\alpha^2} \tag{B.82}$$

$$= \frac{\pi}{4\lambda^2}. \tag{B.83}$$

Substitution back into equation B.79 yields as a final result,

$$TA(N) \equiv \frac{1}{8L^2} \sum_{\vec{R}} \sum_{i=1}^{4} \left\langle \phi^2 \left(\vec{R} \right) \right\rangle \tag{B.84}$$

$$= \frac{1}{4L^2} \sum_{\vec{q}}{}' \sum_{\alpha=0}^{3} \left(\frac{\frac{\pi}{4\lambda_\alpha^2}}{\frac{\pi}{2\lambda_\alpha}} \right) \tag{B.85}$$

$$= \frac{1}{8L^2} \sum_{\vec{q}}{}' \sum_{\alpha=0}^{3} \frac{1}{\lambda_\alpha}. \tag{B.86}$$

Therefore the order parameter for a finite size system on the square lattice can be written in the spin wave approximation as

$$\Psi = 1 - TA(N) \tag{B.87}$$

$$= 1 - \frac{1}{8L^2} \sum_{\vec{q}}{}' \sum_{\alpha=0}^{3} \frac{1}{\lambda_\alpha}, \tag{B.88}$$

and one is reminded that $A(N)$ has been defined rather than explicitly calculated at this point.

B.3.1 Asymptotic behaviour

Calculating the order parameter in the limit as $N \to \infty$ is still not a trivial calculation. This is due to the soft mode in the eigenspectrum. The goal is to calculate

$$TA(N) \equiv \frac{1}{8L^2} \sum_{\vec{q}}{}' \sum_{\alpha=0}^{3} \frac{1}{\lambda_\alpha}. \tag{B.89}$$

For a system of size $N = L \times L$ the sum over $\vec{q}$ is over a finite number of terms defined by

$$q^\alpha = \frac{\pi}{2L}(2n_\alpha + 1), \tag{B.90}$$

where $n_\alpha = 0, \pm 1, \pm 2 \ldots \pm (L-1)/2$. Three branches of the eigenspectrum remain finite as $\vec{q} \to 0$. The fourth branch, which will be labelled as $\lambda_0(\vec{q})$, does go to zero as $\vec{q}$ goes to zero and will cause difficulties in the limit of large N. In the limit as $N \to \infty$ the sums over $\vec{q}$ for all branches except $\lambda_0(\vec{q})$ can be converted to integrals and evaluated. That is

$$\lim_{L\to 0} \frac{1}{L^2} \sum_{\vec{q}} \frac{1}{\lambda_\alpha} = \int d\vec{q} \frac{1}{\lambda_\alpha(\vec{q})} \tag{B.91}$$

$$= TC_\alpha, \tag{B.92}$$

where the temperature dependence of λ_α has been explicitly extracted and C_α is a constant independent of N for large N. For λ_0 one must be careful since

$$\lim_{\vec{q}\to 0} \lambda_0 = D(\hat{q})q^2, \tag{B.93}$$

which will lead to a divergence at $\vec{q} = 0$ in the limit of $N \to \infty$. One can define $\Lambda(\vec{q})$ such that

$$\frac{1}{\Lambda(\vec{q})} = \frac{1}{\Lambda(\vec{q})} - \frac{1}{\tilde{D}q^2} \tag{B.94}$$

where $\tilde{D}$ is the average of $D(\hat{q})$ over all angles:

$$\frac{1}{\tilde{D}} = \frac{1}{2\pi}\int_0^{2\pi} \frac{d\theta}{D(\hat{q})}, \tag{B.95}$$

where θ is the angle $\hat{q}$ makes with the x-axis. Therefore

$$\frac{1}{8L^2}\sum_{\vec{q}}{}' \frac{1}{\lambda_0(\vec{q})} = \frac{1}{8L^2}\sum_{\vec{q}}{}' \frac{1}{\Lambda(\vec{q})} + \frac{1}{8L^2}\sum_{\vec{q}}{}' \frac{1}{\tilde{D}q^2} \tag{B.96}$$

$$= T\Lambda_0 + \frac{1}{8L^2}\sum_{\vec{q}}{}' \frac{1}{\tilde{D}q^2} \tag{B.97}$$

The first term is independent of N in the limit $N \to \infty$ while the second will define the dominant N dependence. Evaluating the second term gives

$$\frac{1}{8L^2}\sum_{\vec{q}}{}' \frac{1}{\tilde{D}q^2} = \frac{1}{8\pi\tilde{D}}\ln(N) + TC_0, \tag{B.98}$$

where C_0 is a constant independent of N.

Finally combining all the contributions gives in the limit of large N gives

$$\frac{1}{8N}\sum_{\vec{q}}{}' \sum_{\alpha=0}^{3} \frac{1}{\lambda_\alpha} = \frac{1}{8\pi\tilde{D}}(\ln(N) + C), \tag{B.99}$$

with C a constant independent of N. C includes all the contributions defined above and is given by

$$C = 8\pi\tilde{D}\,(C_0 + C_1 + C_2 + C_3 + \Lambda_{0\cdot}) \tag{B.100}$$

Thus the order parameter as calculated in the linearised spin wave approximation, varies in the limit of large system size N as a function of temperature and N as

$$\Psi \approx 1 - \frac{T}{8\pi \bar{D}}(\ln(N) + C). \tag{B.101}$$

CENTRE FOR NFLD. STUDIES
JUL 18 1978
MEMORIAL UNIVERSITY
OF NEWFOUNDLAND